Investigation of ON-to-ON Body and ON-to OFF Body Channel Characteristics in Static/Dynamic Human Body Model using High Gain Antennas

A Thesis submitted

in partial fulfilment for the degree of

Doctor of Philosophy

by

Elizabeth George

Department of Avionics Engineering

INDIAN INSTITUTE OF SPACE SCIENCE AND TECHNOLOGY

THIRUVANANTHAPURAM - 695 547

3 April 2023

CERTIFICATE

This is to certify that the thesis titled ***Investigation of ON-to-ON and ON-to OFF Body Channel Characteristics in Static/Dynamic Human Body Model using High Gain Antennas*** submitted by **Elizabeth George**, to the Indian Institute of Space Science and Technology, Thiruvananthapuram, in partial fulfillment for the award of the degree of **Doctor of Philosophy**, is a bonafide record of the original work carried out by her under my supervision. The contents of this thesis, in full or in parts, have not been submitted to any other Institute or University for the award of any degree or diploma.

Dr. Chinmoy Saha
Research Supervisor
Associate Professor
Department of Avionics
Indian Institute of Space Science and Technology

Prof. N.Selvaganesan
Head of the department
Department of Avionics
IIST

Place: IIST, Thiruvanathapuram
Date: 3 April 2023

Declaration

I declare that this thesis titled ***Investigation of ON-to-ON and ON-to OFF Body Channel Characteristics in Static/Dynamic Human Body Model using High Gain Antennas*** submitted in partial fulfillment for the award of the degree of **Doctor of Philosophy** is a record of the original work carried out by me under the supervision of **Dr. Chinmoy Saha** and has not formed the basis for the award of any degree, diploma, associateship, fellowship, or other titles in this or any other Institution or University of higher learning. In keeping with the ethical practice in reporting scientific information, due acknowledgments have been made wherever the findings of others have been cited.

Place: IIST, Thiruvanathapuram
Date: 3 April 2023

Elizabeth George
SC18D038

Acknowledgements

I have been engaged in doctoral research at the **Indian Institute of Space Science and Technology (IIST)**, under the **KSCSTE (Kerala State Council for Science , Technology and Environment)** research fellowship scheme.I am indeed indebted to IIST for providing me with the necessary supports and facilities and KSCSTE for providing me with the financial support during the period of my research work.

First of all, I would like to thank my guide **Dr.Chinmoy Saha**, (Associate Professor, Department of Avionics ,IIST Trivandrum for his constant support and guidance. This research work would not have been possible without the constant encouragement and advice extended to me by him. His perfection and enthusiasm has always inspired me.

Besides my advisor, I would like to thank the rest of my Doctoral Committee: **Dr. Deepak Mishra** (DC chairman, Professor, Department of Avionics ,IIST Trivandrum), **Dr. Basudeb Ghosh** (Associate Professor, Department of Avionics ,IIST Trivandrum), **Dr. Basudev Majumder** (Assistant Professor, Department of Avionics ,IIST Trivandrum) and **Dr. V.S.Sooraj** (Associate Professor, Department of Aerospace, IIST) , not only for their insightful comments and encouragement, but also for the constructive criticism which incented me to widen my research from various perspectives. I sincerely thank to **Dr. B.S.Manoj** (former DC chairman, Professor, Department of Avionics ,IIST) for his valuable support and technical guidance throughout the research. I am also greatful to **Dr. V.K. Dadhwal**, former director for his kindness and support. I also appreciate and acknowledge all the non-teaching staff of Avionics Department especially **Mrs. Archana** and **Mrs. Preetha** for making my life at IIST smooth.

I also express my gratitude and thanks to **Director**, IIST, **Prof.Y.V.N Krishna Murthy**, Registrar IIST, **Prof.A.Chandrasekar**, Dean academics, **Prof. Raju K. George** Dean R & D, and **Prof.Kuruvilla Joseph**, Dean Student activities, for providing me the research facility and ambience during my tenure in IIST.

I am grateful to the support I received from some laboratories. I am thankful to **Dr. K.P.Surendran**, Material Science and Technology Department of the National Institute for Interdisciplinary Science and Technology, Trivandrum. I am also thankful to **Dr. Yahia Antar** (Royal Military College Canada), **Dr. Jawad Siddiqui** (Institute of Radio Physics,

Kolkata), **Dr. Debarati Ganguly** (IISc Banglore) and **Dr.Debdeep Sarkar** (IISc Banglore) for providing me with the resources and technical guidance during my research.I am also thankful to **Dr. Sudhakar Rao**, Northrop Grumman, who was always a source of encouragement.I am greatful to **Dr. T.J Apren**, VSSC, ISRO for his inspiration during my research work.

I express my thanks and wishes to my colleagues, **Ms. Gopika Regunathan**, **Ms. Priya Mariyam Raju**, **Ms. Aswathy**, **Mr. Sumit Diwakar** and also my other friends for sharing their knowledge with me and comfort during my hard times. Thanks for pushing and motivating me during during the college days.

A special thanks to my family. My parents, **Chacha** and **Mummy**, for their love and sacrifice that shaped my life. Though they never understood what I am worried on, it was their love that always made me at ease.

I owe special thanks to a very special person in my life, my husband, **Renjith James** for his selfless love and care during all these years. At times when I thought of quitting, it was he who pushed and motivated me. To our beloved daughter, **Miriam Renjith** who joined us during the last phase of my PhD, thank you so much for giving me unlimited happiness and pleasure. The smile on your face made my thesis writing smooth. Words are not enough to say how thankful I am to you dears. I also thank my in-laws, **Pappa** and **Mummy** for their love, support and valuable prayers.

Last but not the least; Thank You, God Almighty for showering your grace upon me so that my today is always better than yesterday and tomorrow, better than today.

Elizabeth George
SC18D038

To my beloved husband Renjith and our daughter Miriam

Abstract

In the current world, the applicability of wearable devices is not just confined to modern devices like iWatches, fitness bands but also to the healthcare issues as well as safety/security, opening the way towards the vision of internet-of-things (IoT). Presently, body area network finds its importance in the field of sports, health care, multimedia and indoor data transmission system. Wireless communication bands like BCS (5-50Hz), MICS (402-405Hz), WMTS (420-450 Hz, 863-870 Hz), and the mostly used ISM bands (902-928 Hz, 950-956 Hz, 2.4-2.5 GHz) exist for deployment of Body Centric Wireless Communication Services (BCWCs). The ultra-wideband (UWB) technology, ranging from 3-10 GHz also provide some attractive features, like (i) low Power Spectral Density (PSD), (ii) low Interference, (iii) less prone to fading and (iv) high data rates. Hence, along with antennas operating in ISM bands, ultra-wideband antennas are also considered in this thesis. For designing a practical WBAN, it is important to investigate the consequences of on-body electromagnetic (EM) wave propagation while human body is at rest as well in motion. A number of obstacles are there when analysis is based on measurements alone. Hence, a good simulation technique, which is not costly as well as less time consuming is advantageous as it unmasks more comprehensive knowledge of the scenario. For this, a twelve cylinder body model is developed which features critical body parts and can be used to simulate rest as well as moving human body postures. The selection and design of the type of antennas to be used as well the orientation in which antenna is placed is of high importance since they increase the efficiency of the wireless link. The effect of varying orientation of ON-Body antennas is also discussed in the thesis. The work also investigates the gain enhancement techniques considering the OFF-Body antennas. The enhanced gain of an OFF-Body antenna results in a better link budget in case of ON-to OFF-body cases. The present PhD thesis investigates the enhancement of gain in three types of antennas, namely : i) E-shaped linearly polarized microstrip antenna ii) Dual fed square shaped circularly polarized antenna and iii) Dielectric resonator antenna (DRA). In the first two antennas a hybrid substrate is used for enhancing the gain and in the third case, a metasurafce lens is used to enhance the gain of the DRA. A systematic study of the EM wave propagation in ON-Body to ON-Body case as well as ON-Body to OFF-Body case is dealt in the thesis. This includes the investigation of creeping waves on a cylindrical body

model, time domain analysis using UWB antenna on three layered rectangular body model, study of propagation of EM waves during body movement using twelve cylinder body model as well as the study of transmission characteristics with and without the presence of human body while using 'Smart Bag'.

The work is systematically planned and summarized as follows:

- Gain enhancement of linearly and circularly polarized microstrip antenna as well as dielectric resonator antenna which has the potential to be used as OFF-Body antennas is simulated and practically realized.
- Human model which features the critical body segments such as head, shoulder, torso, upper arm, lower arm, thighs and calf is introduced for the study of double arm swing activity. Two cross-slot antennas (CSA) are designed and fabricated, for investigation of the double arm swing activity using the newly introduced twelve cylinder body model. The same CSA is used for creeping wave analysis on cylindrical single layered phantom. Simulations are done in CST Microwave studio suite and experiments are carried out using container filled with distilled water as phantom.
- Characterization of the channel between an ON-Body and OFF-Body UWB antenna in terms of Time Domain characteristics using short pulse electromagnetics is performed using extensive simulation. The experiments are also done by keeping UWB antennas on various positions of a volunteer.
- A smart bag is modelled in SOLIDWORKS and integrated with a patch antenna. The transmission characteristics of this 'Smart Bag' with and without the presence of twelve cylinder human body model is studied.

Table of contents

List of figures

List of tables

Nomenclature

Abbreviations

AR	Axial Ratio
BAN	Body Area Network
BCC	Body Channel Communication
BCWC	Body Centric Wireless Communications
BLE	Bluetooth Low Energy
CMOS	Complimentary Metal-oxide Semiconductor
CP	Circular Polarization
DRA	Dielectric Resonator Antenna
DR	Dielectric Resonator
EBG	Electromagnetic Band Gap
ECG	Electrocardiogram
EM	Electromagnetic
EMG	Electromyography
FSS	Frequency Selective Surface
GHD	Growth Hormone Deficiency
GI	Gastro Intestinal
HBC	Human Body Communication

IBC	Intra Body Communication
ICNIRP	International Commision on Non Ionizing Radiation Protection
IMD	Implantable Medical Devices
IoT	Internet of Things
ISM	Industrial, Scientific and Medical
LHCP	Left Hand Circular Polarization
LOS	Line of Sight
LP	Linear Polarization
MICS	Medical Implant Communication System
MI	Magnetic Induction
MIMO	Muliple Input Multiple Output
MSA	Microstrip Patch Antenna
MSL	Metasurface Lens
NLOS	Non Line of Sight
PICA	Planar Inverted Cone Antenna
PIFA	Planar Inverted F Antenna
RFID	Radio Frequency Identification
RF	Radio Frequency
RHCP	Right Hand Circular Polarization
Rx	Receiver
SAR	Specific Absorption Rate
S-MSA	Square Microstrip Patch Antenna
Tx	Transmitter
UWB	Ultrawideband

WBAN	Wireless Body Area Network
WCE	Wireless Capsule Endoscopy
WMTS	Internet of Things

Chapter 1

Introduction

The study of EM wave propagation on the human body has always attracted the scientists due to its relevance in various fields such as sport, multimedia, healthcare military, and even in fashion world [1]-[4]. The booming of Internet of Things (IoT) increased the importance of this study. An organized exploration of EM wave propagation on human body in rest as well as motion activities is required for proper design of body-worn devices [5]. The data gathered from several sensors placed on the human body is directed to smart devices for further analysis in case of a wireless body area network (WBAN) system [6]. Many difficulties such as need of multiple volunteers, placement of antennas, performing different physical activities arise when experiment based analysis are only taken into consideration [5]. In such cases a simulation strategy should be done in combination with experiments. This helps to get an all-around data in our study [5].

While performing ON-Body to ON-Body studies, the antenna should be oriented in such a way that the radiation from the antenna is along the surface of the body while for ON-Body to OFF-Body cases, the radiation from the antenna should be away from the human body [7]. In literature, the investigation of EM wave propagation is carried out using various phantom model, including, i) rectangular single layer [8], ii) cylindrical single layer [9], iii) cylindrical or rectangular three layer [10], [11], and iv) voxel model [12]. Different ON-Body to OFF-Body cases requires the transmission of data to different distances. In some cases it can be short distance where the patient is in the hospital room while there can be remote applications as well. For long distance transmission of these data, the performance of antenna, especially high gain and efficiency, is highly important as it adds to the channel efficiency. Several gain enhancement techniques are studied in the literature for microstrip antenna as well as dielectric resonator antennas. Various approaches are studied for gain enhancement, which includes the use of superstrate [13], electromagnetic band gap (EBG) structures [14], arraying techniques [15] etc. DRA at higher order modes are also found to

enhance the gain [15]. The improvement of gain in [16] is achieved forming grooves on DRA. Mushroom like structures are also used to enhance the gain [17]. Electromagnetic band-gap (EBG) structures are used in microstrip antennas as well as DRA's [18] for improving the gain. The authors in [19] has considered FSS to increase the gain of the antenna.

In the present thesis, the gain enhancement techniques are investigated for a linearly polarized antenna as well as circularly polarized antenna making use of a hybrid substrate. The gain enhancement is also obtained using metasurface lens for a dielectric resonator antenna. The investigation of the propagation of electromagnetic waves on different types of phantom, namely: i) single layered cylindrical phantom, ii) three layered rectangular phantom and iii) twelve cylinder phantom is performed for various antennas. The study is undertaken for ON-Body to ON-Body as well as ON-Body to OFF-Body scenarios.

1.1 Literature Survey

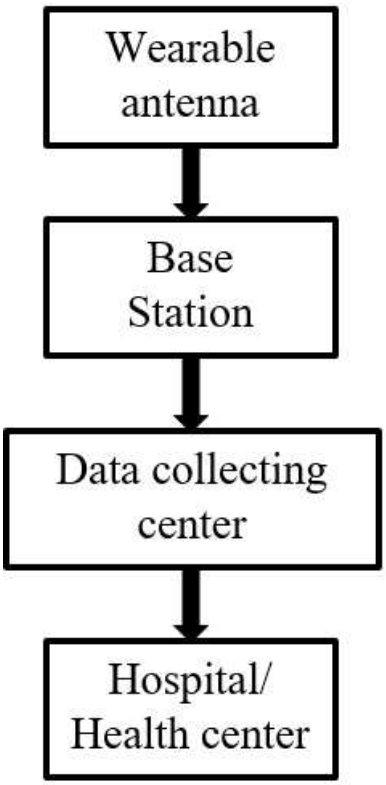

Fig. 1.1 Typical block schematic of smart health monitoring system.

Wearable technology has made exceptional development in recent years, with applications in the medical sector including monitoring of physiological/vital signals, body movement

monitoring and rehabilitation of patients, consumer electronics, sports, artificial intelligence and many. The wearable devices can be positioned on different human body parts as nodes. These nodes are linked to a hub/personal smart device wirelessly. This wireless network is considered as wireless body area network (WBAN). WBANs are the pillar of wearable technology. Its significance can be weighted by the fact that any node breakdown will affect only that particular node while a WBAN crash may impact the entire network/system. Body-centric wireless communications (BCWCs) have potential in various areas, such as E-health systems, consumer systems, home care and entertainment [20]. The Fig.1.1 portrays the working of wearable devices in a smart health monitoring system.

1.1.1 Classification of Wireless Body Area Network (WBAN).

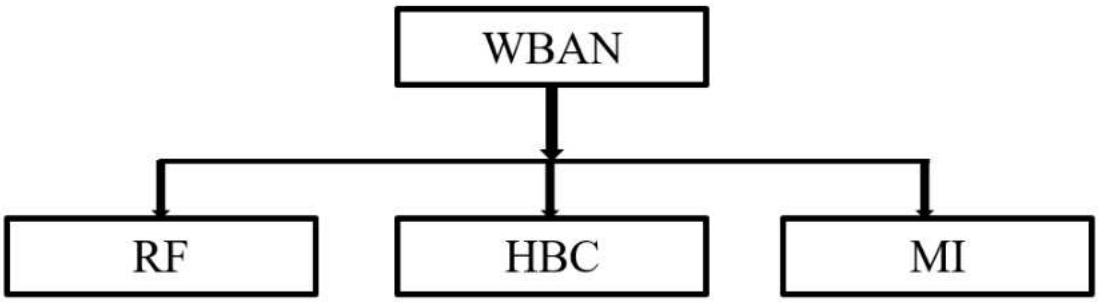

Fig. 1.2 Block diagram showing classification of WBAN

The block depicting the classification of wireless body area network (WBAN) is shown in Fig.1.2. There are three types of WBAN technologies. They are as follows:

- Radio Frequency (RF): This include Bluetooth, BLE, ZigBee and pertinent technologies employing IEEE 802.15.6 standard. RF WBANs can be incorporated with existing wireless technology like smart phones and they are small in size as well as achieve high data rates. The disadvantages of RF WBANs include: a) RF radiation loss via tissues which in turn results in high path loss, b) high power requirements, c) complex channel modeling due to change in channel model for different body parts and surroundings, d) interference from other devices, and e) shadowing effect in the range of 30–40 dB due to dynamic body movement [20].

- Human Body Communication (HBC): This is also known as Intra-Body Communication (IBC), or Body Channel Communication (BCC). Here, the human body is utilized as the channel through which information is transmitted. This is via capacitive or

galvanic coupling, utilizing frequencies centered around 21 MHz as specified under IEEE 802.15.6 standard. As the signals are confined or closer to the human body, HBC favors in terms of security and interference. But the disadvantages of HBCs include: a) high loss, b) high power requirements, c) complex channel modeling, d) bulkiness and safety issues as current flows through the human body [20].

- Magnetic Induction (MI) [7]: Magnetic coupling is used in this method to transmit data between transmitters and receivers positioned on the body. The loss due to human tissues is absent in MI but still it has high loss, mainly when distance between transmitter and receiver increases. Performance degradation also occurs due to human body movement, shadowing effect as in the case of RF WBANs. MI has low data rate [20].

1.1.2 ON-Body EM Wave Propagation

The body centered wireless communications (BCWC) used in various areas [21] such as E-health systems, consumer systems, home care and entertainment, can be categorized on the basis of positions of transmitter (Tx) and receiver (Rx) as: ON-Body, IN-Body and OFF-Body communication systems. In ON-Body systems, both the Tx and the Rx are integrated on one human body, thereby increasing the requirement for EM wave propagation along the human body [22].

Figure 1.3 depicts smart BAN for Internet of Things (IoT). The different nodes like blood pressure node, electrocardiogram (ECG) node, electromyography (EMG) node, artificial pancreas, pulse oximetry and inertial node are positioned on a human body model. Based on the different environments in which humans are engaged, the data can be collected to hubs for short term analysis. Cloud storage of data helps for long term analysis. To design a reliable and power efficient WBAN successfully, a comprehensive idea of ON-Body wireless propagation channels, during static/ dynamic human activities are required. Based on this need, scientists have made both measurement-based and simulation-based analysis techniques to investigate how movement activities affects ON-Body electromagnetic (EM) wave propagation. The measurement-based techniques focus on transmission loss between Tx antennas and Rx antennas worn by human volunteers executing various dynamic activities [5].

In measurement-based analysis human volunteers or human phantom models are used to study the transmission losses between Tx and Rx antennas placed at various positions on the body. Although these investigations have contributed valuable information about transmission loss data, there are still practical restrictions to experiments. This include

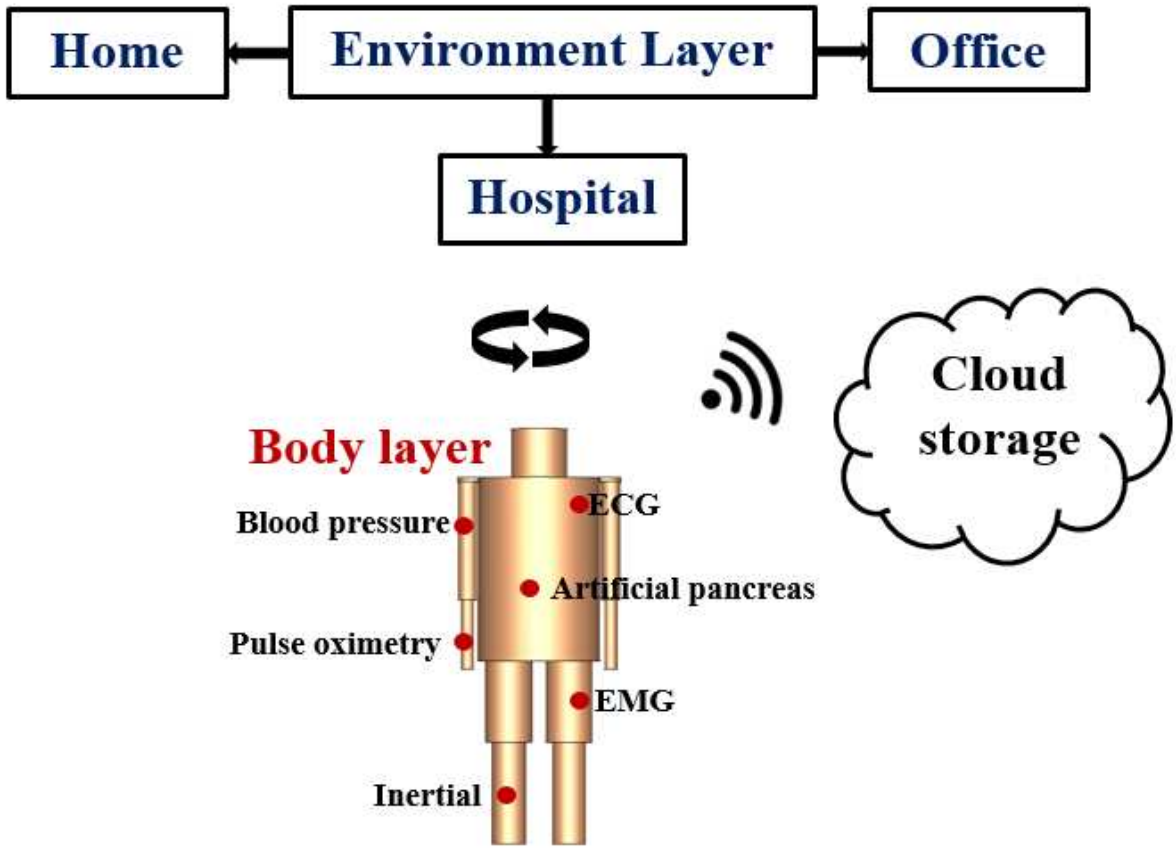

Fig. 1.3 Body area network for Internet of Things.

limitations on dynamic activities like walking, jumping, hopping, antenna placements on different body positions, need for multiple volunteers of different sizes and data resolution. More in-depth information can be obtained with the help of simulation based techniques since transmission loss can be computed for entire EM wave propagation pathways between Tx and Rx antennas. Moreover, simulation techniques give significant flexibility in isolating and optimizing antenna positions for ON-Body EM wave propagation [6].

Analyzing EM wave propagation mechanism along or around the human body/phantom is crucial for designing a reliable as well as efficient WBAN. Scientists have done extensive research over the last decade, and have identified that space wave and surface wave exists mainly for the line-of sight (LOS) along-body propagation, wherein creeping waves dominate for non-LOS, around-body propagation. A creeping wave in electromagnetism is a wave that is diffracted around the shadowed surface of a smooth body such as a sphere and has applications in EM propagation as well as accoustics. Creeping waves greatly extend the ground wave propagation of long wavelength (low frequency) radio. They also cause both of a person's ears to hear a sound, rather than only the ear on the side of the head facing

the origin of the sound. The propagation of electromagnetic waves on the body includes a union of free space propagation, and creeping waves which is due to the diffractions as well as the reflections from the environment. The study of creeping waves around the torso provides more insights on ON-Body to ON-Body propagation. The ON-Body propagation is mainly contributed by creeping waves diffracted from lossy human body phantom and trapped along the body's surface, while the radio waves of OFF-Body links are dominantly line of-sight (LOS) as well as multi-path propagations. Creeping waves are more sensitive to body motions rather than shadowing, fading and multipath effects. Recently, researchers have exploited the ON-Body EM wave propagation characteristics for human activities. Wireless transceivers are used to categorize limb movements by Guraliuc et al. Frequency analysis has been used by Munoz et al. to classify four varying activities, and provided proposal to extract biomechanical data from dynamic WBAN channels. Wang and Zhou investigated activity recognition techniques based ZigBee, RFID, and WiFi. The traditional activity recognition methods based on physical sensors such as motion camera, accelerometer, gyroscope, etc. are costly, provide less power efficiency. The ON-Body propagation methods can be implemented with high classification accuracy [6].

The finite difference simulation techniques in time domain for a numerical human phantom led to the proposal of ON-Body creeping wave mechanism. As EM waves propagates around the human torso, it decays exponentially. This is also verified by measurement data. A formal derivation of analytical path loss model using the diffraction theory was done by Alves et al. This characterizes attenuation of creeping wave around a lossy dielectric cylinder which is along a circular path.

To analyze dynamic creeping wave propagation two antennas have to be positioned, one at the front and other at the back of participants. The authors in [6] used three pairs of quarter-wave monopole antennas, for studying different WBAN bands centered at 433 MHz, 915 MHz, and 2.45 GHz. The transmission data was recorded with the antenna fixed on human volunteers doing different activities.The impedance variation created by positioning an ON-Body antenna due to near-field perturbations during dynamic postures, can be used to identify vital signals for categorizing different dynamic/static human postures [23].

ON-Body EM wave propagation can be used for monitoring human height, especially for determining toddler's health. Monitoring growth helps in early detection of many conditions including Turner syndrome, Crohn's disease, growth hormone deficiency (GHD), short stature, Celiac disease, and obesity which will help to avoid health problems in future. For automating the height monitoring without any obstructions the authors in [24] proposed antenna-impregnated fabrics for wireless recumbent height monitoring on the go. The fabric is integrated with multiple dipole antennas positioned at known intervals from each other.

The transmitting antennas are placed towards the edges of the material whereas the receiving antennas are kept in between. The subject lying on the fabric material causes the detuning of antennas underneath, thereby inducing losses in the wireless transmission paths associated with it. The reduced transmission coefficients of the Tx antennas at the head and feet of the human body/phantom helps in calculating the height of human body/phantom [24].

Another important application of ON-Body EM wave propagation analysis is for monitoring joint flexion which is a crucial part of human movement. To perform activities like running, swimming, climbing, walking etc. the extension of elbow, knee and so on is a must. The ease to monitor joint flexion automates monitoring progress during rehabilitation and personalized training. This also finds application in consumer electronics, gestural recognition, sports etc. The authors in [4] have introduced coils that can be used to examine joint flexion. They are reliable and not sensitive to line-of-sight. When the coils are realized on e-threads, they can be easily integrated to garments.

1.1.3 IN-Body EM Wave Propagation

Biomedical telemetry allows the investigation of physiological data/signals at a distance, through wired and wireless communication technologies. These signals are obtained by usage of transducers and the raw/post-processed data is then transmitted to external processing/control unit. Implantable medical devices (IMDs) is one of the current advancements in bio-medical telemetry [25],[26].

The antennas used in implantable devices should ensure biocompatibility for the safety of the patient and to avoid rejection of the implant. As the human tissues are conductive, direct contact of implantable antenna metallization with the tissue results in a short circuit. To preserve the biocompatibility of the antenna as well as avoid the contact of metal radiator with human tissue, a dielectric superstrate is used. Teflon, MACOR® and ceramic alumina are widely used as biocompatible material. But it is to be noted that drilling and round cuts are not easy with ceramic substrates. Another method used is coating the implantable antenna with a low loss biocompatible layer [26].

Present era has seen the development of ultra-small designs for IMDs. Researchers have developed IMDs with a radius of about 12.5 mm which can be inserted inside the eyeball. The power incident on the implant is limited for patient safety. For 1 gram of tissue, the Specific Absorption Rate (SAR) should be less than 1.6W/kg as per the IEEE C95.1-1999 standard. The SAR value averaged on a 10 gram tissue should be less than 2 W/kg based on ICNIRP restriction [26].

Wireless implanted device facilitates sensing and monitoring of body parameters. It can process the data and transmit physiological processed/raw data of an individual to

the healthcare service centers and hospitals which advances the healthcare system. Organ transplantation is one medical condition where frequent monitoring and hospital visits of the patients are required. For final stage liver diseases, liver transplantation is considered to be the standard treatment by the medical community. But during the first two weeks after surgery, transplantation failure is very high. Traditional techniques for post-surgery includes blood test on a daily basis and tissue biopsy that are meddlesome and gives a slow response to the potential transplantation failure. It is necessary to keep the failure rate of liver transplantation very low due to the limitations of the potential donors. Wireless monitoring using implanted devices for a transplanted organ provides a functional solution for early detection and medication which can prevent a critical damage of the organ. In this process, the implanted wireless device positioned on the top of the transplanted liver transmits physiological information such as hepatic perfusion and oxygenation levels which are the factors indicating risks for a transplanted liver to the ON-Body device/node. From this ON-Body node data is transferred to personal devices and healthcare centers. Thus, even by reducing the hospital stay the patient can be constantly monitored with this application. This also leads to a reduction of recovering periods and medical costs [25].

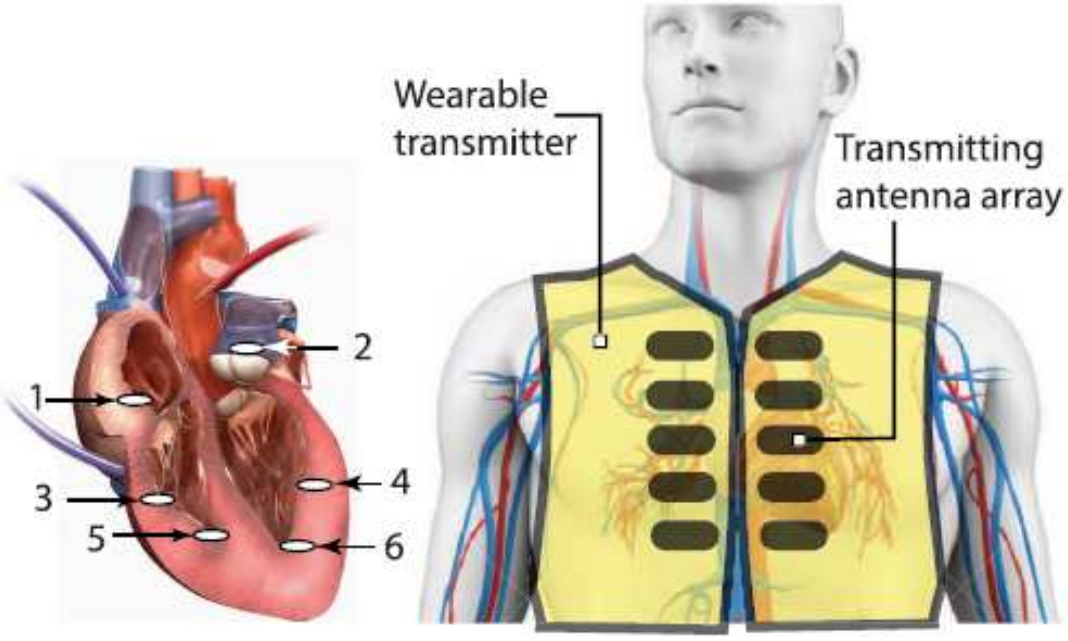

Fig. 1.4 A conceptual illustration envisioning the implantation of multiple leadless pacemakers and a conformal wearable antenna [27].

Continuous operation of the implantable medical devices (IMDs) will need significant energy, which in turn reduce the lifetime of the IMDs. The methods for battery recharge

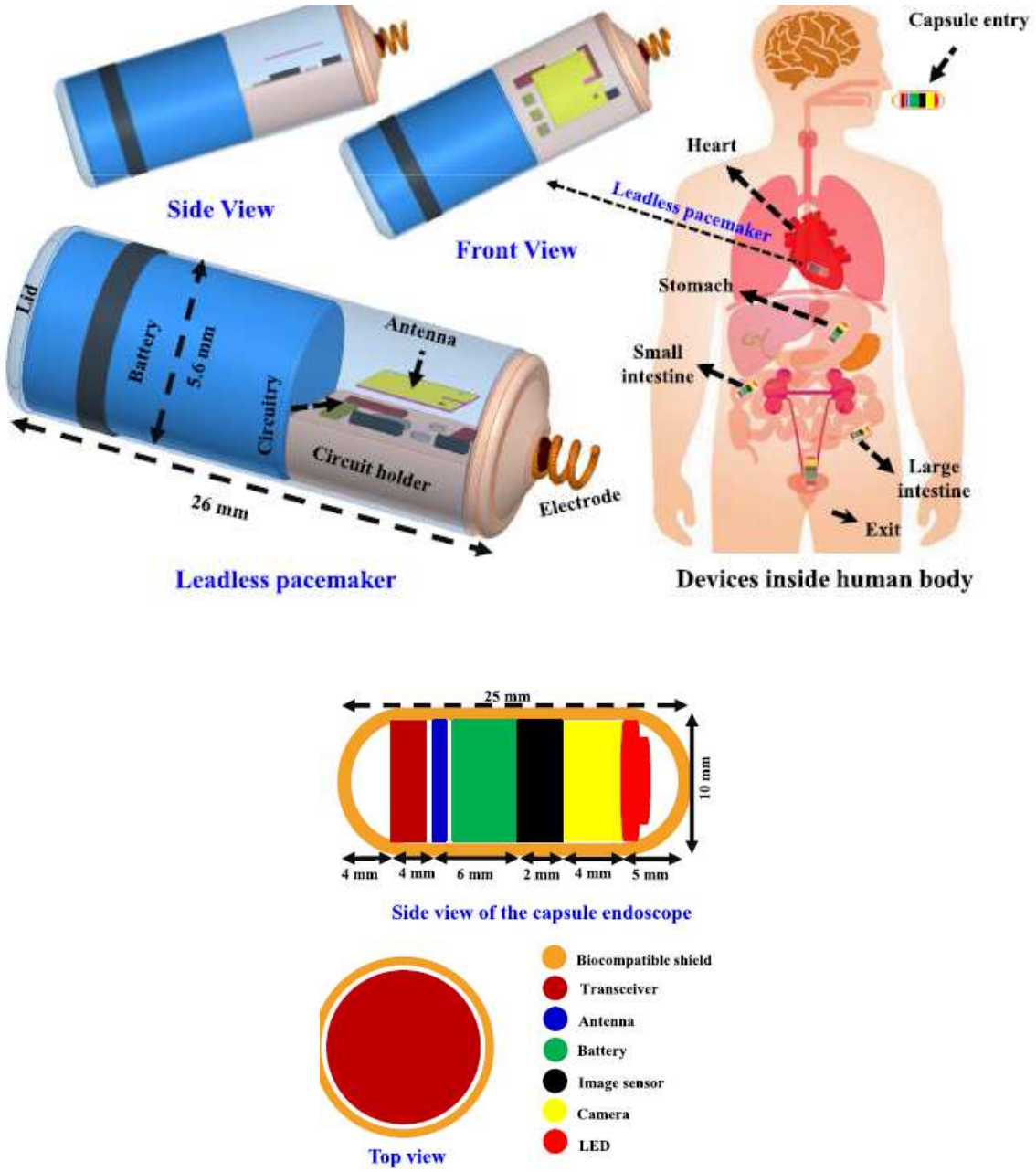

Fig. 1.5 WBAN for leadless pacemaker and capsule endoscopy[29].

includes an inductive-loop approach. It is advantageous to use the bio telemetry link only when necessary. Hence a transmitter receiver system which has two operating bands should be used. This include commercially available Zarlink ZL70101 transceiver. These type of systems uses two frequency bands, one band for “wake-up” and another for transmission. This ensures the transceiver remain in SLEEP MODE consuming less power of 1 W till a WAKE UP signal is given in the 2.45 GHz ISM band. In the NORMAL MODE, the

IMD is kept fully powered, while exchanging information in the MICS band. After the data transfer, the transceiver in IMD goes back to the SLEEP MODE. An external device can be programmed as per doctor's defined schedule to wake up the IMD or only when a threshold patient event is identified [30]. Figure 1.4 depicts wearable transmitting antenna array and leadless pacemakers implanted [27].

Due to the busy schedule, many follow unhealthy food practices. As a result many of the diseases are left unnoticed at an initial stage, including gastrointestinal (GI) tract cancers. Timely detection and diagnosis of GI cancer is important as they are curable at initial stage. Wireless capsule endoscope (WCE) is an effective practical device for early detection of gastrointestinal cancers. These can be used for the observation of gastrointestinal (GI) mucosa, especially for the diagnosis of small intestines. The WCEs are like regular medical pills which can be swallowed easily by individuals which makes the inspection much easier. The conventional endoscopes can examine only a small region of the small intestine but WCEs can inspect the entire area. A WCE communication system consists of four different parts: a Tx in WCE, a Rx array attached to person under test's body, a data receiving and processing box, a viewer on human abdomen, and a workstation with image analysis software. The images taken by the camera are stored in the data receiving box and displayed in real time for physician to see by the viewer. The Rx is usually designed as an array as the signal from the Tx will be weak due to its misalignment inside the human body. Images taken by the camera are then transmitted from the data receiving box to the workstation for investigation by doctors [28]. WBAN for leadless pacemaker and capsule endoscopy can be visualized as shown in Fig.1.5 [29].

For IN-Body scenario, the propagation channel depends on the location of implanted device as varying channel links involves multiple/various organs and tissues resulting in varying channel characteristics. In-Body EM wave propagation channel are reported for chest , brain , torso and embedded in muscle at UWB frequency range [25].

1.1.4 Antennas for Body Area Network

The rise in demand for BANs has made antennas and EM wave propagation for body-centric wireless communications (BCWCs) an area of high importance for research. The main performance requirements for antennas used in BAN networks are as follows: a) influence between the antennas and the human body should be low to ensure antenna efficiency b) low specific absorption rate (SAR), c) size should be small and c) polarization of the antenna should be normal to the body surface, in case of ON-Body communications [30]. To realize low SAR, textile patch antennas, use a large ground plane. But, these antennas are more suitable for ON-to-OFF-Body systems, and not for ON-Body-to-ON-Body systems since

large ground plane results in a narrow beam toward the zenith direction. Hence, a quarter-wavelength monopole antenna which has omnidirectional radiation pattern will be a better choice for ON-Body-to-ON-Body systems. Experimental investigation reveals that in ON-Body-to-ON-Body system, path loss between monopole antennas fixed to the human body is less compared to loop antennas and patch antennas. However, it is not practical to use a quarter-wavelength monopole antenna. Insteaad, antennas like, planar inverted-F antennas (PIFAs) and top-loaded monopole antennas can be used. PIFAs have an added advantage as they are comparatively immune to fading during dynamic body postures due to their non-directivity and multi-polarization.

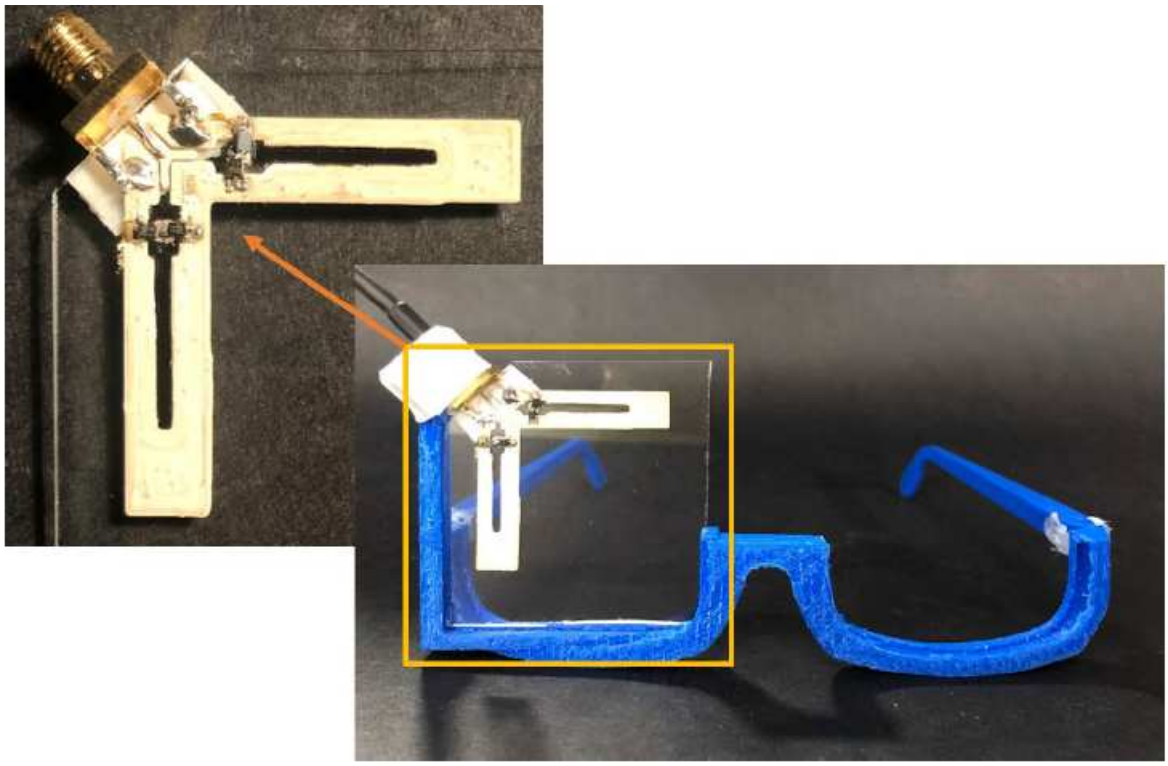

Fig. 1.6 Antenna inside a glass frame [37].

Ultra-wideband (UWB) technology is as an attractive solution for WBAN. UWB provides low-power consumptions, high-data-rate, and robustness against multipath compared to conventional bands [31].It is a demanding task to design an antenna for UWB body-centric communications. The UWB antenna should meet several significant requirements, such as: a) optimized characteristics in frequency and time-domain analysis, b) small size and low profile and c) good ON-Body propagation [30]. The frequency domain and time domain characteristics should be considered and analyzed for antennas kept at different positions on the body. The changes in performance of the antenna due to lossy nature of human

body should also be considered. For wearable applications the UWBs used should be miniaturized. The authors in [28],[30]and[31] have contributed to many miniaturizing designs of UWB antennas. The positioning of the antenna on the human body is significant as for ON-Body to ON-Body propagation the EM wave should propagate along the body. Hence, the omnidirectional planar antennas should be placed normal to the body so that EM wave will propagate along the body. For ON-Body to OFF-Body communications the omnidirectional antenna can be kept parallel to the body which results in the EM wave propagation in and out of the body. If the antenna field polarization is normal to the body surface it will improve the ON-Body propagation. The various reasons due to which a quarter-wavelength monopole is suitable for ON-Body communication are as follows: a) omnidirectional radiation pattern with maximum radiation along the body surface; 2) E-field perpendicular to the body surface. Furthermore, a comparison between two different UWB antennas has been performed showing that the planar inverted cone antenna (PICA) with an omnidirectional monopole-like pattern demonstrates very good performances for on-body communications [30]. Though planar inverted cone antenna and the quarter-wavelength monopole antenna exhibit very good performances, their relatively large ground plane and heights makes them less suitable for ON-Body communication systems.

Since ultra-wideband (UWB) technology enables reduction in size of antenna due to its high frequency levels, they are potential candidates for IMDs. The device lifetime is also increased due to their low power consumption. The high data rate transmission of UWB enables them to be used for drug delivery and micro robots for IN-Body biopsy as well as treatment procedures. The use of biodegradable material reduces the complications of IMD removal from the patient's body. The disadvantage of UWB technology lies in the fact that, UWB signals degrades while propagating through the body making wireless communication links impractical. Hence, an investigation of the propagation characteristics at UWB frequency is important to ensure robust and reliable wireless communication links IN-Body [28].

ON-Body to OFF-Body scenarios requires to send the data to different distances. When the person under test is in hospital room, it is short range but when the person is staying at the comfort of his/her home, it is long range wireless communication. For long ranges antenna performance is crucial for efficient transmission of the data. In order to ensure patient safety the IN-body as well as ON-Body antenna are designed with low gain and the gain of OFF-Body antenna is enhanced using various techniques.

There are various gain improvising techniques reported in open literature: making grooves on the DRA [16], using mushroom-like structures[17], employing electromagnetic band gap (EBG) structures[18], using anisotropic DRA[34], FSS structures[19], use of short horn[35]

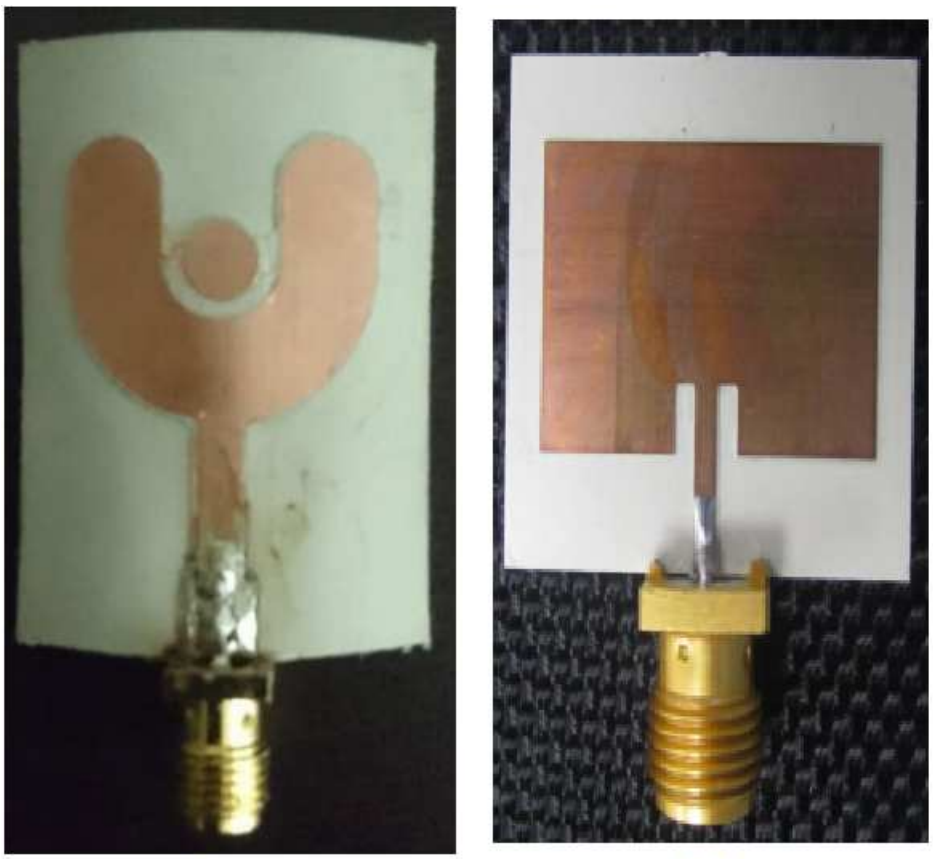

Fig. 1.7 (a) Ultra wideband antenna [33] (b) Microstrip patch antenna[27].

and on-chip CMOS feeding technology[36]. The gain enhancement using small DRA with main DRA[37] and a metamaterial converging lens as a superstrate is other techniques [38]. Parasitic antenna array can also be used to enhance the gain[39].

The selection and design of the type of antennas to be used as well the orientation in which antenna is placed is of high importance since they increase the efficiency of the wireless link. The effect of varying orientation of ON-Body antennas is also important. The enhanced gain of an OFF-Body antenna results in a better link budget in case of ON-to OFF-body cases.

1.2 Motivation Scope and Objective

The investigation of electromagnetic wave propagation in the presence of various biological body models, especially for human body model, is extremely important due to plethora of applications in sport, multimedia, healthcare and Internet of Things (IoT). Various wireless communication bands, such as MICS, WMTS, ISM and UWB bands are being extensively

used for these applications. The design of a practical WBAN necessitates systematic and extensive study of the outcome of on-body electromagnetic wave propagation during human rest as well as movement. A number of limitations crop up when measurement based analysis alone are done including antenna placements, need of volunteers of different physical size and limitations on motion activities. Measurement based techniques can be even more challenging for pregnant women. A simulation technique along with experiments can provide more comprehensive knowledge on dynamic on-body propagation as all EM pathways between the transmitting and receiving antennas are studied. We follow, from above discussion, that there exists a need for investigation of propagation of electromagnetic waves around the human body, study of transmission characteristics in ON-Body to ON-Body scenario as well as ON-Body to OFF-Body scenario. The requirement of performance enhancement of antennas is also evident from the study. This serves us a motivation for our current research work.

1.3 Objective of the Work

The key objective of this thesis is to establish a simplified simulation methodology for dynamic/rest activities of human beings. The work reported in this thesis was taken up with the following objective:

- Study of electromagnetic wave propagation around the human body during rest as well as movement.
- Study the creeping waves around human body.
- Study gain enhancement techniques for OFF-Body antennas.
- To study the best suitable orientation for the antenna kept on human body.

1.4 Thesis Contribution

1.4.1 Ferrite ring loaded hybrid substrate for gain enhancement of linearly and circularly polarized antennas

In this work, a hybrid substrate is formed by the combination of Rogers 6002 and ferrite material for improving the gain of linearly polarized E-shaped microstrip antenna and dual fed square shaped circularly polarized antenna. The E-shaped radiating patch of the antenna is formed by symmetrically designing two slot lines running parallel to each other along the

dominant-mode surface currents of a conventional rectangular microstrip antenna. These embedded slots result in enhanced bandwidth with the presence of additional resonance along with the fundamental TM_{10}-mode resonance. A 90 degree hybrid feed-network is used to obtain the circular polarization in square shaped microstrip antenna. For both the antennas the study is done on conventional Rogers's substrate as well as hybrid substrate of same thickness. The use of hybrid substrate resulted in a gain enhanced antenna due to the constructive interference of surface waves in this newly designed antenna. The study also details on how the position and the size of the ferrite material is concluded in the work.

1.4.2 Metasurface lens integrated dielectric resonator antenna for gain enhancement

A metasurface lens loaded high gain rectangular DRA is detailed in this work. This newly proposed antenna has many applications: i. it can be considered as a single unit of MIMO (Multiple Input Multiple Output) antenna design. ii. It has 5G base station applications. iii. Can be used for IoT applications. This gain enhancement technique can also be used on other antennas with bore-sight radiation. The rectangular design is chosen for antenna as it provides flexibility in the design compared to cylindrical and hemispherical DRA. The proposed antenna is easy to be fabricated also. The DRA is excited by a 50 ohm microstrip line. The circular shaped metasurface lens (MSL) is designed with rectangular copper loops whose dimensions vary from the center of the lens to edges of the lens. The metallic loops are printed on both sides of the dielectric substrate. The varying dimension of the MSL, results in a graded refractive index. The value is highest at the center and slowly decays towards the edges at the design frequency of 4.5 GHz. The incoming radiated waves from the DRA passes through the properly oriented MSL and results in a highly collimated electromagnetic wave at the output side. The distance at which MSL is to be placed is also theoretically discussed in the work. The MSL has to be placed symmetrically above the DRA for proper gain enhancement.

1.4.3 Investigation of creeping waves on a cylindrical phantom

The study aims to obtain an insight on creeping waves around the human body. In this study, a cylindrical body with dielectric constant as two-third of the muscle tissue is modelled in CST studio suite. Two omnidirectional cross-slot antennas operating in the range of 1.8-3 GHz are used. Both the antennas are attached on the cylindrical phantom model. One antenna, Ant1 acts as the transmitting antenna and the other antenna, Ant2 acts as the receiving antenna. The position of Ant1 is fixed, and Ant2 is positioned in circular path around the cylindrical body

model. The transmission characteristics are analyzed for different positions. The experiment was also conducted using a cylindrical plastic container of similar radius to the body model. Two different cases: i) without water (non-lossy medium) and ii) with distilled water of dielectric constant = 78 (lossy medium) filled in the plastic container, were considered for the experiment.

1.4.4 Twelve cylinder Body model

A twelve cylinder body phantom is modelled in CST Microwave studio suite. The twelve homogeneous cylinders (ε_r = 35.15 and $tan\delta$= 1.16 S/m) of this model features the important body parts including head, shoulder, torso, thighs, calf, upper arm and lower arm. This new model is used to simulate the human movement activities apart from human rest.

Double arm swing activity

Here, we modelled this twelve-cylinder body model for a double arm swing activity which occurs in the sagittal plane in reciprocal direction similar to our hand movement while we walk. The Ant1 (Cross slot antenna) is placed on the chest of the model and Ant2 (Cross-slot antenna) is placed on lower arm of the model and the transmission characteristics for each cases are performed.

Integration of Smart Bag with Twelve cylinder body model

A bag is modelled in SOLIDWORKS which is then imported to CST Microwave studio suite to integrate it with a patch antenna (Ant1) operating at 3.45 GHz making it a 'Smart Bag' model. A similar patch antenna is used as the OFF-Body antenna (Ant2) to study the ON-Body to OFF-Body characteristics. In our study the bag material was chosen to be cotton material with a dielectric constant $\varepsilon_r = 1.9$ and $\tan\delta = 0.092$ This 'Smart Bag' is then integrated with the twelve cylinder body model and transmission characteristics in presence of human body is studied.

1.4.5 Time Domain Analysis for ON-Body to OFF-Body scenario using UWB antenna

In this work, two UWB monopole antennas are used to study ON-Body to OFF-Body time domain characteristics. A three layered rectangular body model featuring skin, fat and muscle is used for simulation. The experiment is also repeated by using UWB monopole antenna for the same scenario. Multiple experiments are conducted by using UWB Monopole as well as

Vivaldi antenna on various positions of the human body to get an understanding of varying transmission characteristics. This method of inspecting the transient Figures of Merit is a step towards obtaining an all-inclusive knowledge to channel modeling and estimation with the aid of short pulse electromagnetics.

1.5 Thesis outline

This thesis deals with the investigation of propagation of electromagnetic waves around the human body, study of transmission characteristics in ON-Body to ON-Body scenario as well as ON-Body to OFF-Body scenario. The work also investigates the performance enhancement techniques of OFF-Body antennas.

The background information/knowledge including literature survey, methodologies, motivation, objective, research contributions are discussed in chapter-1. The chapter discusses on different types of wireless body area networks, ON-Body EM wave propagation and IN-Body EM wave propagation.

Chapter-2 is dedicated to the technique for gain enhancement in linearly and circularly polarized microstrip antenna using a hybrid substrate. The hybrid substrate used is a Rogers-Ferrite combination which blocks the surface waves to make them contribute to broadside radiation by constructive interference. The technique is applicable on linearly polarized and circularly polarized antennas. The increase in surface waves due to increased height of antenna can be reduced by using this technique.

Technique for gain enhancement in Dielectric resonator antennas using metasurface lens is discussed in Chapter-3. For this a dielectric resonator antenna operating at 4.5 GHz is designed using microstrip feeding. A metasurface lens operating at 4.5 GHz is also designed. The MSL is kept above DRA to enhance antenna gain. The positioning of the MSL above the DRA is discussed theoretically. This is realized and experimentally validated. This technique can be used on any type of antenna. The MSL can also be redesigned for various frequencies.

Analysis of creeping waves on a cylindrical phantom model is studied using simulation as well as experiments. Experiments on container with and without water are done and observations are interpreted. A twelve-cylinder body model is proposed which can be used for modelling rest as well as dynamic activity of humans. The sagittal plane and coronal plane of the body are discussed in the chapter. This model is used for the study of double arm swing activity in the sagittal plane as well as to analyze the transmission characteristics of a patch antenna integrated on a bag model. The EM wave propagation for ON-Body to ON-Body scenario as well as ON-Body to OFF-Body scenario is discussed in detail in Chapter-4.

In Chapter-5, a line of sight (LOS) scenario for ON-Body to OFF-Body scenario is simulated using a three layered phantom model with two similar UWB monopole antennas functioning in the bandwidth of 3-10 GHz to provide the time domain characterization of the channel. Experiments corresponding to the simulations are also carried out. Experiments are also done with near field, far field and various elevation angles. Experiments with Vivaldi antenna is also discussed in the chapter. Multiple experiments at different positions of the body gives an insight to the variation of the transmission characteristics of the antenna.

Chapter-6 summarizes the work of the present thesis and discusses the future scope of the work. The need of ON-body and OFF-Body analysis as well the importance of the study of different types and orientation are discussed in this chapter. The major contributions of the research work are summarized in this chapter.

Chapter 2

Ferrite Ring Loaded Microstrip Antenna

2.1 Introduction

Microstrip patch antennas(MSA) is one of the best choices for planar antenna technology due to many reasons including easy fabrication, cost effectiveness, and their simplicity to integrate with microwave circuits. These antennas are generally narrow-band, but different research groups have worked on enhancing the bandwidth of MSAs [40]-[43]. When two parallel slots are cut on the MSA to make it E-shaped MSA the impedance bandwidth increases substantially to 32.3% but at the cost of increased height to 10 mm using air as the substrate medium [44]. E-shaped MSA has been used for variety of applications by scientists from different research groups.

The authors in [45] reported that the use of transmission line model theory resulted in a 27.7% simulated impedance bandwidth when an air substrate of 10 mm height is used. In [46], a 13.86% impedance bandwidth is realized on FR4 substrate of height 3.2 mm. Researchers have also worked on realizing circular polarized patch antennas by using various methods such as , i) cutting small triangles from the two diagonally opposite corners of a nearly square MSA, ii) making diagonal slots on MSA; which provides effective CP polarization by generating equal/ nearly equal orthogonal currents in phase quadrature [47]-[50]. Another method to provide CP radiation is by using a hybrid coupler which enables dual feeding. But the use of hybrid coupler will make the antenna less compact due to the extra space requirement. An impedance bandwidth of 62.3% and axial ratio bandwidth of 61.73% is attained by authors in [51]. This is attained by designing the antenna on a 17 mm height thick substrate.

Ferrite is used for various applications in antenna. This is due to the fact that it has many advantages [52], such as, i) antenna miniaturization, ii) better radiation efficiency, iii)

bandwidth enhancement [52] and iv) aids in antenna frequency tuning [53]. These substrates are also reported for radar [54] as well as beam scanning [55] operations.

This chapter discusses the gain enhancement technique in MSA employing a hybrid substrate which includes Rogers 6002 and ferrite material. The technique is used for enhancing gain in linearly polarized and circularly polarized antennas. The base antennas used for the demonstration of the concept are linearly polarized E-shaped MSA and circularly polarized dual fed MSA. The E-shaped MSA using the 6.35 mm height hybrid substrate provides 18.63% impedance bandwidth. The dual fed CP MSA on hybrid substrate of 7.112 mm provides an axial ratio (AR) bandwidth of 24.09% and impedance bandwidth of 27.2%. The feed-network and ground plane are designed on a separate substrate and the ground is sandwiched between the top substrate on which antenna is printed and bottom substrate on which hybrid coupler is present. In both the antennas a ferrite ring embedded within the Rogers substrate aids in gain enhancement. These antennas can be used as OFF-Body antennas in ON-Body to OFF-Body communications. The antenna designed is fabricated on Rogers 6002 and analysis is done on the hybrid substrate, in CST microwave simulation software [56]. The Chapter is sectioned as follows. The design of E-shaped MSA with linear polarization operating in the S-Band is discussed in section 2.2. Section 2.3 details the design of Dual feed circularly polarized S-MSA . The gain enhancement technique using the combination of Rogers 6002 and ferrite material is for the antennas discussed in section 2.2 and section 2.3 is detailed in section 2.4. The chapter is concluded in Section 2.5.

2.2 Linearly polarized E-Shaped MSA

This sections details the design and implementation of an E-shaped antenna with linear polarization. The impedance, E-field and H-field pattern of the realized antenna is then compared with the simulation results.The Agilent PNA-X N5224A network analyzer is used to characterize the S_{11} of the antenna. The E-field and H-field pattern is measured using a broadband preamplifier (Agilent 83051 A) and a broadband dual ridged horn as the transmitting reference antenna in a fully calibrated far-field anechoic chamber.

2.2.1 Antenna Design

The proposed E-shaped MSA is illustrated in Fig. 2.1 (a). Rogers 6002 ($\varepsilon_r = 2.94$ and tan $\delta = 0.0012$) [57] is used to realize the antenna. The E-shaped MSA is design by embedding two parallel slots of equal dimensions along the dominant mode surface currents of traditional MSA. The wider bandwidth in E-shaped MSA is due to the additional resonance contributed

by the symmetrical parallel slots with the fundamental TM10-mode resonance. The increased bandwidth is achieved by varying the length, width and position of the slots together with the height of Rogers substrate. The height of 6.35 mm is attained by stacking two Rogers substrate of height 3.175 mm vertically. The Table I gives the detailed dimensions of the designed antenna. The image of the fabricated antenna prototype is as shown in Fig.2.1(b).

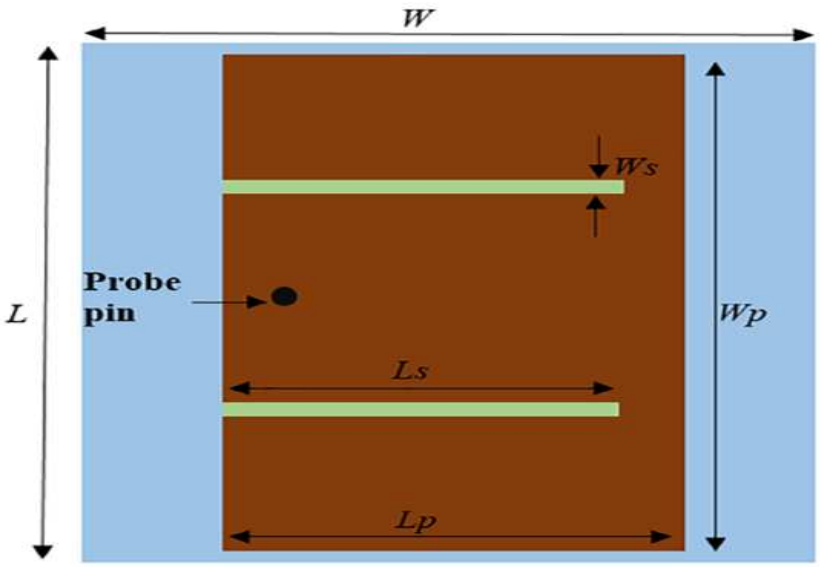

(a)

(b)

Fig. 2.1 (a) Schematic diagram of E-shaped patch antenna, (b) Fabricated image of E-shaped patch antenna.

Table 2.1 Design Parameters of E-shaped MSA on conventional substrate

Parameter	Dimension	Parameter	Dimension
L	70	W	70
L_s	27.55	L_p	32.6
W_p	67	W_s	0.5

2.2.2 Results and Discussion

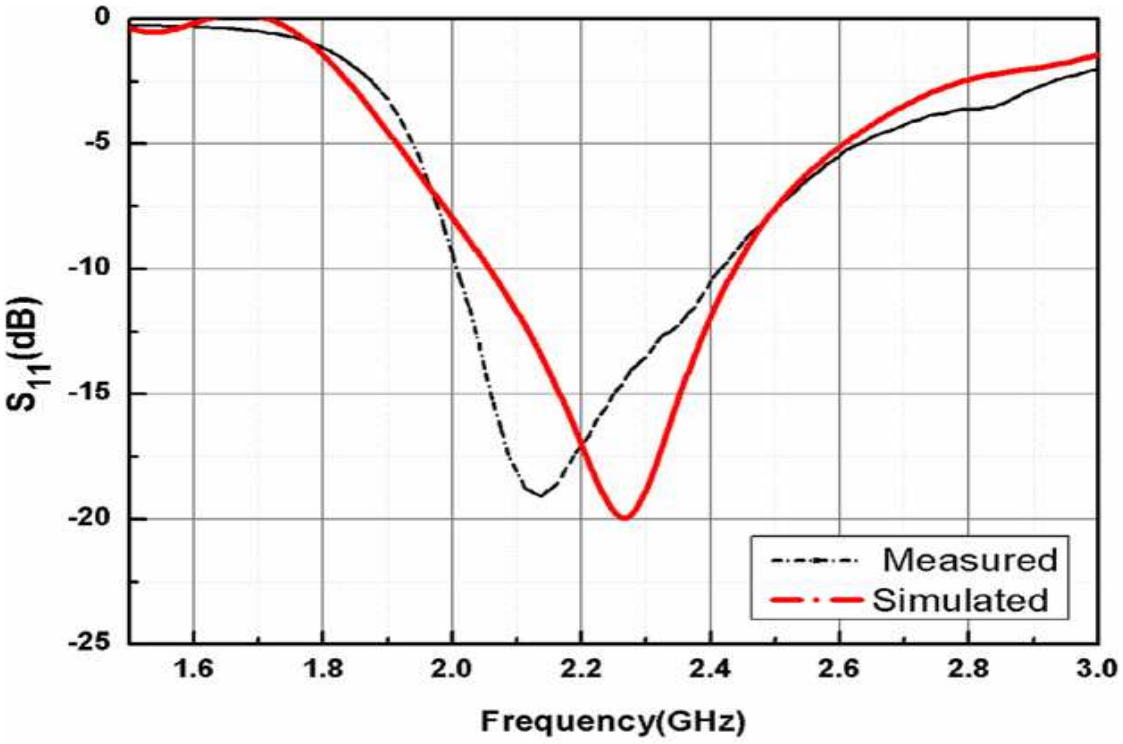

Fig. 2.2 Simulated and Measured S_{11} of E-shaped patch antenna

The E-shaped MSA which is linearly polarized is designed and analyzed using CST microwave design suite [56]. Figure 2.2 shows the simulated as well as measured impedance characteristics of the antenna. The plot reveals that the antenna covers a bandwidth ranging from 2.05 GHz to 2.43 GHz (17.27%) in the simulation and 2.01 GHz to 2.42 GHz(18.63%) in the measurement.

The simulated and measured E-plane and H-plane radiation patterns at 2.05 GHz is shown in Fig. 2.3(a) and Fig.2.3(b) respectively. The E-plane and H-plane pattern reveals a 3-dB beam-width of 118° and 73° respectively. The measured results exhibits reasonably good

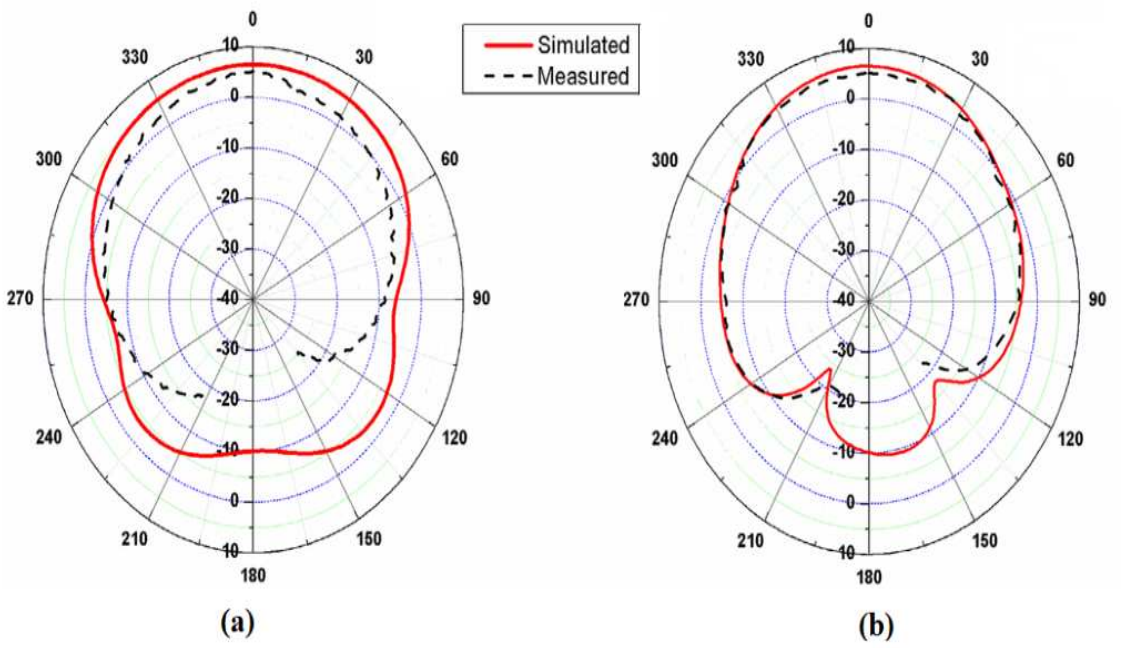

Fig. 2.3 Simulated and Measured radiation pattern: (a) E-plane (b) H-plane

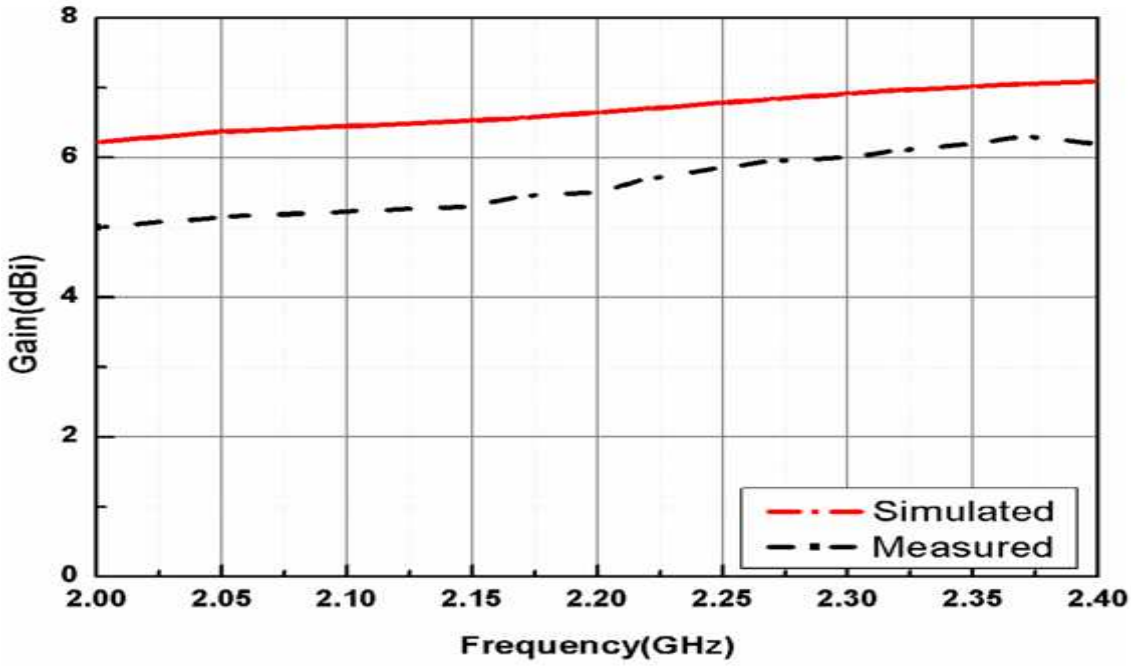

Fig. 2.4 Simulated and measured Gain of E-shaped patch antenna using conventional substrate.

agreement with the simulation. The maximum realized gain is shown in Fig.2.4. The pattern shows that antenna gain varies between 5 dBi and 6.1 dBi in the designed region.

2.3 Circularly polarized Dual-fed Square MSA

To attain circular polarization in an antenna, two equal or nearly equal orthogonal modes has o be excited in phase quadrature. Various techniques of CP generation include: i) dual-feeding via 90° hybrid coupler ii) trimming small triangles diagonally opposite to each other on a square/nearly-square patch, iii) diagonal/cross slots on the radiator and iv) combinations of (i)-(iii). Though all these techniques has attracted the research community, in this work a CP S-MSA with with hybrid coupler is used.

2.3.1 Design of Circularly Polarized S-MSA

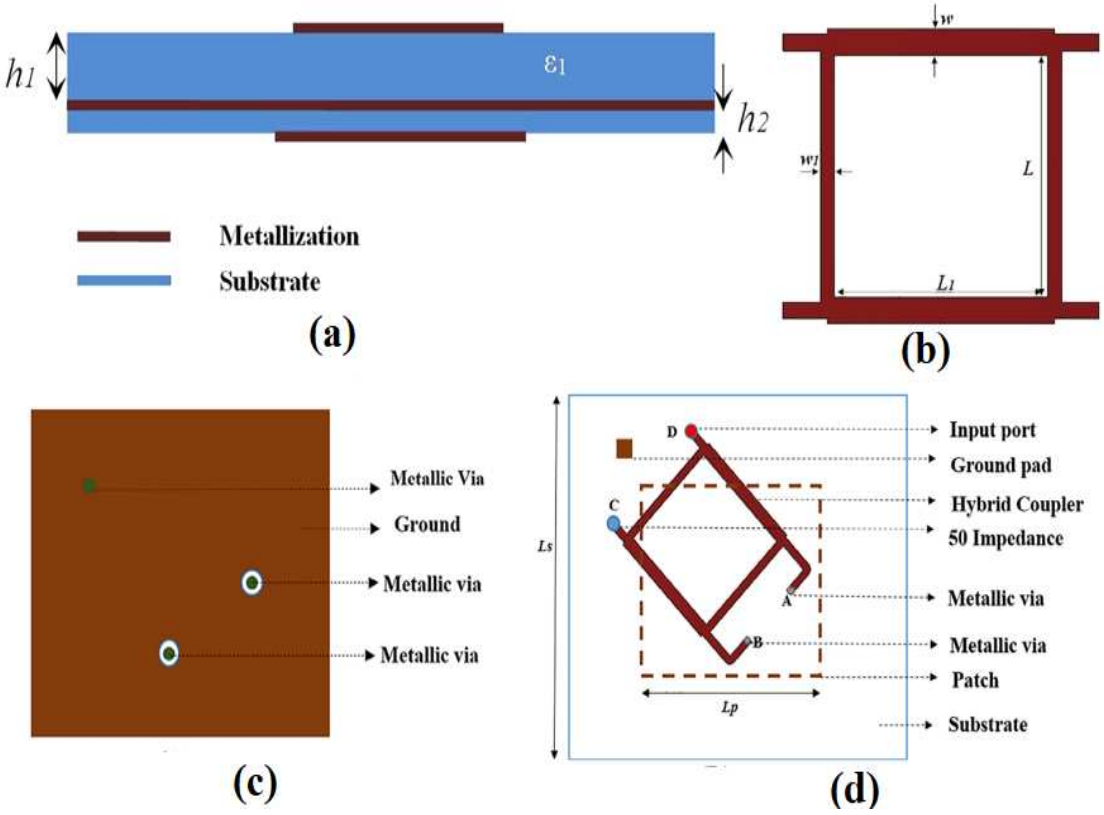

Fig. 2.5 Schematic diagram of Dual feed CP antenna: (a) 3D structure, (b) Hybrid coupler, (c) Ground and (d) Top view

The schematic of the proposed circularly polarized S-MSA is as shown in Fig.2.5. The antenna is designed on a Rogers 6002 substrate. The radiator is square shaped with a size of Lp × Lp printed on the top substrate with height h_1. Another substrate of size h_2 is placed vertically below the antenna substrate to embed hybrid coupler. As seen in Fig.2.5(a), the

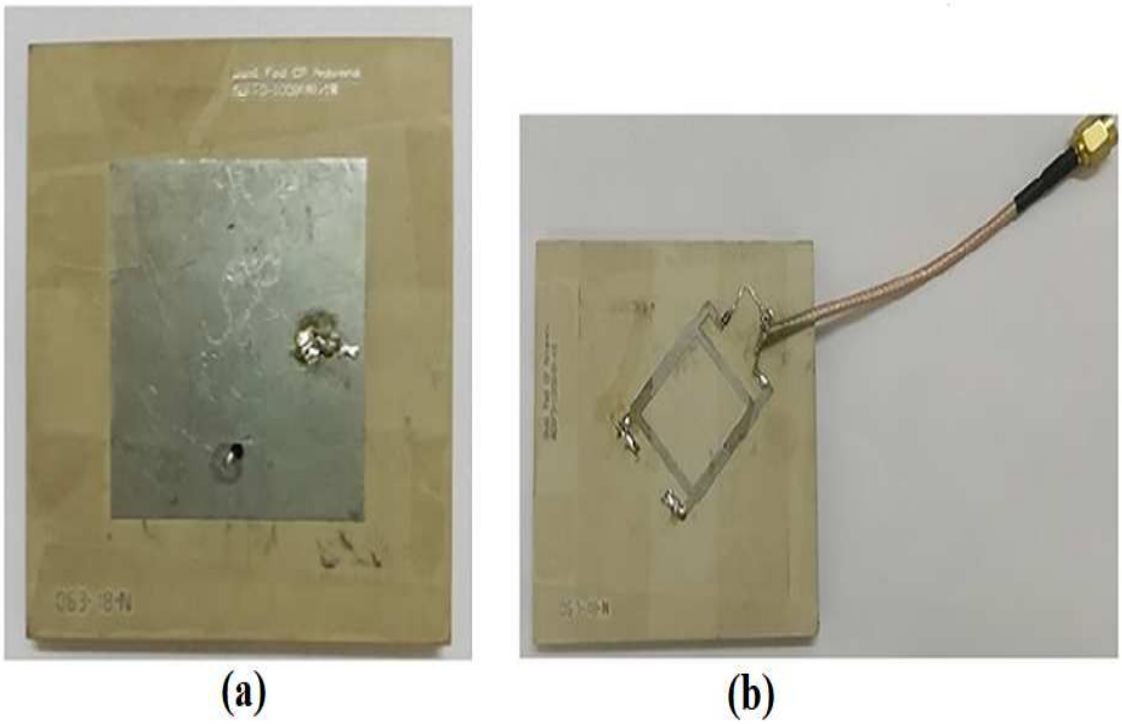

Fig. 2.6 Image of fabricated antenna (a) Top view (b) Bottom

ground plane of the antenna is sandwiched between substrate for radiator and substrate for hybrid coupler. Figure 2.5(b) shows the feed points A and B on the hybrid coupler positioned 45° from the origin. Vertical vias/probes are used to connect from the coupler to the raditor.

The LHCP/RHCP signal is generated by exciting the antenna input terminals. A 50-ohm connector fastened at any of the input terminals of the 90° coupler generates the desired signal. The coupler position and thereby points A, B, C and D in Fig.2.5(d) are optimized to attain impedance matching and the generation of two orthogonal modes. Two circular shaped etchings are made on the ground plane so that the probe pins/vias are not shorted due to the sandwiched ground plane in between radiator and hybrid coupler, as shown in Fig. 2.5(d). To facilitate the easy connection of 50 ohm connector to the ground plane for launching the signal, a ground pad of 1 mm × 1 mm is designed near hybrid couple.The ground pad and main ground plane are connected via a shorting pin. The overall size of the proposed antenna is $L_s \times L_s \times (h_1 + h_2)$. The antenna is suitable for LHCP/RHCP application as two feed ports are present. The dimensions of the dual feed CP antenna, are detailed in the Table 2.2. The images of the fabricated antenna are as shown in Figure 2.6(a) and (b).

Table 2.2 Design Parameters of S-MSA on conventional substrate

Parameter	Dimension	Parameter	Dimension
L_s	60	L	17.93
L_p	29.20	L_1	19.51
h_1	6.35	w	2.26
h_2	0.762	w_1	1.66

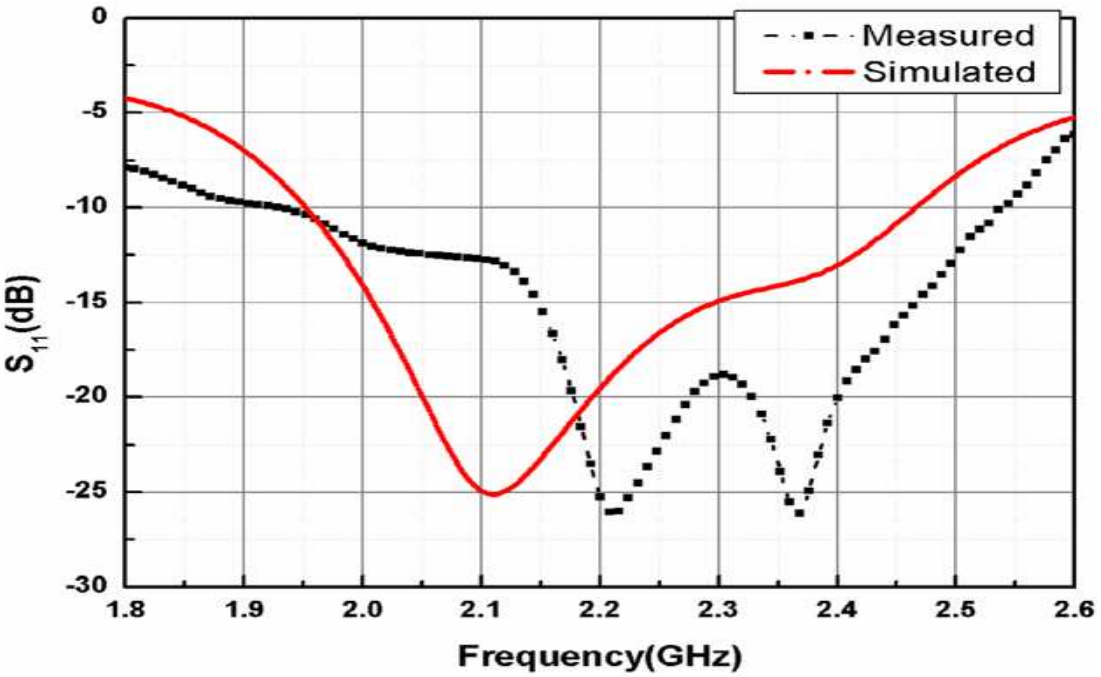

Fig. 2.7 Simulated and measured S_{11} of dual feed CP antenna without ferrite.

2.3.2 Results and Discussion

The simulated and measured impedance characteristics of the CP S-MSA is shown in Fig. 2.7. As we can see from the plot, the CP S-MSA produces a 23.18% impedance bandwidth in simulation, which ranges from 1.95 GHz to 2.46 GHz, and a 27.27% measured impedance bandwidth, ranging from 1.95 GHz to 2.55 GHz. The antennas exhibits 3-dB beam width of 89.10° for RHCP excitation and 85.50° for LHCP excitation as seen in Fig. 2.8(a) and (b).

The axial ratio (AR) vs. elevation angle of CP S-MSA is shown in Fig.2.9. The plot shows the AR in phi=0° and phi=90° plane at 2.14 GHz. A 3-dB AR beamwidth of 160° is exhibited by the antenna in both the planes. Figure 2.10 shows the AR vs. frequency plot, which shows that antenna gives circular polarization (AR$<$3 dB) ranging from 1.94 GHz-2.47 GHz exhibiting an AR of 0.2414 dB at 2.2 GHz. Measured AR vs. frequency is

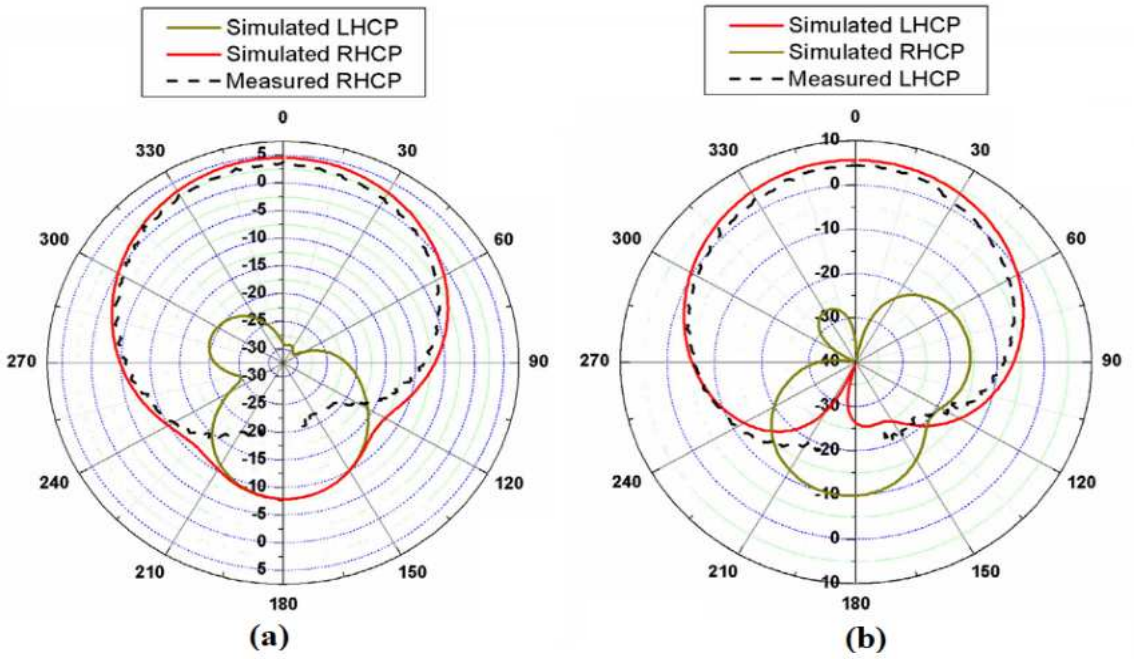

Fig. 2.8 Simulated and measured E-plane radiation pattern at 2.15 GHz: (a) Feed point C, (b) Feed point D.

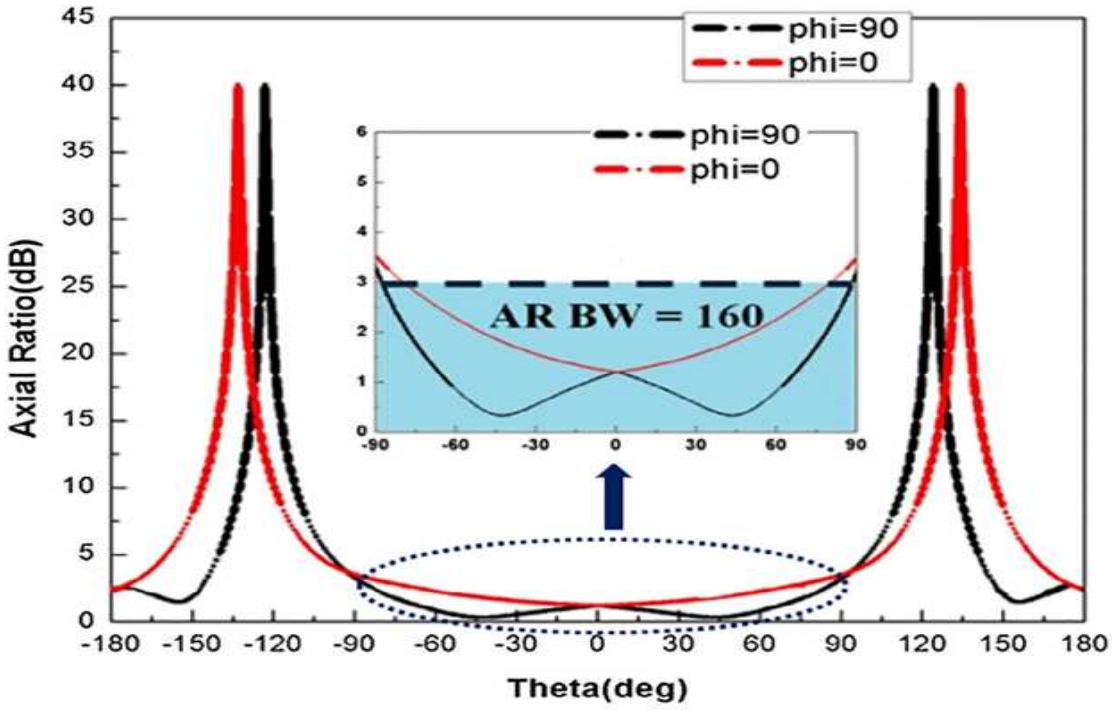

Fig. 2.9 Axial-ratio vs. theta variation at phi=90° and phi=0° at f= 2.14GHz

in good correlation with the simulated plot. The realized gain of the proposed antenna is shown in Fig.2.11. The simulation and measurements shows good matching. The antenna parameters for both E-shaped MSA and CP S-MSA is summarized in TABLE 2.3.

Table 2.3 Comparative Look of simulated and measured results of E-shaped and S-MSA on Conventional Substrate

		E-shaped MSA	S-MSA
Impedance BW%	Simulated	17.27	23.18
	Measured	18.63	27.27
Maximum Gain	Simulated	7	6.5
	Measured	6.1	5.5
Axial Ratio BW%	Simulated	NA	24.09
	Measured	NA	22.72

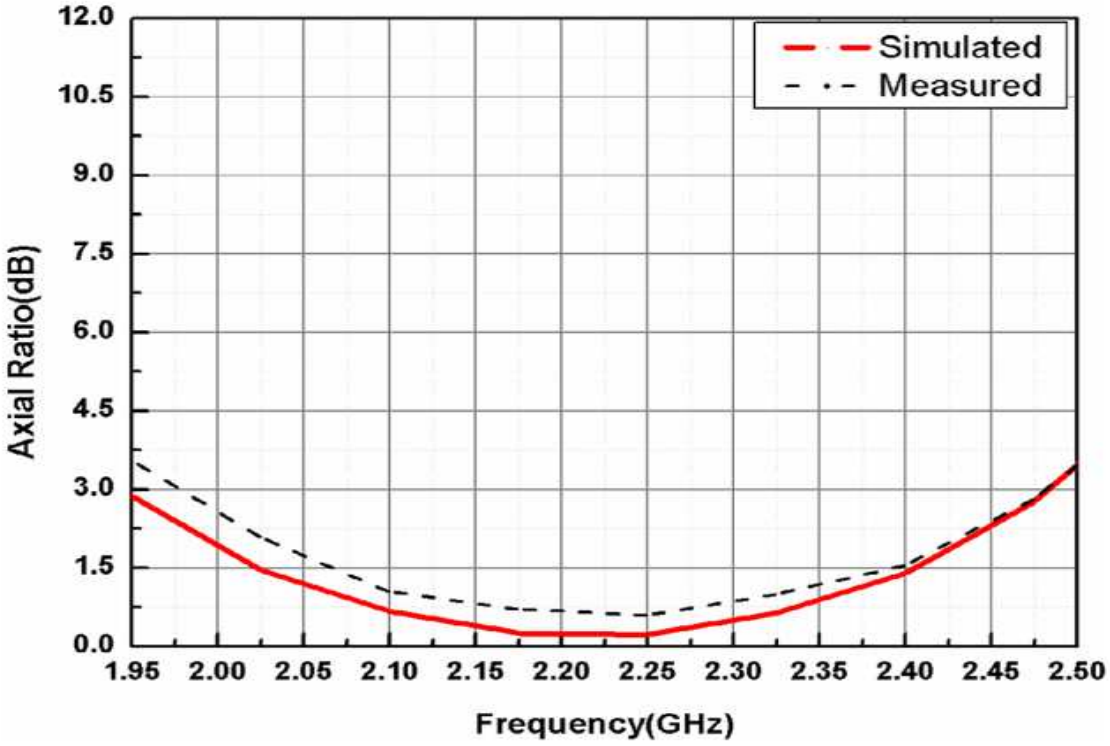

Fig. 2.10 Simulated and measured axial ratio of Dual feed CP antenna.

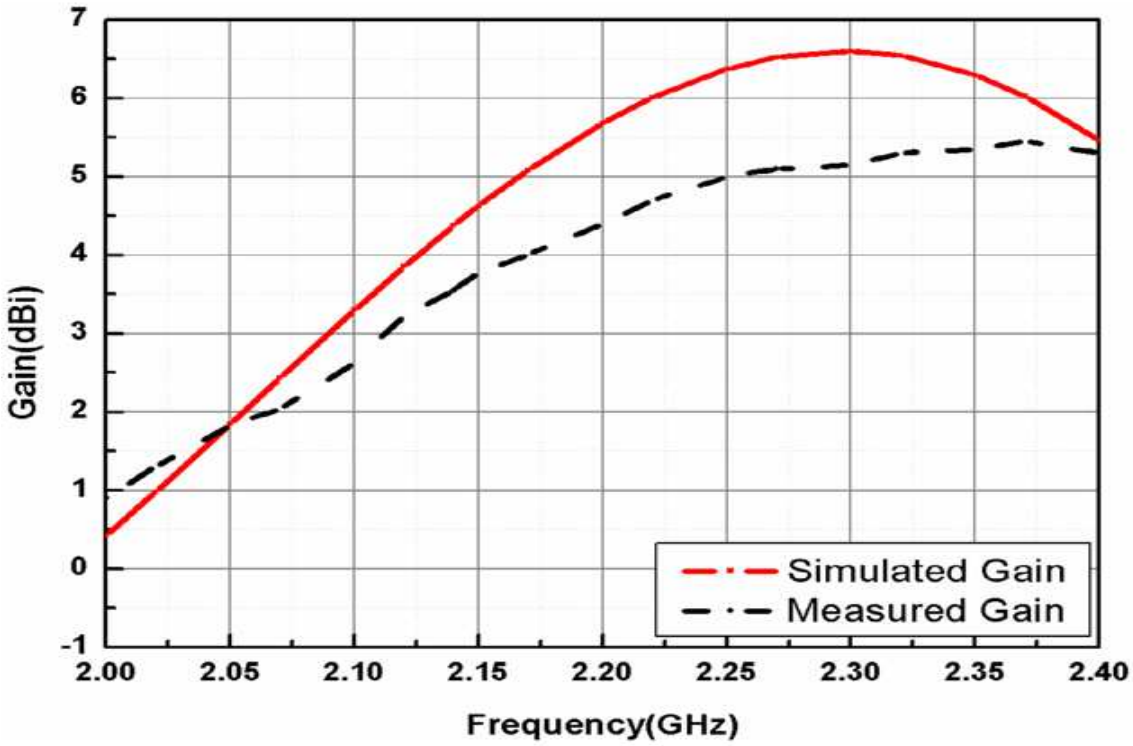

Fig. 2.11 Simulated and Measured gain of Dual feed CP antenna

2.4 Enhancement of Antenna Gain with Hybrid Substrate

The antennas considered in previous section, is designed and realized with thick substrate in vertical configuration. This stacked configuration of the antenna reduces the efficiency of the antenna. This is due to the losses created by the surface waves propagating along antenna substrate which are not in the direction of main beam of the antenna. If the antenna design is modified to direct this surface wave in the main beam direction losses can be reduced, thereby increasing the gain of the antenna [58]. This can be attained by various methods including, use of hybrid substrates, electromagnetic band gap (EBG) structures, photonic band gap (PBG) structures, AMC structures etc. [58]-[61]. Some of these structures increases the design/fabrication complexity of the antenna. Following a systematic technique introduced by Balanis et. al. [58], ferrite rings are embedded in the substrates of E-shaped MSA and S-MSA [62]-[66]. This is done by making grooves in the conventional Rogers 6002 substrate mechanically and filling with the ferrite ring of proper dimension. This results in a well-designed hybrid substrate with Rogers 6002-ferrite-Rogers 6002 composition. The same surface waves which are the reason for losses in the antenna designed on thicker conventional substrate when designed using hybrid substrate enhances the gain of the antenna. This is because the excited surface waves strike on two interfaces, namely: i. dielectric-ferrite and

ii. ferrite-dielectric. The energy is partially reflected as well as transmitted across the two interfaces. The dimensions of the ferrite ring, its position in the conventional substrate, relative permittivity and permeability are factors which determines the enhanced gain of the antenna. The reflected and incident waves interfere constructively contributing to the main beam direction generating enhanced gain.

2.4.1 Design of Hybrid Substrate

On the antennas with conventional substrate, discussed in section 1 and 2, circular groove is made around the radiating patch. The ferrite ring with thickness h which is same as that of of the Rogers 6002 substrate, inner and outer radius d_i and d_o respectively is introduced into this groove. The design of the antenna substrate using Rogers 6002 and ferrite results in a hybrid substrate which has interfaces: i. dielectric-ferrite interface which is positioned at d_i and ii. ferrite-dielectric interface positioned d_o from the center of the antenna radiator. The design parameters of hybrid substrate for E-shaped MSA and S-MSA are given in Table 2.4 and 2.5 respectively (remaining parameters are as given in Table 2.1 and 2.2 respectively).

Table 2.4 Design Parameters of E-shaped MSA on hybrid substrate

Parameter	Dimension	Parameter	Dimension
L	160	W	160
d_i	40	d_o	65

Table 2.5 Design Parameters of S-MSA on hybrid substrate

Parameter	Dimension	Parameter	Dimension
L_s	150	d_i	35
d_o	60		

The enhancement of gain using hybrid substrate is demonstrated for both LP and CP antennas discussed in section 2.2 and 2.3. The inner diameter of the embedded circular ring of ferrite material in E-shaped MSA and S-MSA should be greater than one fourth of λ, where λ relates to the dominant mode resonant wavelength. The E-shaped MSA and S-MSA using hybrid substrate are designed and analysis is done in CST microwave studio. The size of the antenna using Rogers 6002 discussed in previous sections is increased and analyzed initially. No variations in gain was observed when the size of the conventional substrate alone was increased and but when a combination of dielectric and ferrite substrate is used

making it a hybrid substrate, the gain of the antenna increased. Fig.2.12 depicts the top view of the redesigned E-Shaped MSA and S-MSA.

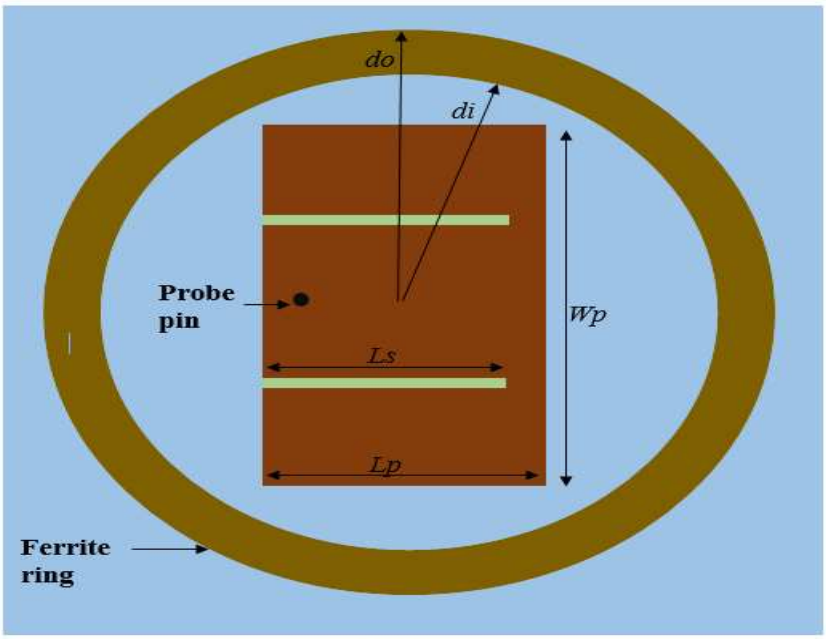

(a)

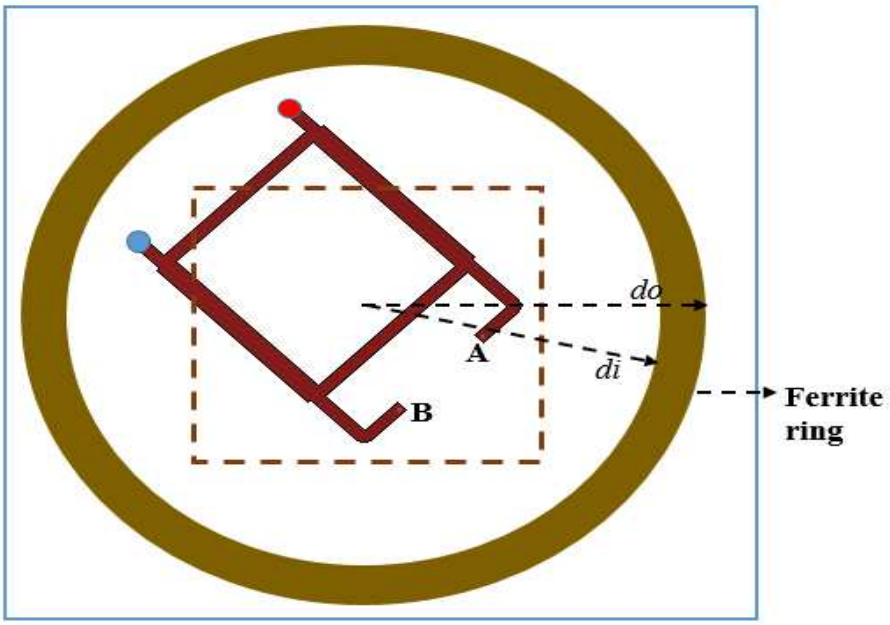

(b)

Fig. 2.12 Schematic diagram of:(a) E-shaped patch antenna, and (b) Dual feed CP antenna with hybrid substrate.

2.4.2 Results and Discussions of linearly polarized antenna with ferrite

The simulated impedance characteristics of the E-shaped MSA loaded with ferrite ring for its varying widths (W_{FR} unit in mm) is shown in Fig. 2.13(a). It can be clearly noted that the impedance bandwidth shifts for different values of W_{FR}. The plots in Fig. 2.13(b) depicts the maximum realized gain when width W_{FR} = (d_o- d_i) of the ferrite ring is fixed and its positions is changed. The parameter d_i is fixed as 40 mm and the width W_{FR} is varied and maximum realized gain is plotted as shown in Fig. 2.13(c). The systematic parametric studies as seen from Fig.2.13, reveals that a value of W_{FR} = 25 mm and d_i = 40 mm is considered best for the required gain profile and impedance bandwidth. In Fig.2.14 a comparison of the the S_{11} the of E-shaped MSA with conventional as well as hybrid substrates is studied for W_{FR} = 25 mm. As exhibited in Fig. 2.14, proposed antenna with hybrid substrate exhibits a simulated impedance bandwidth ranging from 2.08 GHz to 2.49 GHz. A notable gain enhancement is obtained in the frequency range from 2 GHz to 2.4 GHz for the antenna designed using hybrid substrate compared to the one on conventional substrate as seen in Fig.2.15. The simulated 3-D radiation pattern in Fig. 2.16 shows that, the E-shaped MSA on dielectric-ferrite substrate generates a maximum gain enhancement of 4.46 dBi at of 2.05 GHz compared to the E-shaped MSA on conventional substrate with no embedded ferrite ring.

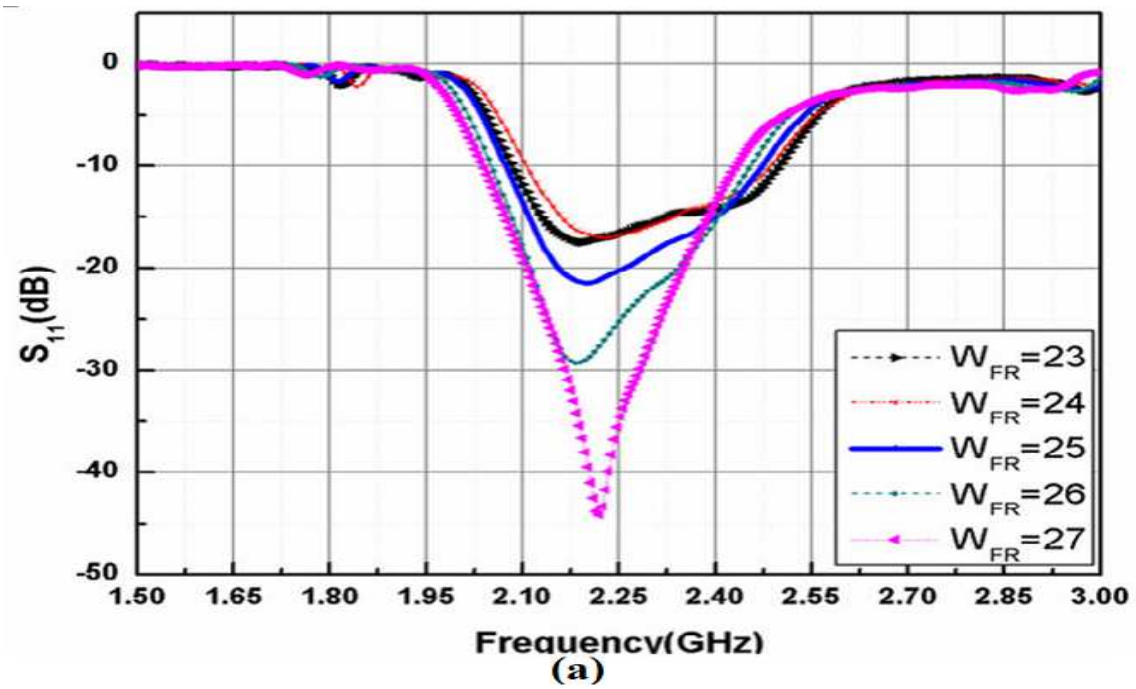

(a)

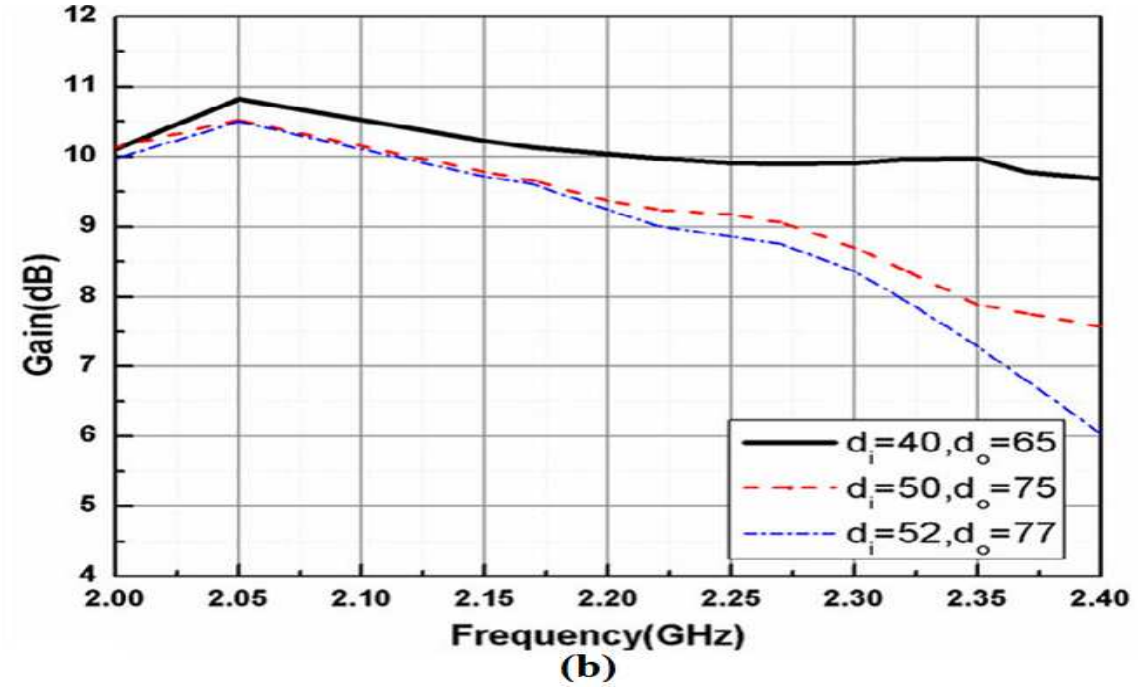

(b)

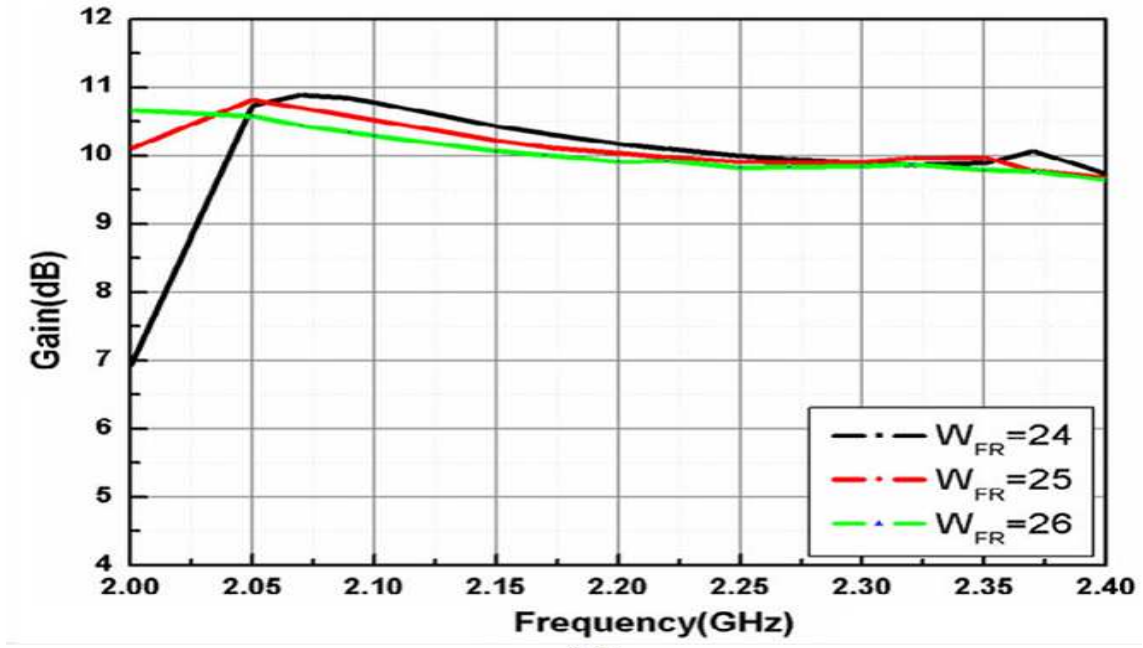

(c)

Fig. 2.13 Parametric studies of ferrite ring loaded E-shaped patch antenna. (a) Simulated S_{11} for varying W_{FR}, (b) Maximum gain for varying positions of the ring with fixed $W_{FR} = d_o - d_i = 25$ and (c) Maximum gain for varying WFR of the ring with fixed d_i =40 (W_{FR}, d_o and d_i are in mm).

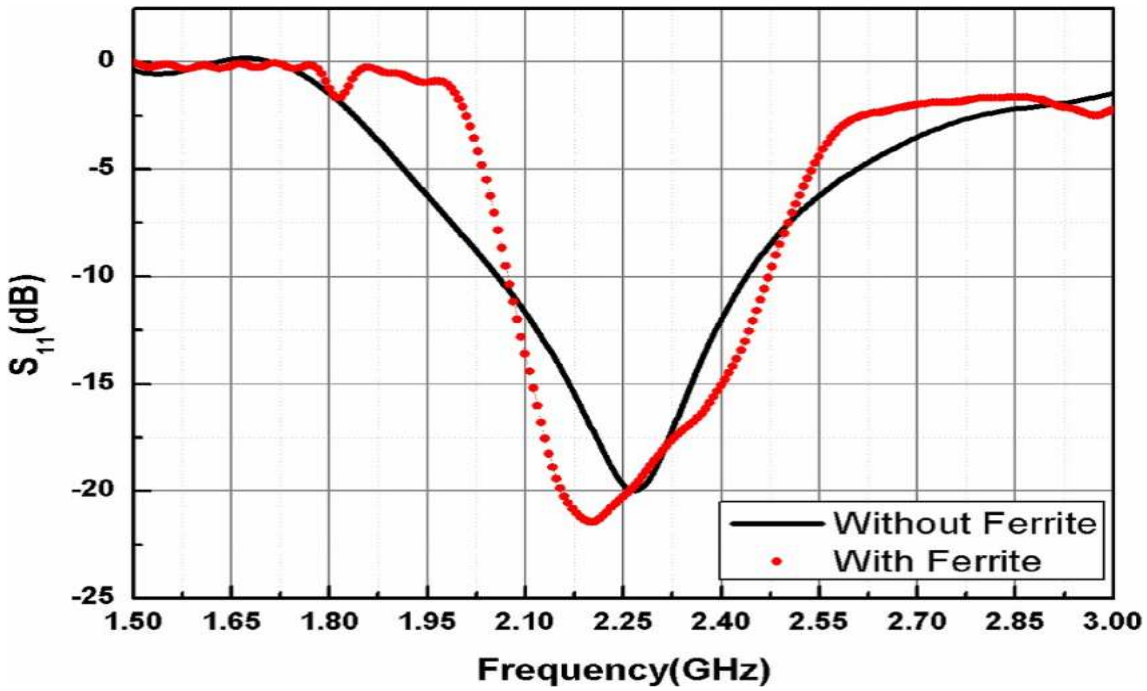

Fig. 2.14 Simulated S_{11} of E-shaped patch antenna with and without ferrite ring (W_{FR} = 25 mm and di = 40 mm).

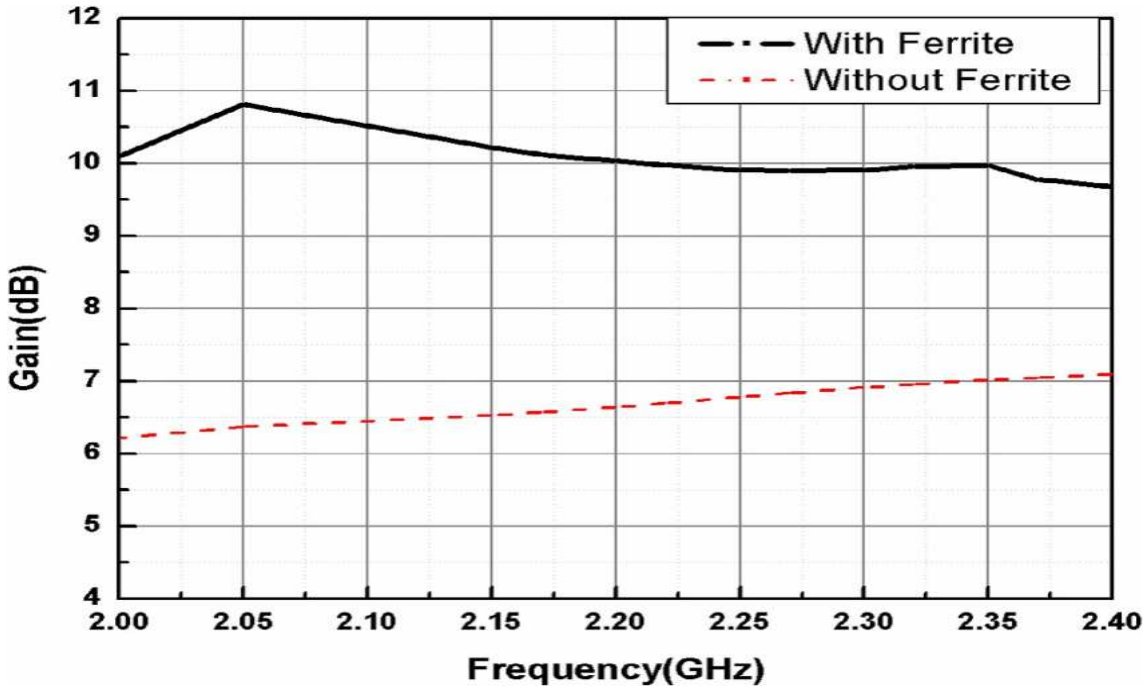

Fig. 2.15 Simulated gain of E-shaped patch antenna with and without ferrite (W_{FR} = 25 mm and d_i=40 mm).

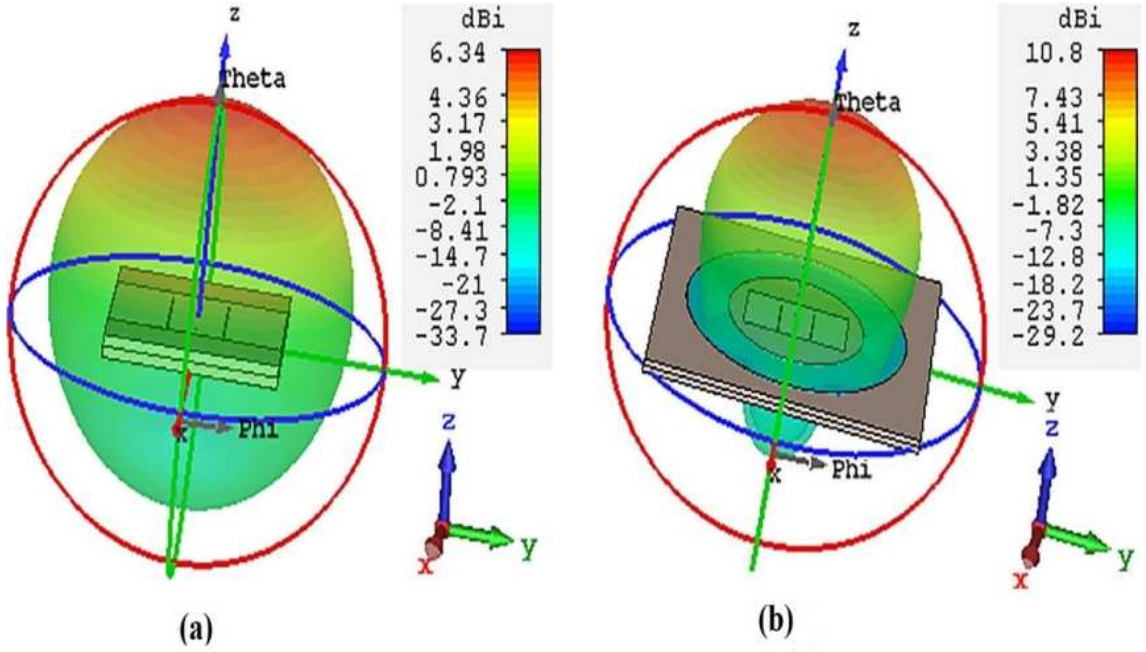

Fig. 2.16 Simulated 3-D gain pattern of E shaped patch antenna at 2.05 GHz (a) without ferrite (b) with ferrite ring (W_{FR} = 25 mm and d_i = 40 mm).

2.4.3 Results and Discussion of circularly polarized antenna with ferrite

A ferrite ring with its parameters optimized in CST Microwave studio is embedded around the radiating patch of S-MSA like E-shaped MSA. The simulated impedance bandwidth for variations in W_{FR} for S-MSA is shown in Fig. 2.17. Figure 2.18 and 2.19 exhibits the simulated impedance bandwidth as well as maximum realized gain of S-MSA with and without ferrite ring of W_{FR} =25 mm. As observed from these plots, the impedance bandwidth with and without the ferrite ring are almost similar but the gain is enhanced by 3.61 dBi in case of S-MSA with ferrite ring embedded in the conventional substrate. The enhanced gain from 2 GHz to 2.4 GHz as seen in Fig.2.19, can be used for S-band operations. A slight reduction in the gain of the S-MSA on hybrid substrate at higher frequencies is attributed to the inevitable non-optimum placing of the ferrite ring. The distance of ferrite ring from the central radiator gets highly detuned when frequency increases thereby reducing the gain slightly.

The circular polarization is conserved from 1.97 GHz to 2.5 GHz as seen from Axial ratio vs.Frequency plot exhibited in Fig.2.20. Figure 2.21 (a) exhibits the radiation pattern in the E-plane of the S-MSA with ferrite ring, which shows a 57.4° 3-dB beam width at 2.15 GHz for RHCP excitation. As seen in Fig.2.21 (b), for LHCP excitation, the same antenna generates a 3-dB beam width of 51.3° at 2.15 GHz . It is very clear that when these patterns

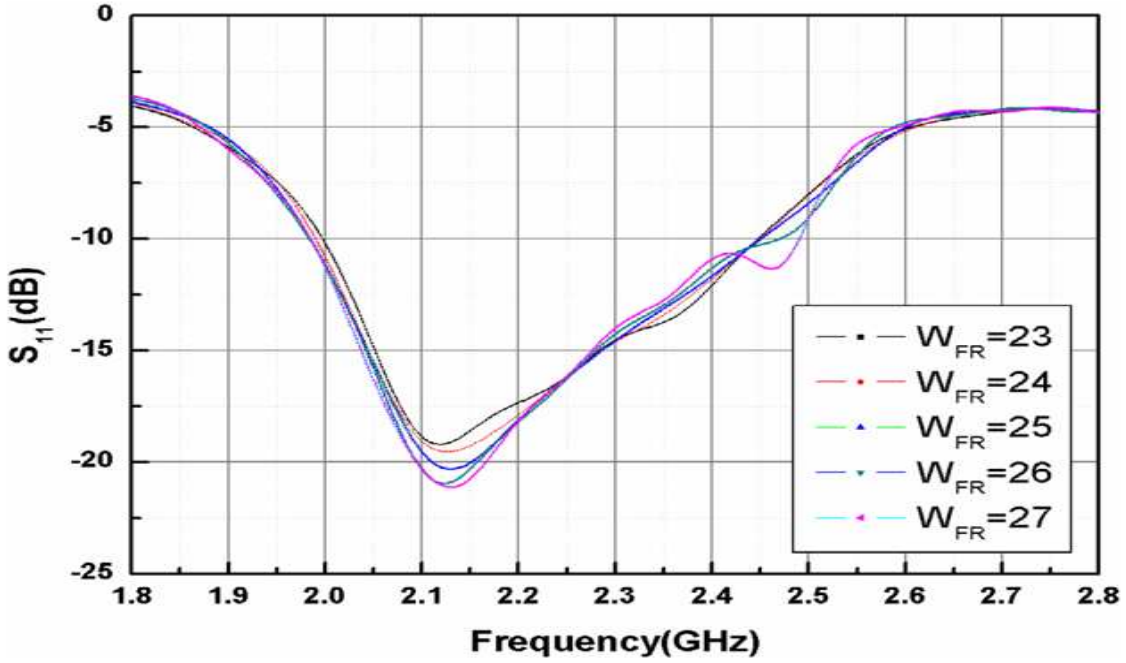

Fig. 2.17 Simulated S_{11} of Dual Fed CP antenna by varying W_{FR}

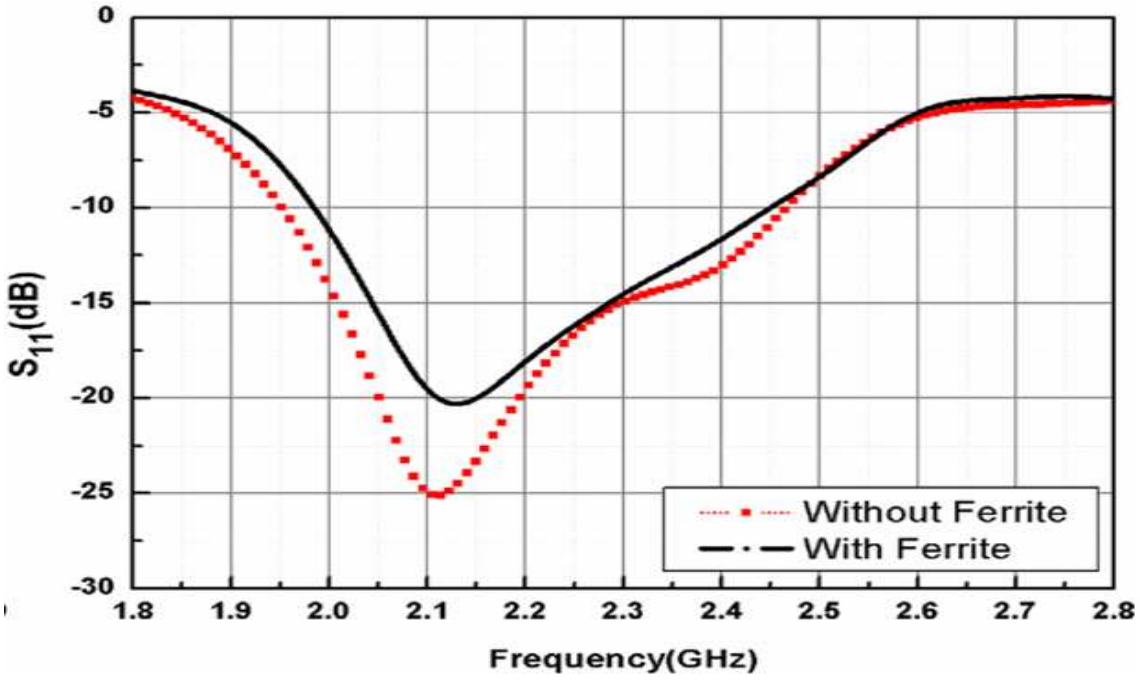

Fig. 2.18 Simulated S_{11} of Dual feed CP antenna with and without ferrite.

are compared with that of the antenna on conventional substrate a much directional pattern is generated while using the hybrid structure.

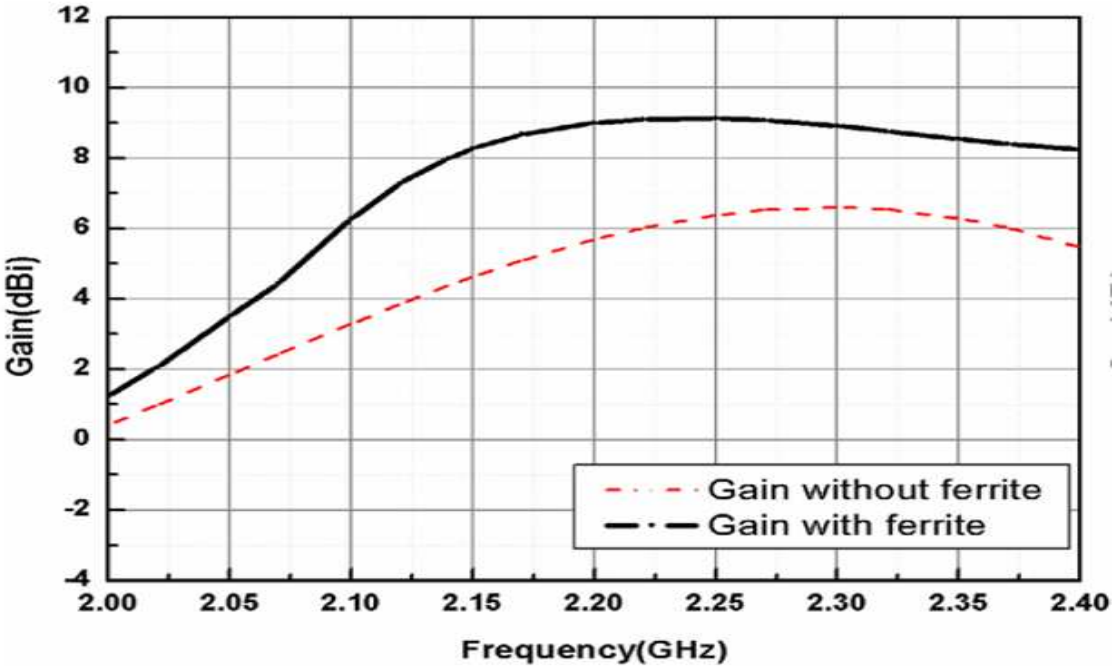

Fig. 2.19 Simulated Gain on Dual feed CP antenna with and without ferrite.

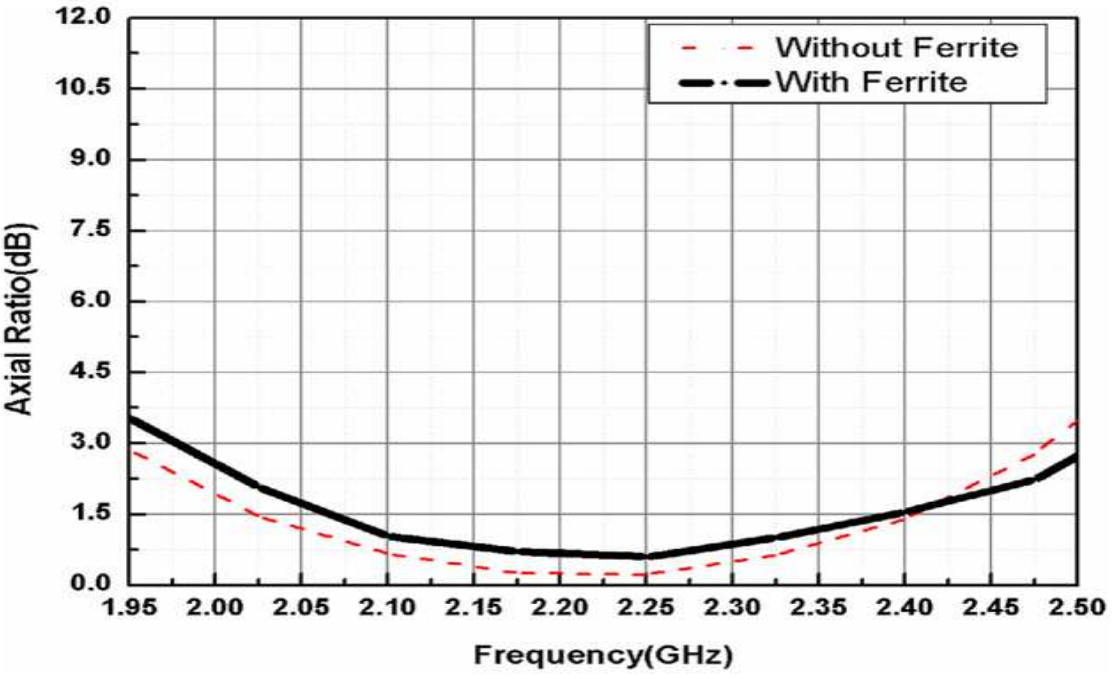

Fig. 2.20 Simulated axial ratio on Dual feed CP antenna with and without ferrite.

The 3-D radiation pattern of the S-MSA on conventional and hybrid substrate is shown in Fig.2.22. The plot clearly reveals a gain enhancement of 3.61 dBi for the antenna on hybrid

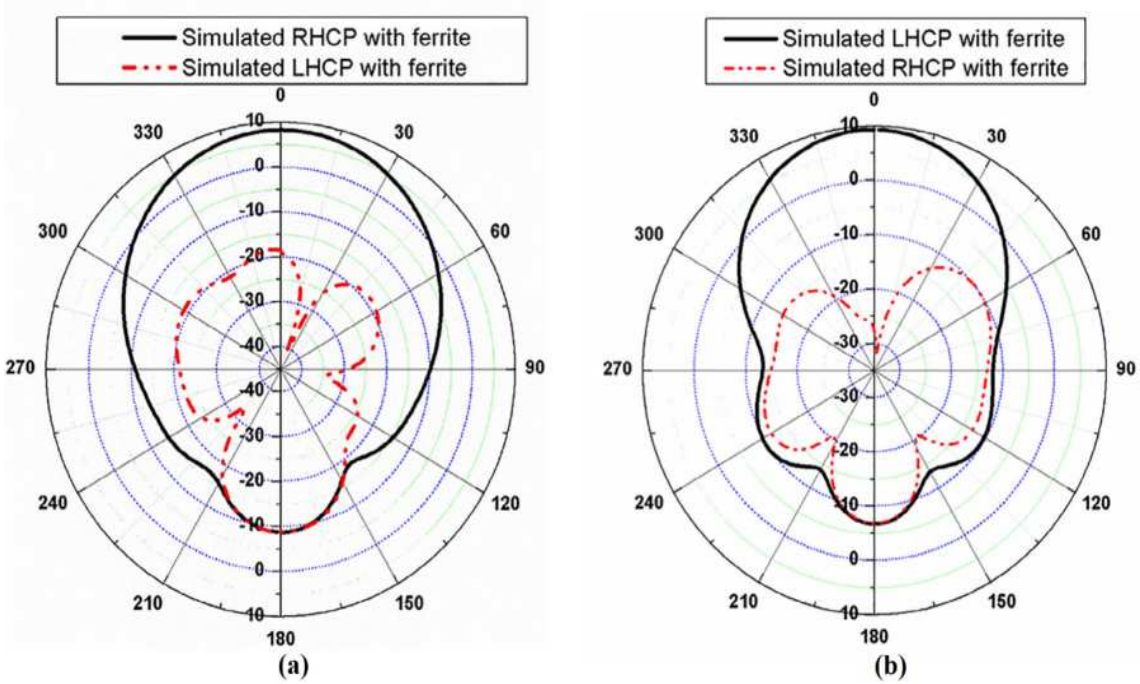

Fig. 2.21 E-plane radiation pattern of dual feed CP antenna at 2.15 GHz: (a) Feed point C, (b) Feed point D.

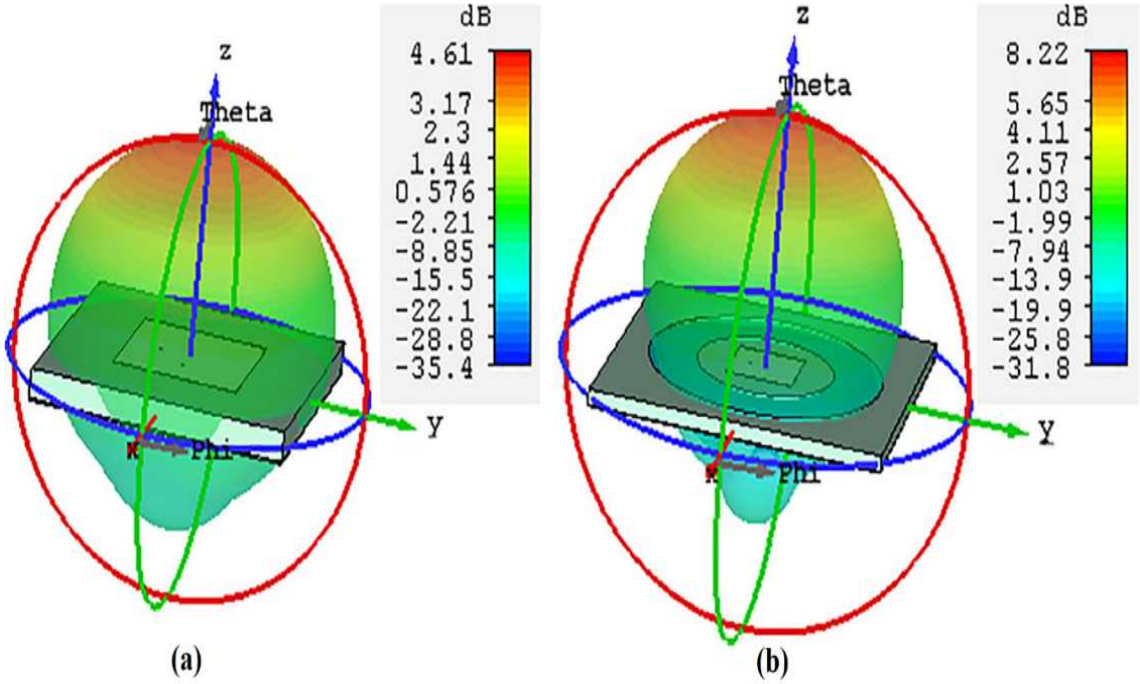

Fig. 2.22 Simulated 3-D gain pattern of Dual fed CP patch antenna at 2.15 GHz: (a) without ferrite, (b) with ferrite.

substrate. Table 2.6 details a comparison of different antenna parameters of the E-shaped

Table 2.6 Performance comparison of E-shaped MSA and S-MSA on conventional and hybrid substrate

	E-shaped MSA		S-MSA	
	Conventional	Hybrid	Conventional	Hybrid
Simulated Impedance BW%	17.27	17.9	23.18	21.36
Maximum Gain (dBi)	7	10.8	6.5	8.22
Simulated Axial Ratio BW%	NA	NA	24.09	24.09

MSA and the S-MSA using conventional as well as hybrid substrate, which reveals a notable gain improvement for hybrid-substrate design for both the antennas with all other parameters of the antenna remaining the same.

2.5 Conclusion

A new method for gain improvement using ferrite rings in linearly and circularly polarized wideband MSAs using a hybrid substrate is discussed in this chapter. The E-shaped MSA and S-MSA on hybrid substrate radiates in the broadside direction with an increased maximum gain of 10.8 dBi at 2.05 GHz and 8.22 dBi at 2.15 GHz for E-shaped MSA and S-MSA respectively. The technique discussed in this chapter is independent of the geometry of antenna and can be used on other configurations as well. The technique makes use of the increased surface wave existing in the antenna due to thick substrate by converting it into broadside radiation. This technique of using hybrid substrate can be used to reduce mutual coupling effects in microstrip array applications.

Chapter 3

Metasurface Lens for Gain Enhancement

Higher gain, improved bandwidth and reconfigurable features are the necessities of present era wireless communication systems. Dielectric antennas are formed with dielectric resonators(DR) and Dielectric antennas (DRA) exhibits various interesting and appealing features, such as, higher impedance bandwidth, reduced size and good radiation efficiency. These antenna, popularly known as DRA, can be excited by various techniques [67], [68]. One important feature of Dielectric Resonator Antenna (DRA) is the absence of surface waves [69]. This feature makes DRA a more suitable candidate over microstrip patch antennas for some applications. The shape, size and ε_r are the parameters that determines the fundamental frequency of the narrow band DRA [68]. Over the past years many research groups have reported different structures of DRA including T-shaped, L-shaped, U- shaped, E-shaped, triangular etc. which uses different feeding methods[69]. Various mechanisms used for enhancing the gain such as, the use of superstrate [13], electromagnetic band gap (EBG) structures [14], formation of array antenna [15] are reported by various research groups [16]-[18],[70]-[72],[74]. It is found that DRA which operates with higher order modes provides improved gain [15]. Grooves are made on the DRA to get an enhanced gain in [16]. In [17], gain is improved using mushroom like structures. EBG is used in [18] for enhancing the gain of the antenna. With the introduction of anisotropic DRA, researchers in [34] attained a gain of 8.4 dBi. The researchers in [19] introduced FSS to improve antenna gain. Short horn is used in [35] to enhance the gain. On-chip CMOS feeding mechanism is used in [36] while a small DRA along with another main DRA [37] generates enhanced gain. The metamaterial converging lens as superstrate is used in [38], to increase the gain of a cylindrical DRA. An electromagnetic simulation software optimizes the distance between the metamaterial and ground plane in [38].

In this chapter, a rectangular DRA loaded with metasurface (MS) lens is discussed. This MS lens loaded DRA with improved gain has applications in various fronts: i. it can be

utilized in high-gain MIMO (Multiple Input Multiple Output) antenna as a unit element, ii. as different operators in Japan and many other nations has allocated frequency ranging form 4.5 GHz to 4.9 GHz for 5G , array of this antenna can be used in 5G base station, iii. unmanned aerial vehicle (UAV) (4.4-4.5 GHz) and iv) military applications. The design of MS lens and antenna on which MS lens is integrated are not mutually dependent, which allows this concept of gain enhancement to be exploited in other antenna configurations generating bore-sight maximum radiation. The chapter also details the technique used to fix the height of the MS lens above the dielectric resonator antenna.

3.1 Design of the Antenna

3.1.1 The Dielectric Resonator Antenna

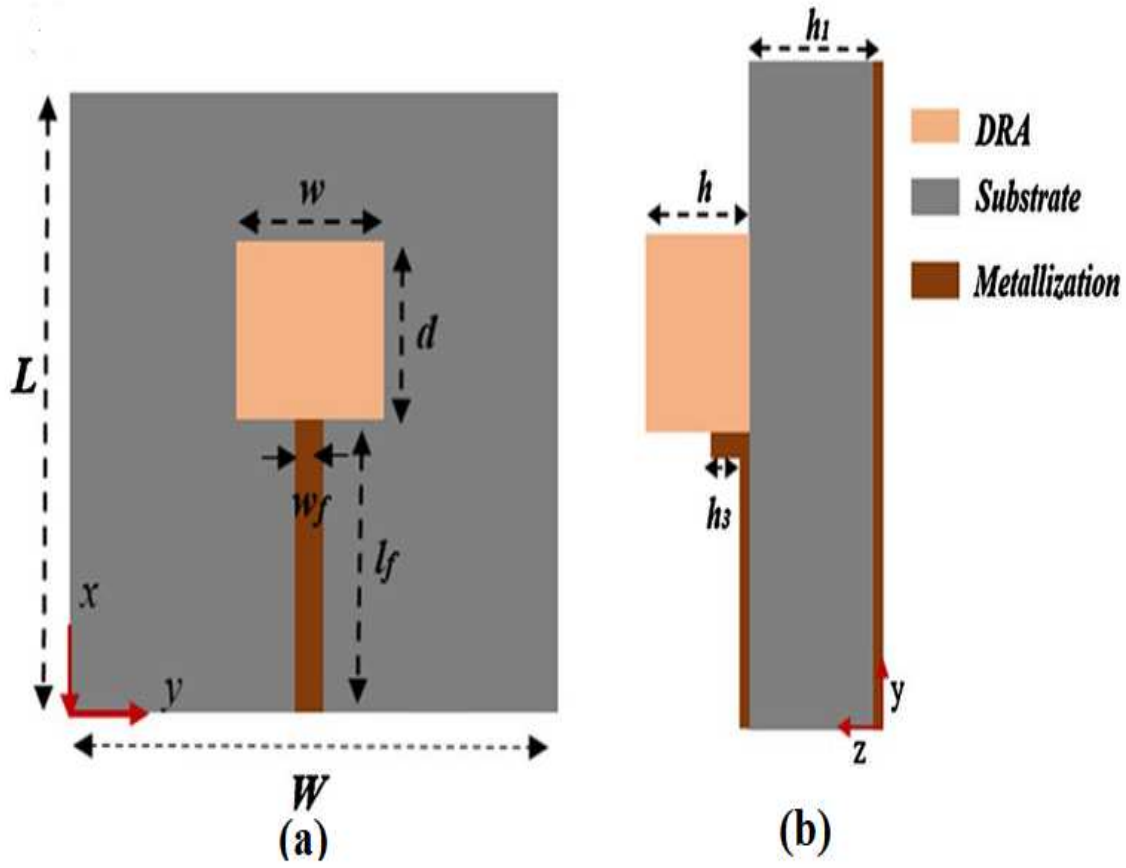

Fig. 3.1 Schematic of the Dielectric Resonator Antenna: (a) Top view, (b) Side view .

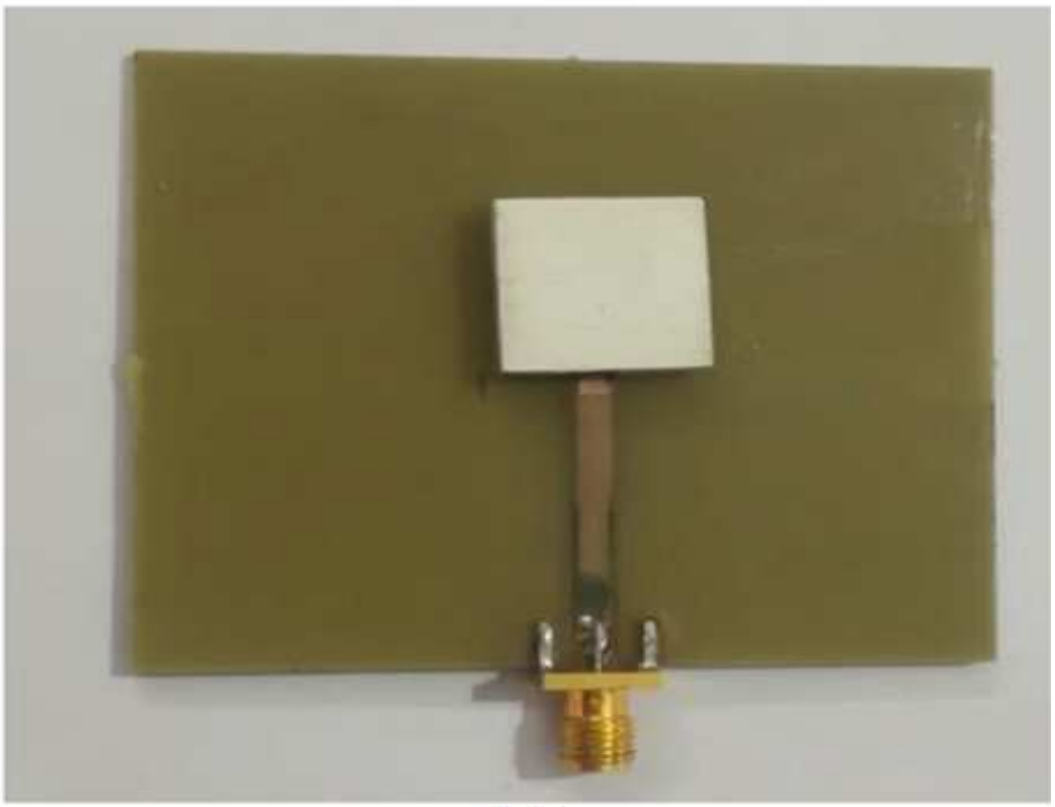

(c)

Fig. 3.2 Image of fabricated antenna.

A piece of dielectric resonator (DR) with specifications of length d, width w, height $h = \frac{b}{2}$ and a dielectric constant ε_r is used to design the rectangular dielectric resonator antenna (DRA). The choice of rectangular DRA is due to the fact that this design is for narrow band applications with high gain. The ratios $\frac{w}{h}$and $\frac{w}{d}$can be considered independently in rectangular DRA. Rectangular shape of the DRA provides design flexibility over cylindrical and hemispherical DRA. The proposed antenna geometry is simple and can be easily fabricated. To excite the resonant frequency, the dielectric resonator mounted on the ground plane is connected to a microstrip line . The resonant frequency depends on the dimension and ε_r of the DR sample. The resonant frequency f_0 can be solved by using the transcendental equation [76],

$$f_0 = \frac{c}{2 \times \pi \sqrt{\varepsilon_r}} \times \sqrt{k_x + k_y + k_z} \tag{3.1}$$

$$k_x = \frac{\pi}{w} \tag{3.2}$$

$$k_z = \frac{\pi}{2b} \tag{3.3}$$

$$d = \frac{2}{k_y} tanh \frac{(k_{y0})}{(k_y)} \tag{3.4}$$

$$k_{y0} = \sqrt{k_x + k_z}$$

where k_x, k_y, k_z denotes the mode wave number in x, y and z directions respectively. It is also possible to calculate the resonance by making use of the empirical formula introduced in [76],

$$f_{GHz} = \frac{15 \times F}{w_c m \pi \sqrt{\varepsilon_r}} \tag{3.6}$$

where F denotes the normalized frequency. The resonance frequency of the DRA as calulated using equation 3.6 is approximately 4.9 GHz. By calculating the resonant frequency using equation 3.1-3.4, it is obtained as as 4.8 GHz, revealing a good correspondence with the procedure in equation 3.6.The schematic diagram of the of the proposed rectangular Dielectric Resonator Antenna of dimension d × w × h with a relative permittivity ($\varepsilon_r = 18$ and tan $\delta = 0.0287$) positioned on a grounded FR-4 substrate (($\varepsilon_r = 4.2$ and tan $\delta = 0.03$)) of thickness h_1 is depicted in Fig.3.1. The image of the fabricated antenna is as shown in Fig.3.2.

The 50 ohm microstrip line which excites the DRA is elevated to a height h_3 vertically along the rectangular DR block. The height h_3 can be modified to control the coupling from the microstrip line to the DR block. Hence, the height h_3 is optimized in HFSS software to attain a suitable reflection coefficient over the desired impedance bandwidth.

3.1.2 Synthesis of DR Material

The DR material is prepared by mixing Barium and polyethylene in proper ratio. The mixture contains 36 volume percentage of barium (Ba) mixed with 64 volume percentage of polyethylene. The density of the composite ρ can be determined by,

$$\rho = \frac{\rho_1 v_1 + \rho_2 v_2}{v_1 + v_2} \tag{3.7}$$

where ρ_1 and ρ_2 represents the density of polyethylene and barium titanate respectively and the volume percentage of polyethylene and barium titanate is represented as v_1 and v_2 respectively. This mixture is then placed inside a hot press in a rectangular mold at a temperature of 165° C for two hours. The solid piece obtained from the hot press is cooled down before it is made to the required size. A sample sheet of this mixture which has a

thickness of 1.5 mm is fabricated initially to experimentally measure the dielectric constant. It was found that the dielectric constant of this material synthesized using a Network Analyzer connected to QWED WARSAW electromagnetic design software is 18.

3.1.3 Results and Discussion

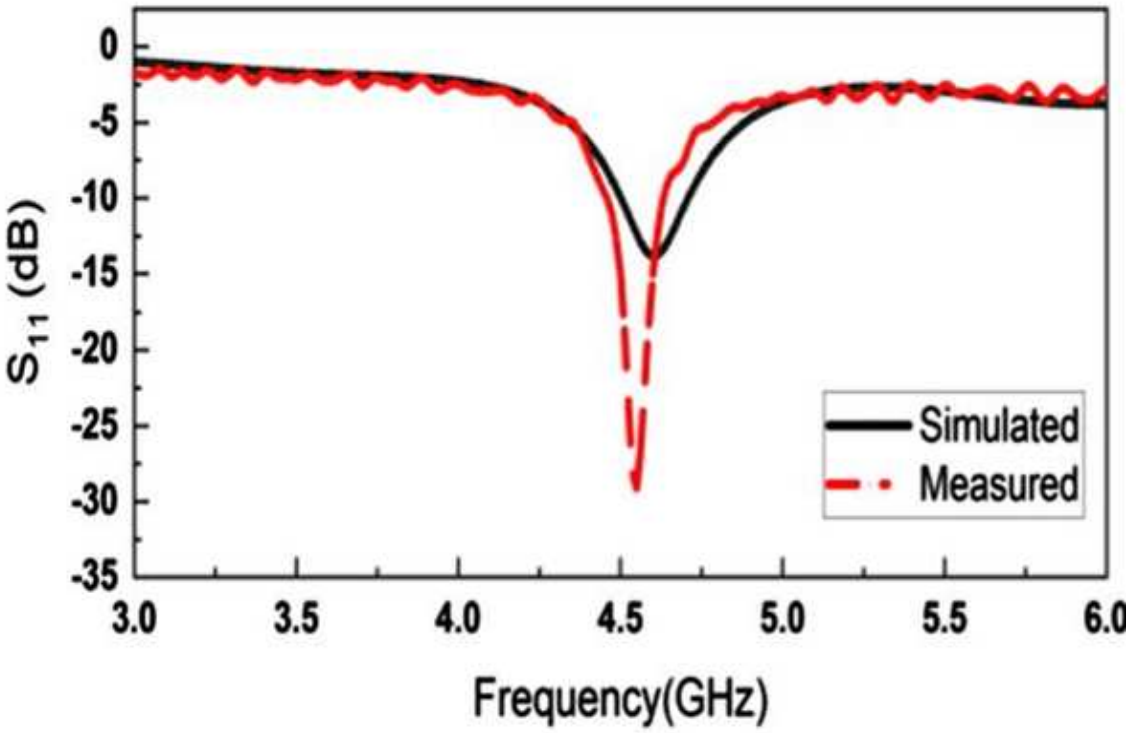

Fig. 3.3 Simulated and measured reflection coefficient of stand-alone DRA.

The HFSS simulated as well as measured impedance bandwidth of the DRA is depicted in Fig.3.3 . The measurement is done using an Agilent PNA-X N5224A network analyzer. An excellent matching is obtained for the standalone DRA at around 4.5 GHz. The simulated and measured impedance bandwidth attained is 200 MHz and 140 MHz respectively. To perform the radiation pattern measurements, a fully calibrated far-field anechoic chamber which has a broadband preamplifier (Agilent 83051 A) and a transmitting reference broadband dual ridged horn antenna is used. Figure 3.4 (a) and (b) exhibits E- and H-plane radiation pattern of the proposed DRA. Both for simulation and measurement plots in Fig.3.4 (a) and (b), a broadside radiation pattern is achieved. The simulated gain is 5.8 dBi while the measured gain obtained is 4.3 dBi. The pattern reveals that the half power beam-width is 90 degree. The minor difference in the measured and simulated gain is due to various practical issues, including, i) fabrication tolerance of the DRA, ii) micro-mismatch in placing the DRA on

the grounded substrate etc. In actual cases, for antennas which have full ground plane, the measurement of the back-lobe can lead to ambiguous results, mainly if the positioners as well as other metallic parts are not properly shielded. This causes the transmitting antenna to illuminate the metallic parts along with the AUT leading to ambiguous results. Taking this into consideration, for the DRA, the entire back lobe measurement was not done.

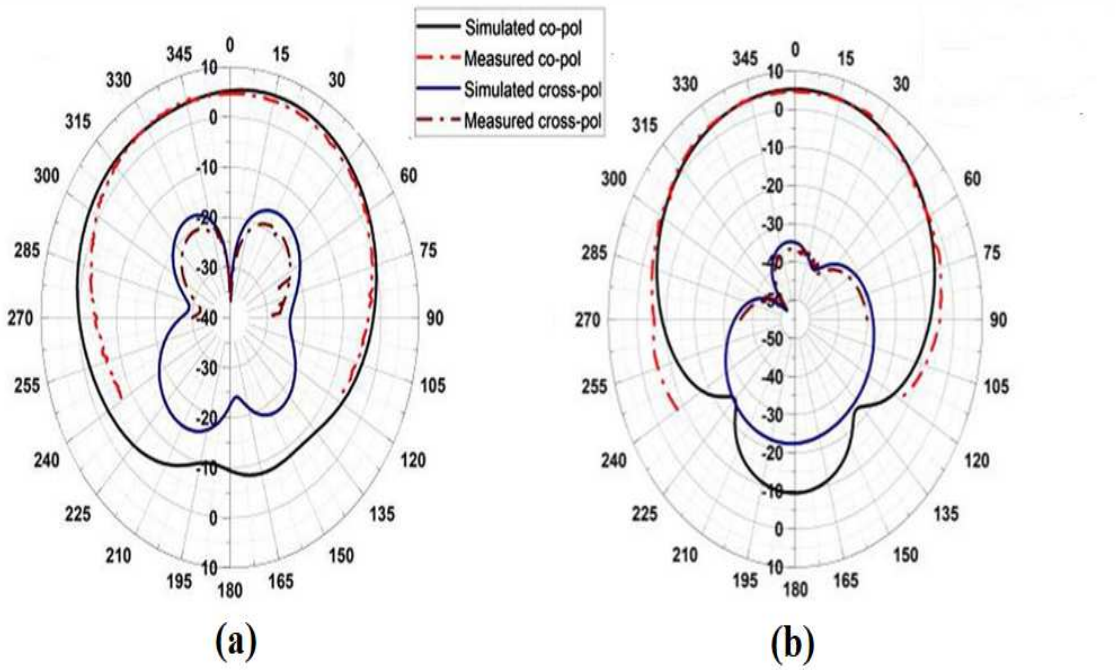

Fig. 3.4 Simulated and measured radiation pattern of stand-alone DRA at 4.5 GHz: (a) E-plane, (b) H-plane.

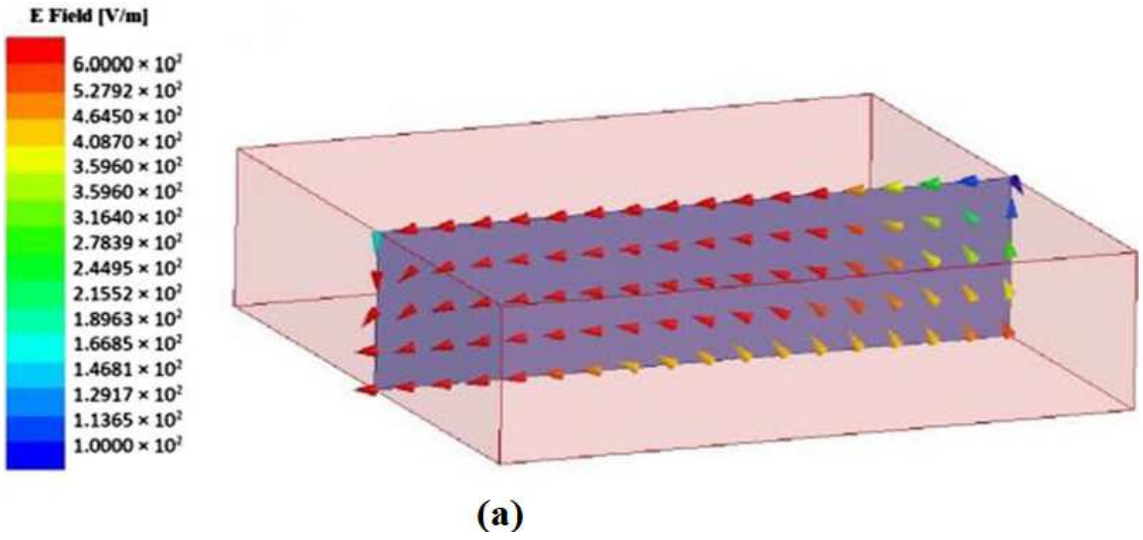

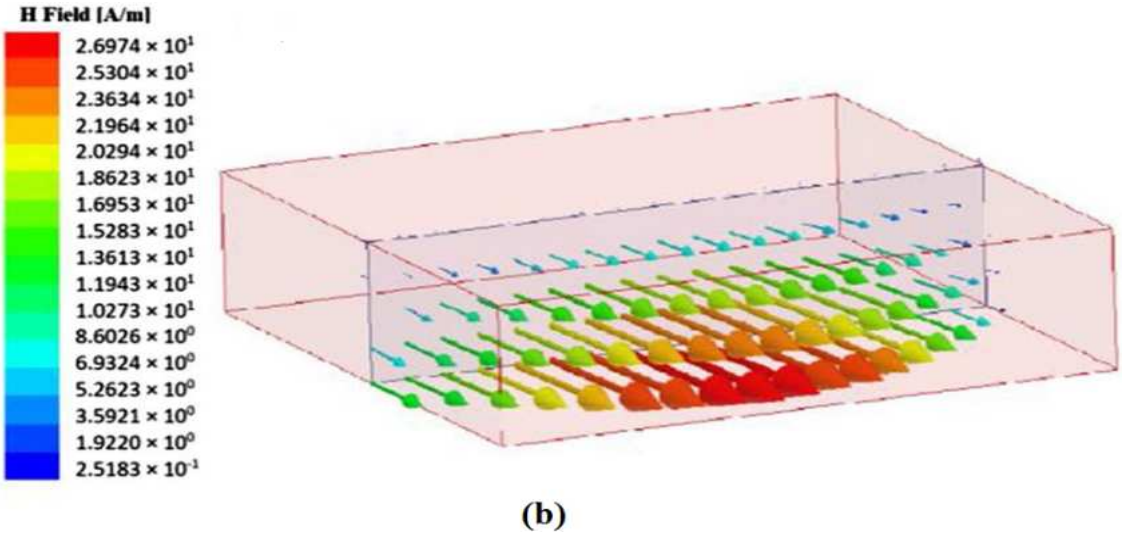

(b)

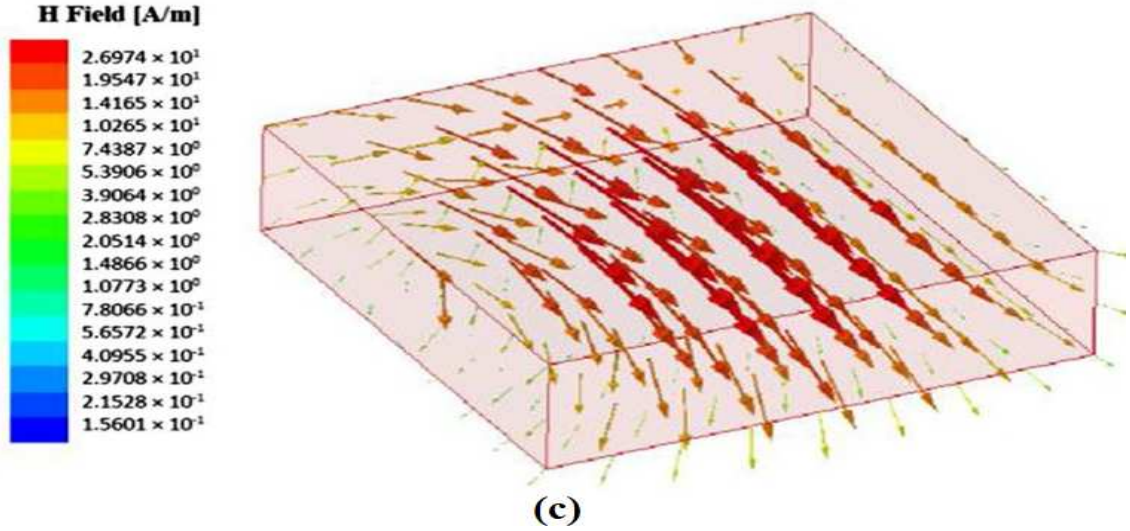

(c)

Fig. 3.5 (a) Electric field along the x-direction (on a non-modal plane), (b) Magnetic field along the y-direction (on a non-modal plane), and (c) Magnetic field in cross-sectional view for proposed rectangular DRA at 4.5 GHz.

The Fig.3.5 (a)shows the plot with E-field pattern in x-direction and Fig.3.5 (b) depicts the H-field in y-direction. The cross-sectional view of H-field is shown in Fig.3.5 (c). The field plots shown in Fig.3.5 confirms lower mode with $m = n = 1$ excitation.

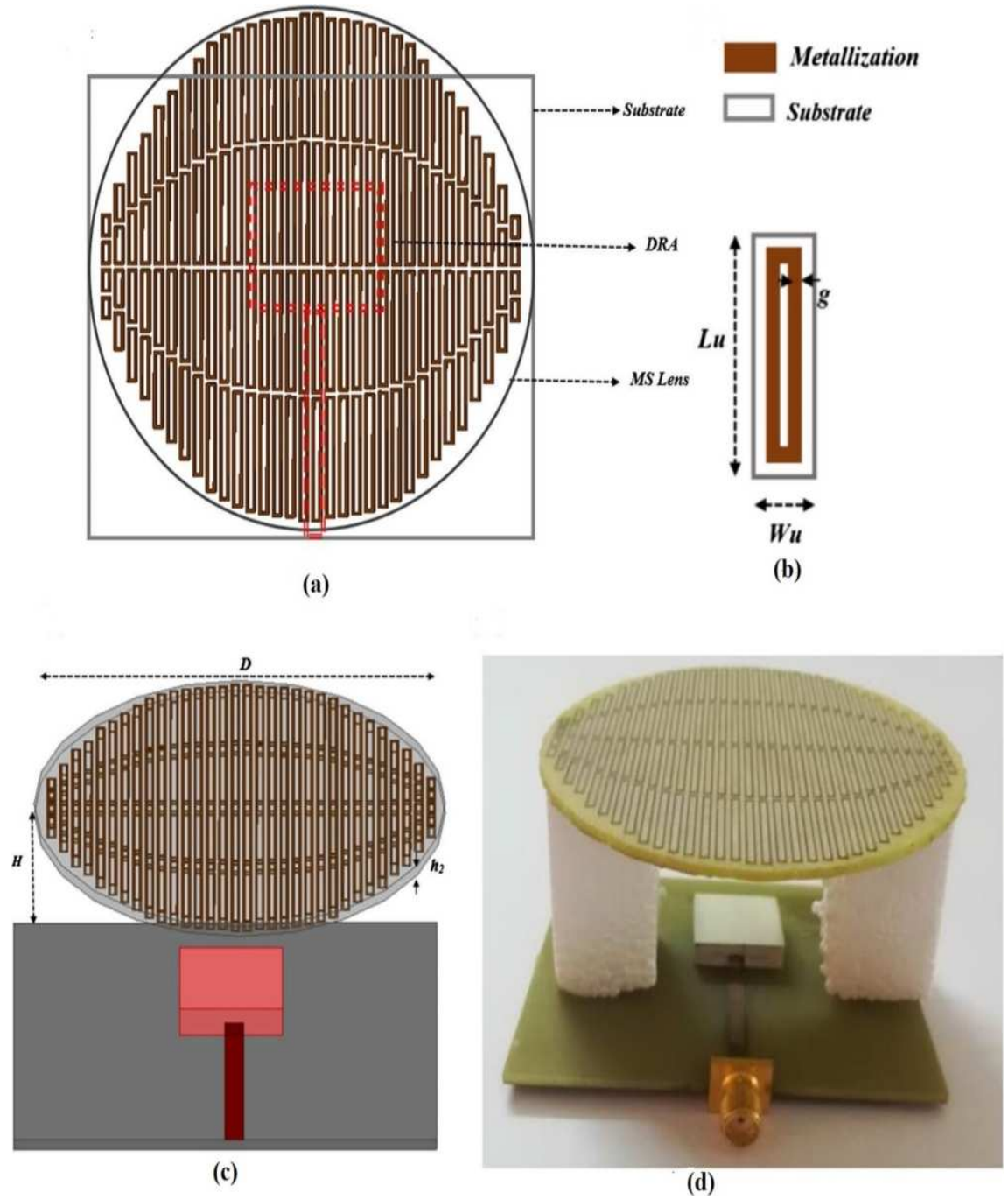

Fig. 3.6 (a) Top view of the proposed antenna with MS lens, (b) enlarged view of schematic of a unit cell of the MS lens, (c) 3D view of the DRA with the MS lens and (d) Image of the fabricated antenna.

3.2 The MS Lens loaded Dielectric Resonator Antenna

3.2.1 Design of Metasurface lens (MSL)

The MSL, is designed with many rectangular shaped metallic loops of varying dimensions. These metallic loops are printed on both the sides of a dielectric substrate with circular geometry having radius 68 mm, height 1.575 mm and $\varepsilon_r = 4.2$. The varying dimensions of the metallic loops on the MSL, results in a graded refractive index profile having greatest value at the center which gradually decays towards the edges at 4.5 GHz [74]. This MSL operating at 4.5 GHz is mounted on top of the DRA designed in the previous section at a height vertically above the DRA as $\lambda_0/2$,where λ_0 is the wavelength at the frequency of operation of the DRA. The DRA which is excited by a 50 ohm microstrip line results in TE_{11} mode. The EM waves radiated from the DRA proceeds through the MSL which is properly oriented resulting in a highly collimated EM wave at the output side of MSL. For required gain enhancement the MSL has to be positioned symmetrically above the DRA which otherwise will affect the gain improvement. The schematic diagram of the DRA loaded with MSL is shown in Fig.3.6. The top view of the antenna is portrayed in Fig.3. 6(a). The unit cell schematic is as shown in fig. 3.6(b). The unit cell parameters are length L_u, width Wu and metallization width g . Figure 3.6(c) shows the 3D view of the DRA loaded with MS lens and the photograph of the realized MSL loaded DRA is depicted in fig. 3.6(d). This MSL can be used together with other sources, like microstrip radiator, to achieve an improved gain.

The unit cell's refractive index is theoretically calculated using the Kramer's Kronig Algorithm [74]. The transmission -reflection data is used to identify effective magnetic permeability and electric permittivity of a composite EM structure in the algorithm. These are calculated as follows:

$$\mu_{eff} = N_{eff} \times Z_{eff} \tag{3.8}$$

$$\varepsilon_{eff} = \frac{N_{eff}}{Z_{eff}} \tag{3.9}$$

where N_{eff} is the complex refractive index and Z_{eff} is the complex wave impedance [77]. In this design, the unit cells on both sides of the MS lens are of constant width $0.022\lambda_0$ as well as constant gap along x-axis resulting in thirty two unit cells on the x-axis. A 1-D periodicity is maintained by each unit cell which repeats four-times in the orthogonal direction. As the designed surface (lens) is an engineered structure which yields a differing refractive index profile for collimating the radiated EM wave from the source antenna, this surface is named as a metasurface lens. The positioning of MSL vertically above DRA is determined by the

refractive index range of the MSL. To identify the appropriate distance H for placing the MS lens, the ratio is set as follows:

$$\frac{H}{D} = k \tag{3.10}$$

where D is the diameter of MSL. In this work the refractive index range is designed to be 9.4, which results in a k value of 0.5 [74]. The following equation shows the relation between k and the range of refractive index [74]:

$$n(r) = 43.75(\sqrt{k + \frac{1}{4}} - k) \tag{3.11}$$

The increase in the length of cell leads to an increased refractive index. The scatterers are rectangular shaped and their dimensions are differed to obtain required constitutive parameters [74]. These are spread on both sides of the FR-4 (ε_r = 4.2) substrate of diameter D = λ and thickness h_1, where λ is the wavelength corresponding to the frequency o operation f = 4.5 GHz. Thickness of the substrate used for MS lens design is h_2. Here FR-4 substrate was chosen as it was readily available in the lab. The length L_u of the unit cells are varied along the x-axis with a length of $0.12\lambda_g$ in the central region to $0.01\lambda_g$ at the border of the circular FR-4 substrate. The dimensions of rectangular unit cells along y-axis is kept same. This results in an MSL which has 32×4 rectangular rings on both sides as indicated in Fig. 3.6. This design of MSL with its unit cells results in a graded refractive index (GRIN) profile [74]. The EM waves radiating from the DRA strikes on the MSL with differential phases and gradually degrading phase profile from the centre to the edges of the lens. The GRIN (graded index) profile design of the MSL, contributes to the uniform phase profile of the EM waves incident from the source antenna from the other side of the MS lens which leads to a constructive interference resulting in a gain enhanced antenna design. The heterogeneous sized unit cells and polarization matching results in the GRIN profile of the MS lens [74]. The working principle of this MSL with GRIN profile is to some extent similar to reducing the dispersion in the multi-mode fibers via graded refractive index profile. The profile and hence the dimension of the cells is designed based on the operating frequency of the source antenna. Hence, the overall size of MSL is determined by the source radiator size. Here, the cells are arranged to generate a refractive index of 12.4 in the middle of the MSL which degrades gradually to 3.15 at the border of the substrate along x-axis. Detailed discussion of design parameters of the MSL loaded DRA is given in Table 3.1.

Table 3.1 Design parameters of proposed antenna

Parameter	Dimension(mm)	Parameter	Dimension (mm)
D	68	$w = d$	17
H	34	h	4.2
L	60	h_3	2
W	70	h_1, h_2	1.575
L_f	29	W_u	1.47
W_f	3	g	0.375

3.2.2 Results and Discussion

The simulated and measured impedance bandwidth of the MSL loaded DRA is depicted in Fig.3.7 . The MSL integrated DRA generates a better impedance matching (S_{11}= -37 dB) over the standalone DRA (S_{11}= -14 dB) due to the positive interference of MSL material loaded above the source DRA. The MSL loaded DRA generates a bandwidth of 140 MHz and 180 MHz in simulation and measurement respectively. When MSL is loaded above the source DRA, an electromagnetic coupling occurs resulting in a small variation in the resonance frequency of the antenna loaded with MS lens in comparison with the standalone DRA. This can also be due to fabrication tolerance and slight uncertainty in ε_r of the synthesized DR material.

Figure 3.8 (a) and (b) depicts the radiation pattern in E-plane and H-plane of the DRA integrated with MSL. An image of the S_{11} and radiation pattern measurement mechanism is pictured in fig.3.9. A metallic structure kept at the bottom region of Fig.3.9(b) provides the mechanical stability while performing the experiment. Since this structure is behind the measured antenna ground plane (fully grounded DRA) it has negligible consequence on the radiation pattern measurement. The DRA is fixed on the grounded FR-4 substrate at exact location using an index matched dielectric glue. This is then loaded with MSL at theoretically calculated height with a foam structure to support the MSL. It is observed from the fig. 3.8 (a) and (b) that the combination of MSL and DRA results in a broadside radiation pattern with peak gain of 9.90 dBi and 9.3 dBi in simulation and measurement respectively. There is a reduction in half power beam-width to 40 when MSL is used. This increase in gain is due to the designed MS lens with GRIN profile which generates a collimated beam with improved peak gain.

The enhancement in gain of the MSL integrated DRA compared to the stand-alone DRA is also validated by plotting the 3-D radiation pattern of DRA integrated with and without the MSL as depicted in fig. 3.10(a) and (b) respectively. The rise in current distribution on the

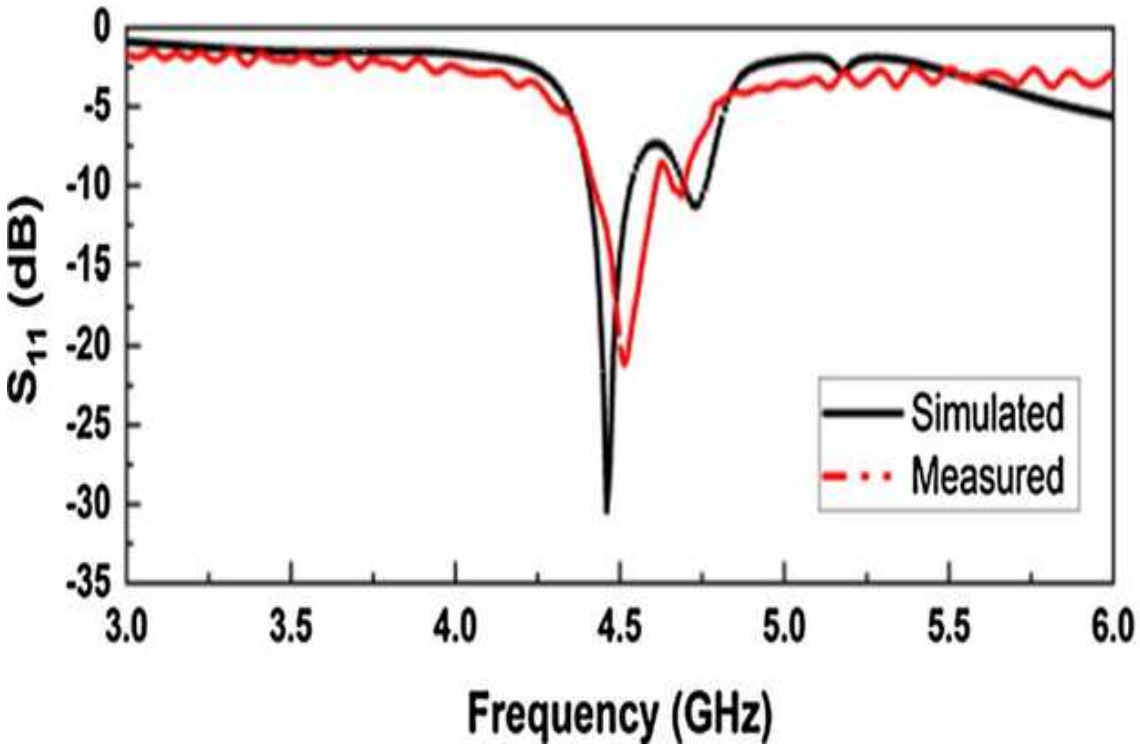

Fig. 3.7 Simulated and measured reflection coefficient of the DRA .

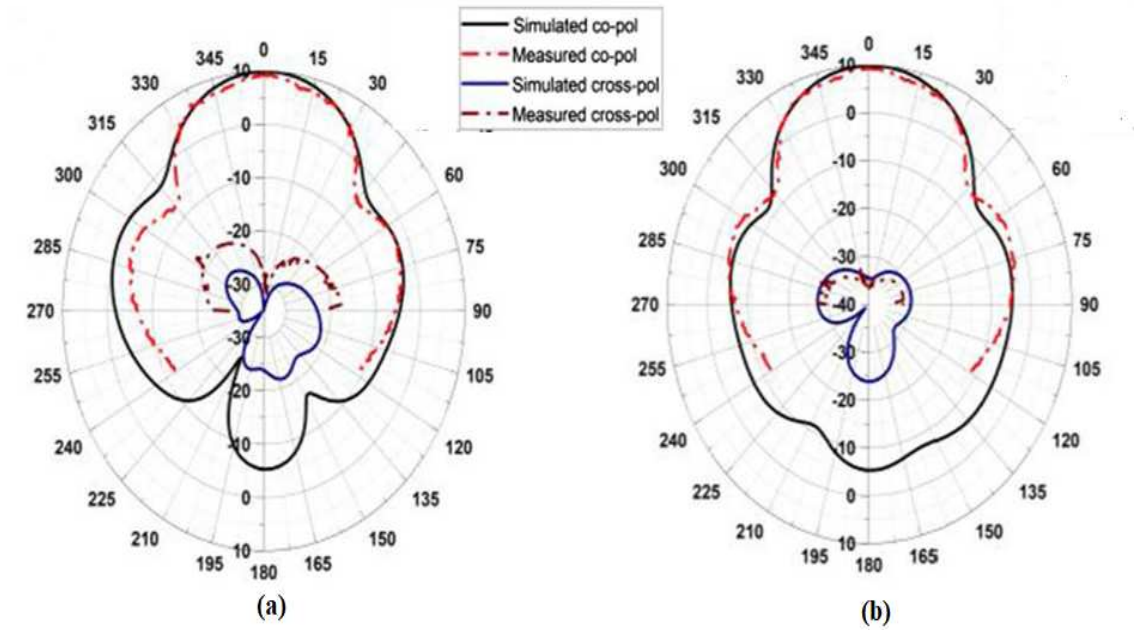

Fig. 3.8 Simulated and measured radiation pattern at 4.5 GHz of the DRA with MS lens: (a) E-plane, (b) H-plane.

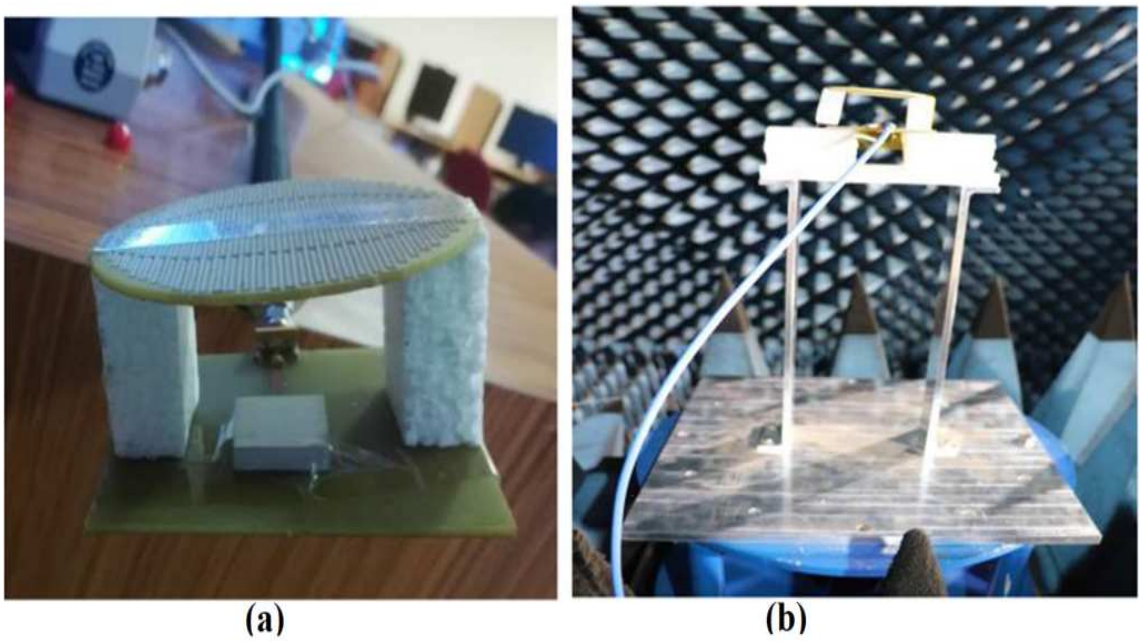

Fig. 3.9 Image of the measurement setup used for measuring (a) S_{11} and (b) Gain of the DRA loaded with an MS lens.

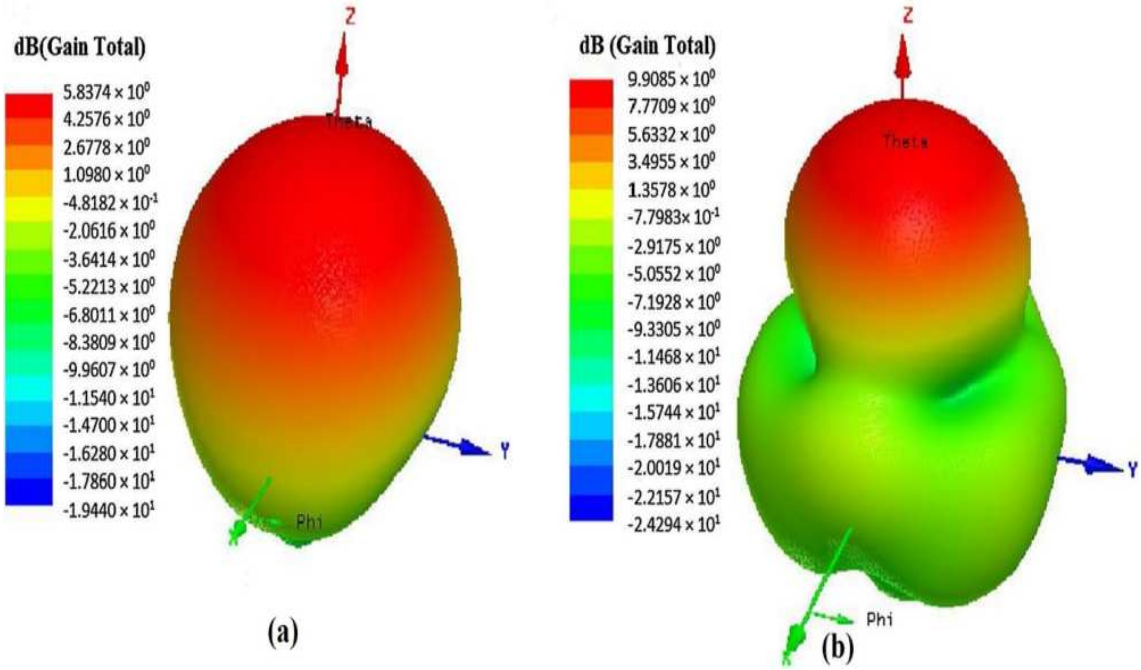

Fig. 3.10 3D Gain at 4.5 GHz: (a) DRA without, and (b) with an MS lens.

MSL is observed in fig.3.11. This results due to the focused EM waves along the bore sight

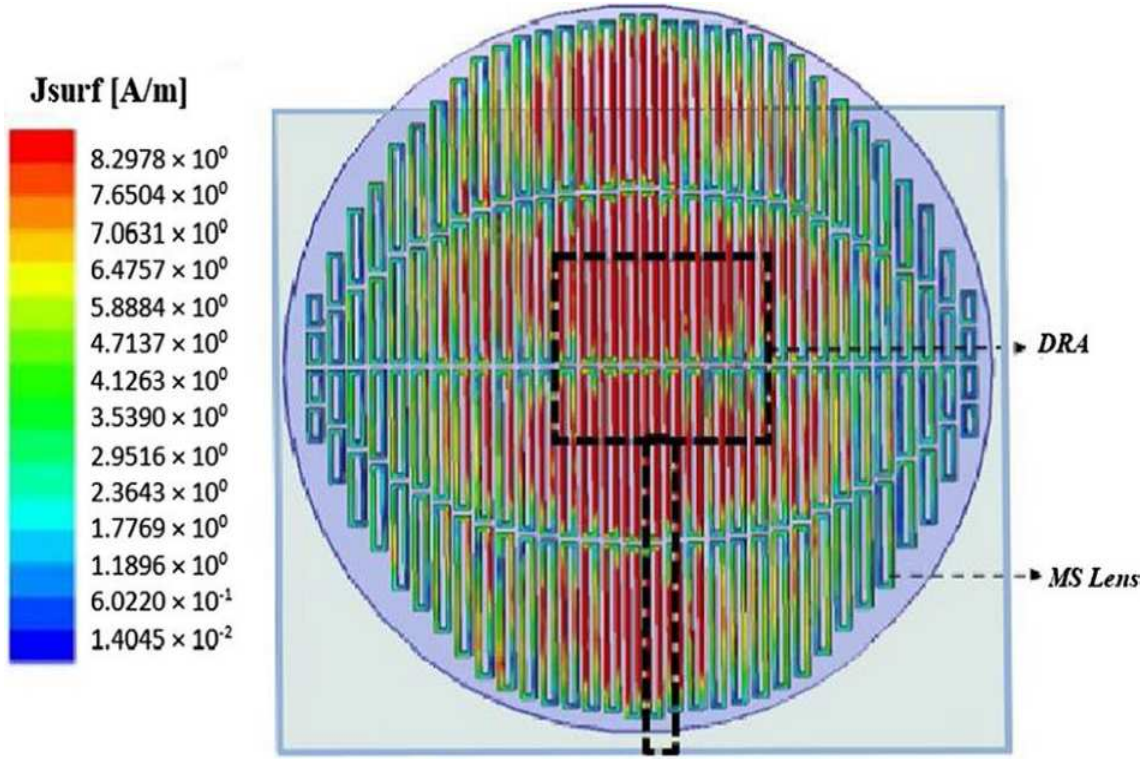

Fig. 3.11 Current distribution on the MS lens at 4.5 GHz.

of the DRA integrated with MSL as seen in the fig.3.11. Table 3.2 presents a comparison of simulation and measurement results of the DRA integrated with and without the MSL.

3.3 Conclusion

A dielectric resonator antenna integrated with MSL is discussed in this chapter. Kramer's Kronig algorithm extracts the effective magnetic permeability and electric permittivity of the unit cell designed from the S-parameters generated. The placement of unit cells on FR-4

Table 3.2 Comparative look of simulated and measured results of standalone DRA and DRA loaded with an MS lens

		Standalone DRA	DRA with MS lens
Impedance BW%	Simulated	200	140
	Measured	140	180
Maximum Gain	Simulated	5.8	9.9
	Measured	4.6	9.3

substrate results in a graded index profile. Thus the EM waves from the standalone DRA antenna follows a uniform phase profile leading to a constructive interference which thereby enhances the gain of the DRA with MSL by 4.1 dBi in simulation against measured value of 4.7 dBi. The proposed mechanism of gain improvement provides a notable rise in gain for the source antenna with a compact structure.

Chapter 4

Investigation of EM Waves on ON-Body to ON-Body and ON-Body to OFF-Body scenarios using Twelve Cylinder Body Model

The study of electromagnetic (EM) wave propagation around/along the human body has always arouse the curiosity of the researchers as it has variety of applications in multimedia, healthcare system, military and sport [1]-[5]. The onset of IoT followed a considerable exploration in the area of wearable devices. The development of wearable devices requires an organized investigation of EM wave propagation while humans are at rest and movement [5]. In a typical wireless body area network (WBAN), sensors which collect relevant information from the human body is positioned on the body which are then transferred to patient's personal devices and then to health care service centers for further processing [6]. The study based on measurement analysis alone has various constraints like antenna positioning, requirement of volunteers of varying sizes, need of analyzing wearable devices on multiple material and the difficulty to do various physical activities on many volunteers [5]. A simulation technique combined with experimental analysis can provide a comprehensive information on rest and dynamic ON-Body propagation and the EM wave propagation between transmitting (TX) and receiving (RX) antennas [5].

In case of ON-Body to ON-Body EM wave propagation, antennas which radiate along the body surface should be used whereas for ON-Body to OFF-Body systems antennas with broadside radiation like textile patch antennas are more suitable [7]. The analysis of ON-Body to ON-Body channel characteristics is executed using various types of human body models/numerical phantoms, including, i) single layer rectangular [8] ii) cylindrical single

layer/torso [9] iii) three layer [10], [11] and iv) voxel model [12]. Software like 'POSER6' [78] "Phase Space Recap 2" are used for modelling the channels on dynamic human bodies [5].

In this chapter, investigation of creeping wave characteristics is reported with a simple yet effective cylindrical human body model. A human model with crucial body parts such as head, shoulder, torso, upper arm, lower arm, thighs and calf is introduced for dynamic human activities. The double arm swing activity is performed using this model to analyze the transmission characteristics. Two similar cross-slot antennas (CSA) are designed, analyzed and then fabricated, to study the creeping waves characteristics and the double arm swing activity on the newly modelled twelve-cylinder human model. The double arm swing activity is done giving consideration to various dynamic body postures. During this activity positioning of Ant1 is on the chest and Ant2 on the lower arm. The use of this newly introduced model remarkably lowers the measurement procedures and research cost. The simplified twelve cylinder body model can be easily modified to do multiple analysis. All the simulations are done in CST Microwave studio [114]. The chapter is arranged as follows: the creeping wave characteristics is explained in section 4.1 . The double arm swing activity is briefed in section-4.2 using the new model. Section 4.3 details the simulation set-up of 'Smart Bag' followed by discussion on integration of 'Smart Bag' with human body model in section 4.4.

4.1 Creeping wave Characteristics:An Investigation

Alves et al. introduced the concept of creeping waves on body surfaces at microwave frequencies [79]. The propagation of creeping wave in case of a wearable antenna is dicussed in the article [79]. A creeping wave in electromagnetism is a wave that is diffracted around the shadowed surface of a smooth body such as a sphere and has applications in EM propagation and as well as accoustics. Creeping waves greatly extend the ground wave propagation of long wavelength (low frequency) radio. They also cause both of a person's ears to hear a sound, rather than only the ear on the side of the head facing the origin of the sound. The propagation of electromagnetic waves on the body includes a union of free space propagation, and creeping waves which is due to the diffraction as well as the reflections from the environment. The study of creeping waves around the torso provides more insights on ON-Body to ON-Body propagation. The ON-Body propagation is mainly contributed by creeping waves diffracted from lossy human body phantom and trapped along the body's surface, while the radio waves of OFF-Body links are dominantly line of-sight (LOS) as well

as multi-path propagation. Creeping waves are more sensitive to body motions rather than shadowing, fading and multipath effects.

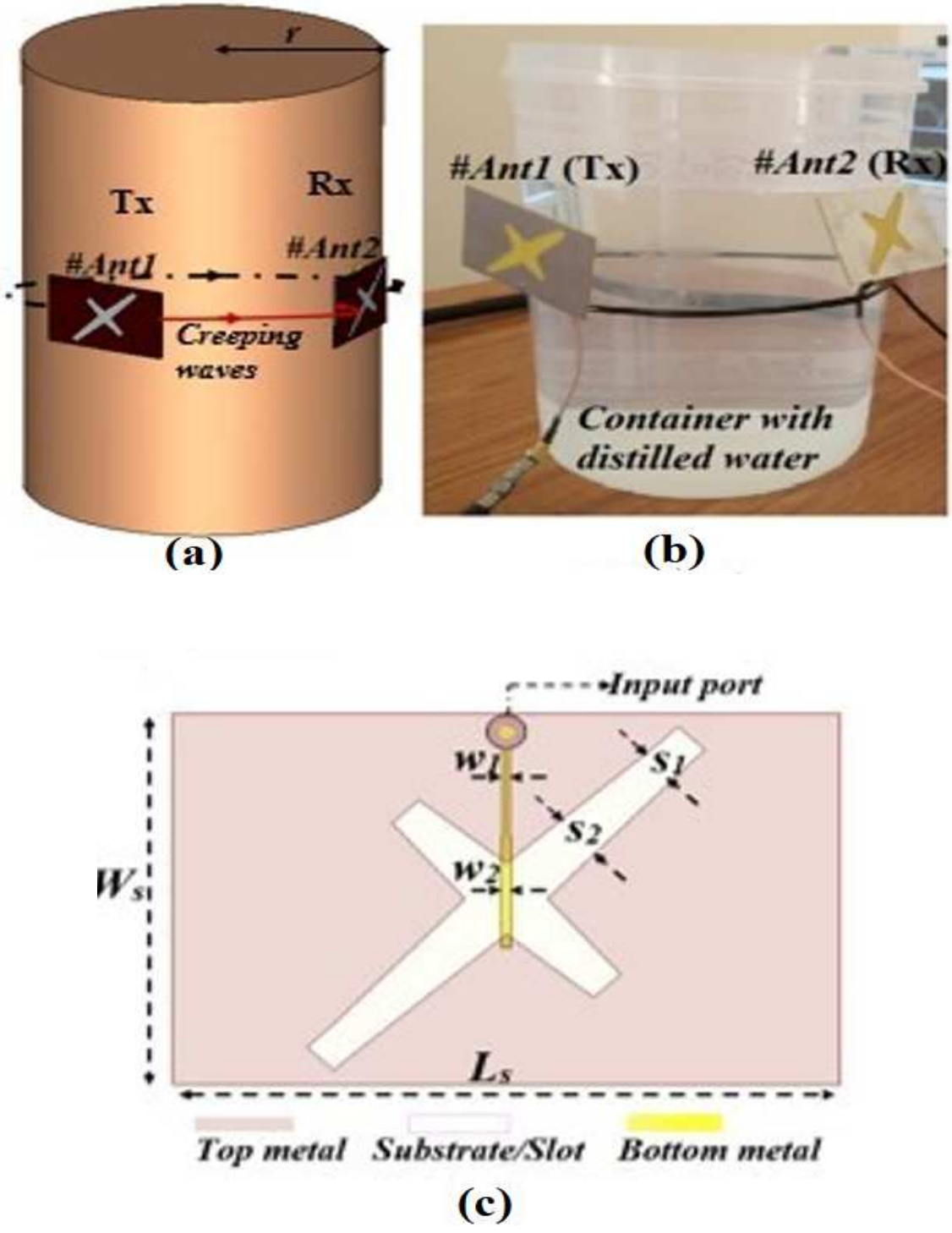

Fig. 4.1 (a) Creeping wave simulation setup using CSA on phantom model. (b) Experimental setup using container with distilled water. (c) Schematic of the antenna.

In present work, a cylindrical phantom and omnidirectional CSA of size $L_s \times W_s \times$ h is used to analyze the creeping wave characteristics. The designed antenna operates in the frequency range of 1.8 to 3 GHz [80]. The simulation methodology and experimental set up for EM wave analysis is depicted in Fig. 4.1 (a) and (b). The antenna schematic is depicted in Fig. 4.1 (c). The design dimensions of the CSA are provided in Table-4.1. In the simulation set-up shown in Fig.4.1(a), homogeneous cylindrical phantom models of, length l = 300 mm, and radius $r = r_1 = 64$ mm and $r = r_2 = 98$ mm are considered.

Table 4.1 Design Parameters of CSA

Parameter	Dimension (mm)	Parameter	Dimension (mm)
L_s	70	s_1	5.8
w_1	0 .7	h	1.58
W_s	45	s_2	6.2
w_2	0.85		

The S_{11} is simulated for two scenarios: i) CSA in free space and ii) CSA on human body model. This is depicted in Fig 4.2 which shows that for both scenarios a 1.2 GHz impedance bandwidth is attained. The experiment is performed on CSA fabricated on FR4 (ε_r = 4.4 and $tan\delta$ =0.02 material. The S_{11} is measured for two scenarios: i) standalone CSA and ii) CSA on container filled with distilled water is as depicted in Fig.4.2.

The homogeneous body model has dielectric constant ε_r= 35.15, and conductivity 1.16 S/m. This value is the average permittivity of human body which is two-third of muscle tissue [81]. The $Ant1$ and $Ant2$ are positioned on the homogeneous phantom model. The $Ant1$, on the model is the transmitting antenna (Tx) while $Ant2$ on the phantom model, acts as a receiving antenna (Rx). The position of $Ant1$ is fixed and $Ant2$ is moved in a circular path around the cylindrical phantom model. As EM waves travel around the cylindrical phantom models an exponential decay of EM waves is noted.

Figure 4.3 depicts the simulated transmission data used to study the creeping waves. In case of the cylindrical body model of radius $r_1 = 64$mm, the receiver antenna #Ant2, is placed directly on the backside of the transmitting antenna $Ant1$ at the wrapping span of 200 mm ($\pi \times r_1 = 200$ mm). Likewise, a back-to-back position of the antennas are obtained for the body model with radius r_2 = 98 mm, at a wrapping span of 300 mm ($\pi \times r_2 = 300$ mm). A constructive interference of the EM waves in clockwise and anti-clockwise direction are observed when antennas are placed back-to back. This phenomenon can be noticed clearly as #Ant2 is fixed at more number of points near the backside of #Ant1 and analyzed. The vertical dotted line marked in Fig.4.3 marks the point at which this constructive interference occurs.

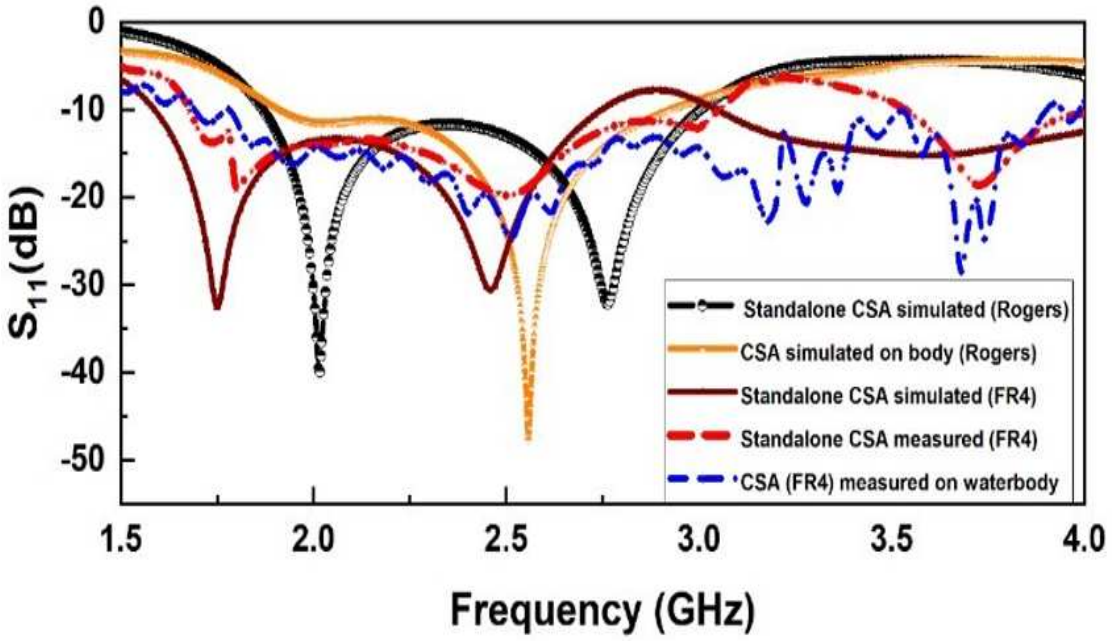

Fig. 4.2 Simulated and measured S_{11} of the CSA.

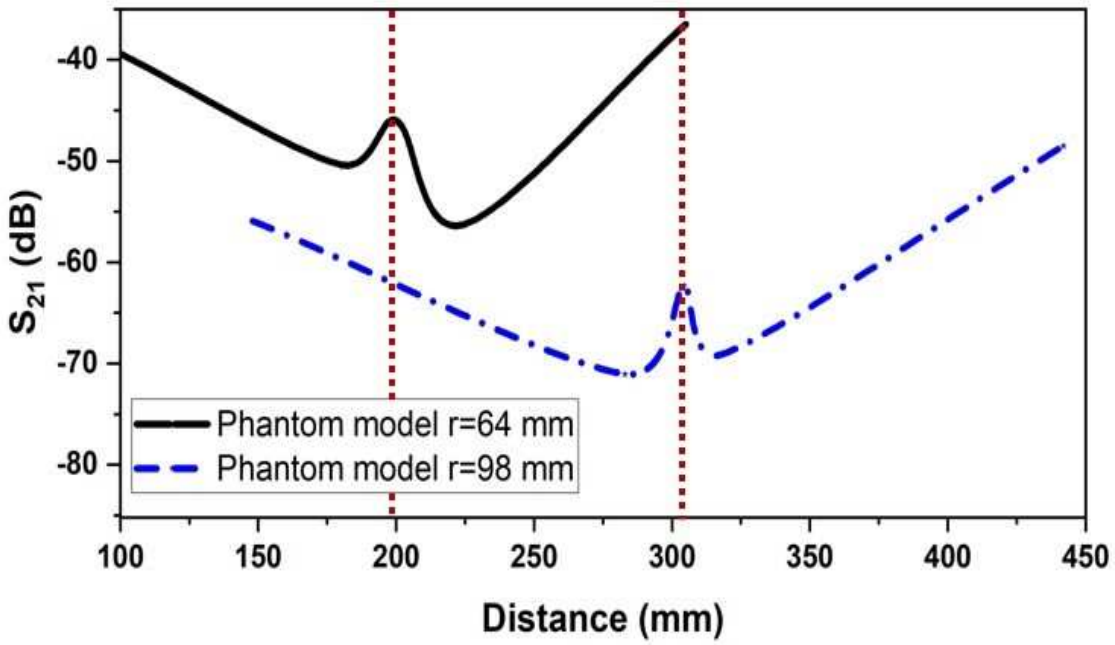

Fig. 4.3 Simulated transmission values for phantom model of varying radius at 2.4 GHz.

In order to further understand the phenomenon of creeping waves, experiments for the corresponding simulations were performed at IIST RF and Microwave Lab facility. The

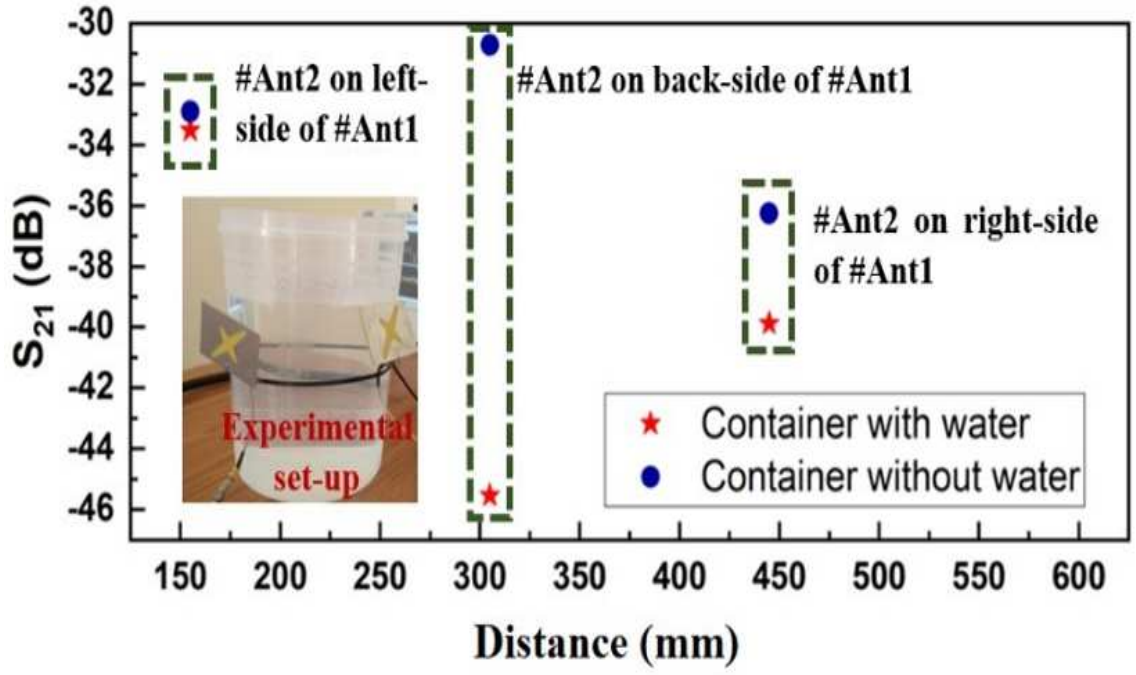

Fig. 4.4 Experimental study using CSA and a container with and without distilled water at 2.4 GHz.

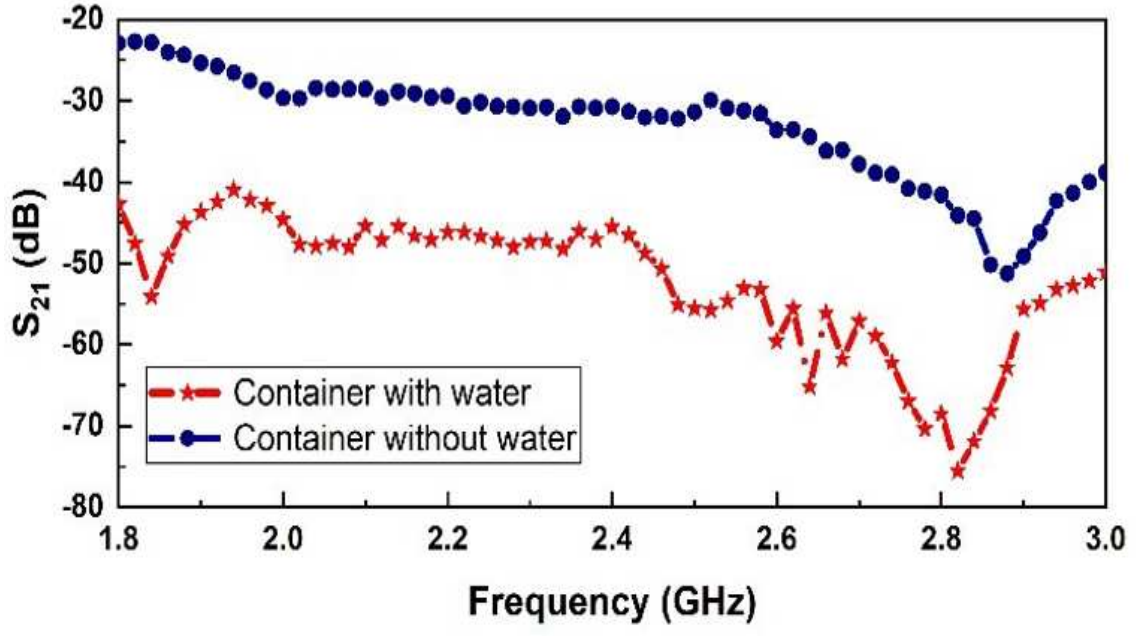

Fig. 4.5 Transmission characteristics using CSA and a container with and without distilled water vs. frequency.

experiment was done by using a plastic container with radius 100 mm for two scenarios: i) empty container (non-lossy medium) and ii) conatiner filled with distilled water($\varepsilon_r = 78$) making it as lossy medium as depicted in Fig.4.4. The experiment is done using distilled water, as water is a major constituent of human body. The water content in adults is 60 percentage while in children the percentage is still higher [82], [83]. The Rx antenna, #Ant2 was fixed on the left, back and right side of #Ant1 to obtain transmission characteristics at those positions. In case-(i) (empty container), the transmission characteristics is better when #Ant2 and #Ant1 are positioned back-to-back compared to all other placements of CSAs as this orientation gives maximum EM wave transmission. But in case-(ii) (with distilled water), it is noticed that the transmission characteristics decays significantly as the #Ant2 is placed directly opposite to #Ant1. This substantial decrease in strength of the EM waves is due to the presence of lossy water medium in the container.

The S_{21} when #Ant2 and #Ant1 are directly opposite to each other are plotted against frequency for two cases: i) container filled with distilled water and ii) empty container as shown in Fig.4.5. When filled with water, the container becomes a lossy medium reducing the transmission values during experiment when compared to the medium without water. The transmission losses also increases towards higher frequency.

4.2 Double Arm Swing Activity in the Sagittal Plane

The twelve cylinder homogeneous body model with ε_r= 35.15, and conductivity 1.16 S/m [81] designed can be modelled for rest and dynamic activities . The head, shoulder, torso, thighs, calf, upper arm, lower arm are featured using individual homogeneous cylinders. The coronal as well as sagittal plane of the human body model and schematic of the newly proposed twelve-cylinder homogeneous body model are shown in Fig.4.6. This model is developed to perform the analysis of dynamic scenarios and postures. Here, this twelve-cylinder body model is used to model dynamic postures in a double arm swing activity. This activity is performed by hand movement in reciprocal direction in the sagittal plane which is similar to our hand posture as we walk.

The ten frames showing different postures during double arm swing activity using this simplified model is depicted in Fig. 4.7. In present work, the #Ant1 is positioned on the chest of this model and #Ant2 is positioned on the lower arm of the phantom model. At t = 0, position is depicted by frame P1 and t = 1 second it is depicted as frame P10. All the other intermediate frames are equally time spaced and shown in the Fig.4.7.

While performing this activity, more number of frames are studied in the first half cycle, where hand is moved from front side of body model to back-side of the model to get a

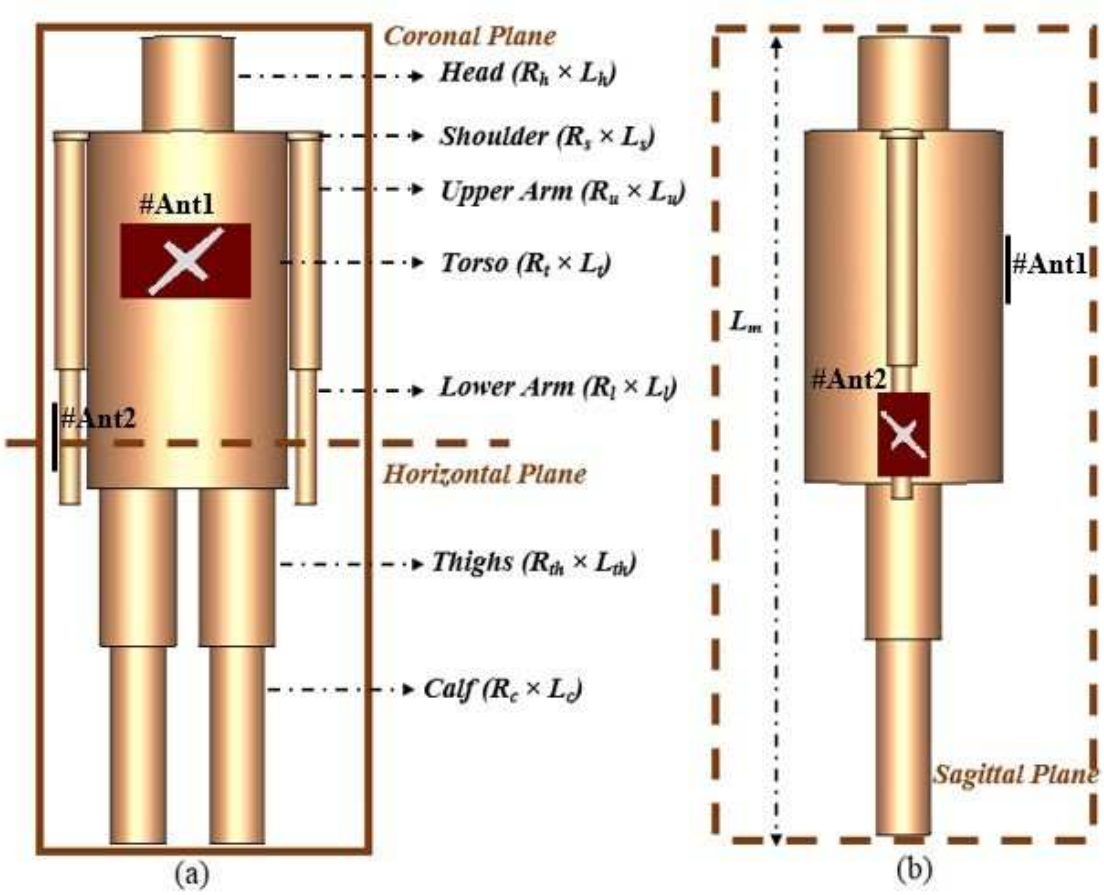

Fig. 4.6 Schematic of twelve-cylinder phantom model: (a) Front view, and (b) Side view.

comprehensive information of the transmission characteristics. In the next half cycle, the hand is moved from back to the front-side of the phantom model almost along the same path. The detailed dimensions of the model are provided in Table 4.2.

Experimental investigation using multiple frames shows that the signal loss is lower when lower-arm where #Ant2 is positioned is in the front side of the body and #Ant1 is on the chest as seen in Fig.4.8. The transmission value reduces as #Ant2 placed on the lower arm is on the backside of the body model in double arm swing activity. As seen from Fig.4.8, the S_{21} of this simulation results in a cosine pattern.

The response of changing the orientation of CSA is studied using a four-year child model whose design values are given in Table 4.3. Figure 4.9(a) shows the child model simulated with Ant1 and Ant2 positioned parallel to the body surface while in Fig. 4.9(c) CSAs are fixed normal to the surface of the body resulting in the movement of EM waves along the surface of the body. This is understood from the omnidirectional radiation pattern of the CSA shown in Fig. 4.9(b). Figure 4.10 depicts the experiment performed on a female volunteer

Table 4.2 Dimensions of twelve-cylinder Body Model

Parameter	Dimension (mm)	Parameter	Dimension (mm)
R_h	30	L_h	60
R_l	7 .	L_l	85
R_s	15.9	L_S	5
$R_t h$	25	$L_t h$	100
R_u	9	L_u	145
R_c	18	L_c	125
R_t	65	L_t	225
L_m	550		

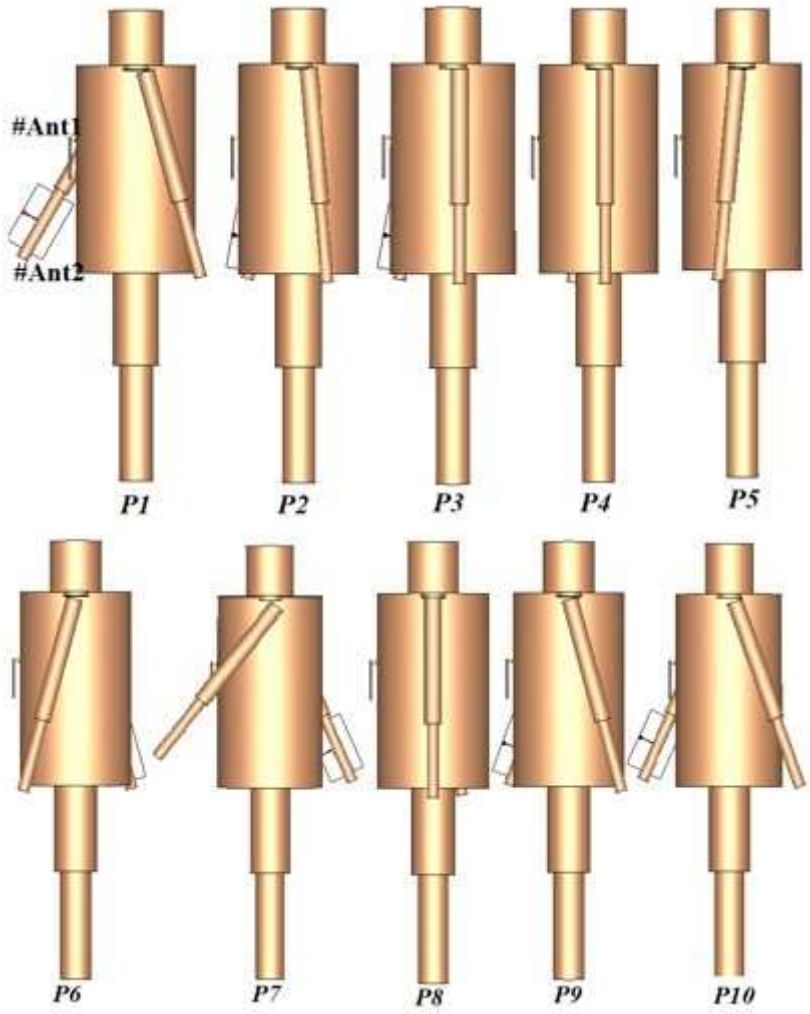

Fig. 4.7 Frames P1-P10 illustrating the double arm swing activity.

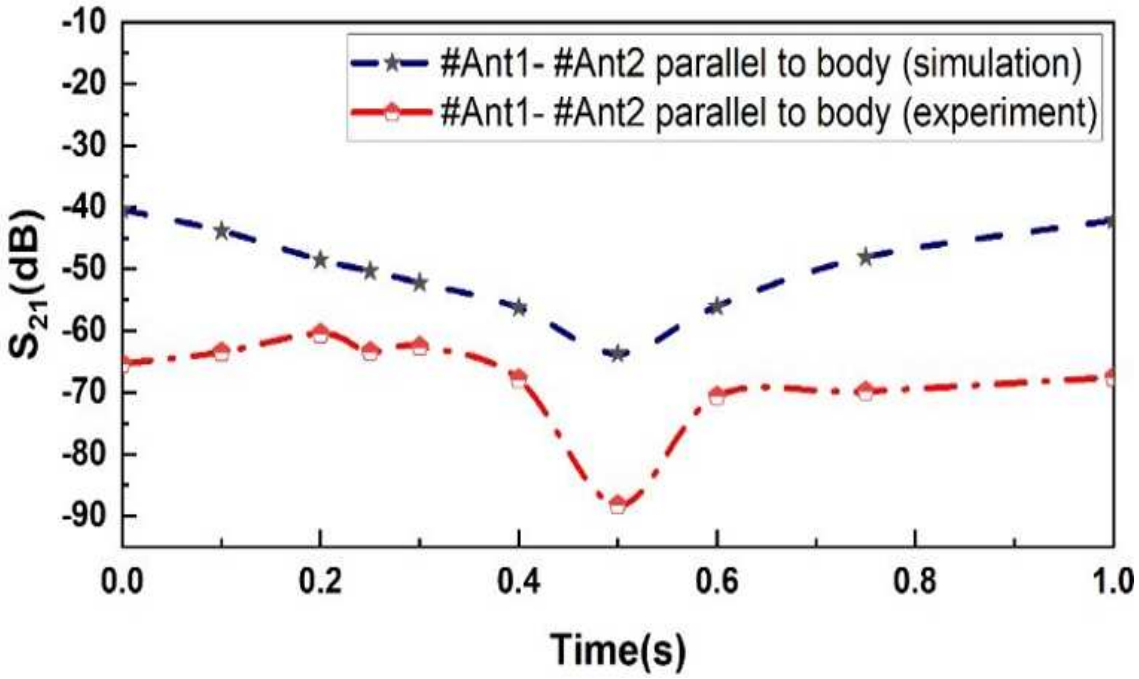

Fig. 4.8 Transmission characteristics of double arm swing activity for single cycle.

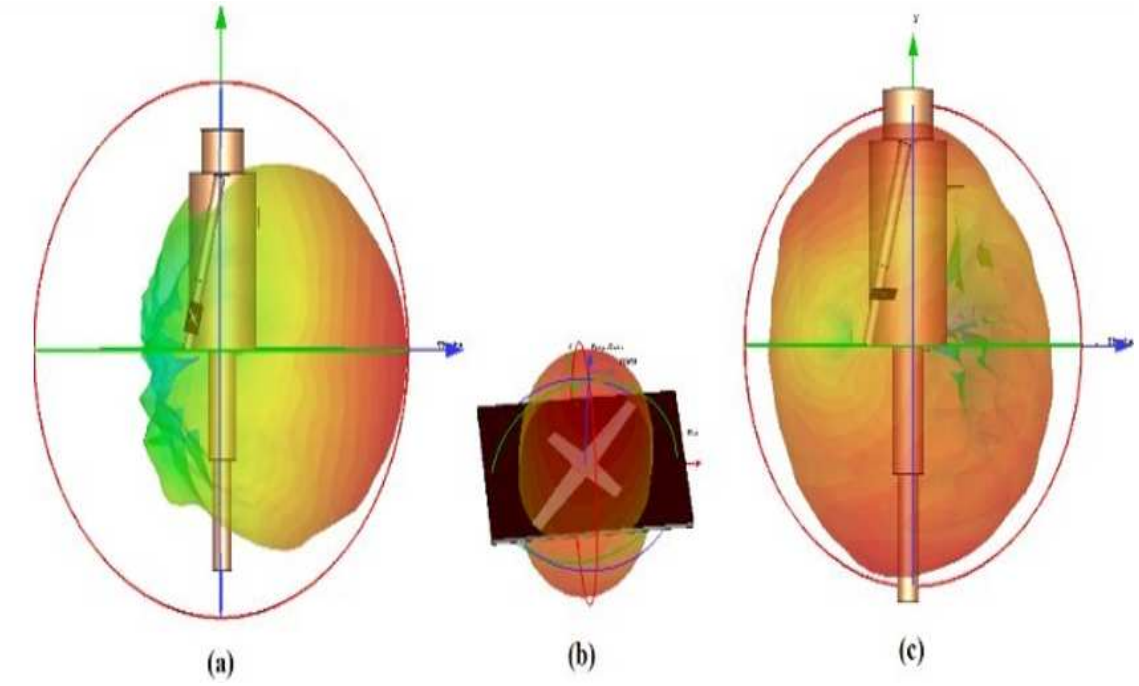

Fig. 4.9 (a) *Ant*1 and *Ant*2 parallel to the model (b) Radiation pattern of the CSA and (c) *Ant*1 and *Ant*2 perpendicular to the model.

of height 157 cm and weight 54 kg. When CSA is fixed parallel to the lossy human body,

Fig. 4.10 (a) $Ant1$ and $Ant2$ parallel to the volunteer (b) $Ant1$ and $Ant2$ perpendicular to the volunteer

the efficiency is significantly reduced as seen in Fig.4.11. Placement of CSA parallel to the human body surface is more efficient for a communication system with ON-Body to OFF-Body set-up rather than ON-Body to ON-Body scenario.

Table 4.3 Dimensions of the four-year child Model

Parameter	Dimension (mm)	Parameter	Dimension (mm)
R_h	70	L_h	100
R_l	15 .	L_l	160
R_s	27	L_S	5
R_th	45	L_th	250
R_u	18	L_u	245
R_c	30	L_c	250
R_t	110	L_t	400
L_m	1000		

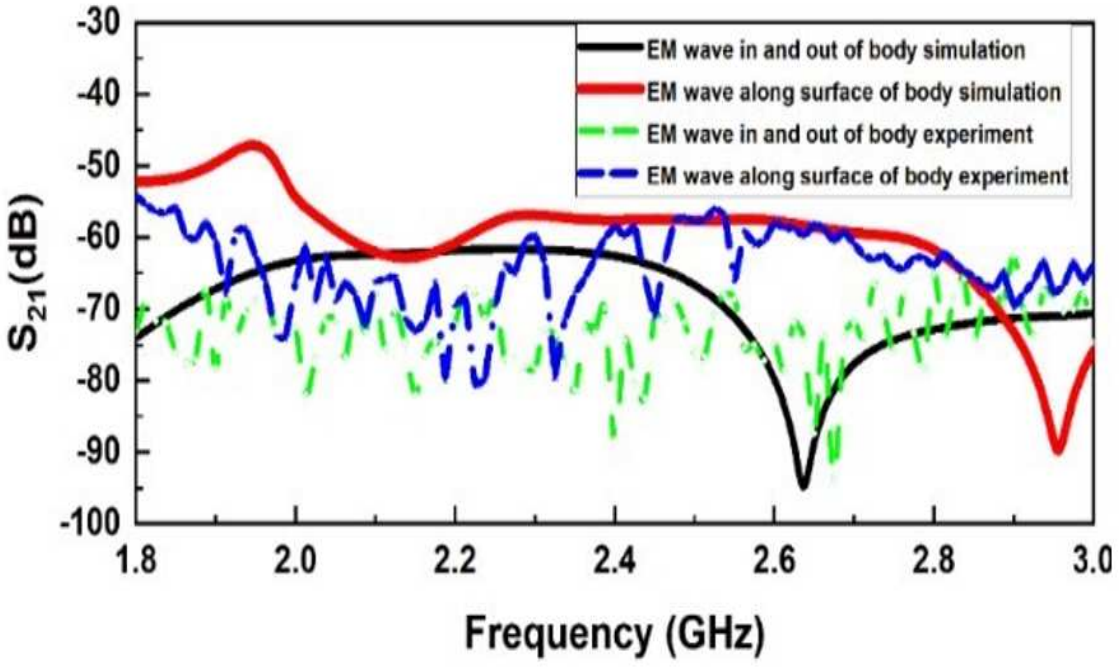

Fig. 4.11 Transmission characteristics with varying antenna orientation.

4.3 ON-OFF Body Analysis for Smart Bag

With the development of Internet of Things (IoT), Body area network will create a big leap in the near future [1]. Wearable devices are an essential part of IoT [2]. Antenna is one essential component of wearable devices as the efficiency of wireless link depends on them[2]. The transmission characteristics changes with varying position of antenna.A 'Smart Bag' can be made if an RF transmission system is inbuilt on the bag. The Smart Bag can send its location to customer mobile through cellular communication which will helps him/her identify the location of bag.This section deals with the ON-OFF Body analysis by varying the position of antenna which in turn changes the transmission characteristics. This analysis can be extended to different materials of bag as well as on different household and consumer equipment which are expected to be a part of the Internet of Things (IoT).

4.3.1 System Simulation

Figure 4.12 shows the bag model designed in SOLIDWORKS [84] which is used for ON-Body to OFF-Body analysis.

The bag modelled in SOLIDWORKS [84] and then imported to CST [56] for doing the analysis. The material used for bag model simulation is cotton material with dielectric constant ε_r = 1.9, $\tan\delta = 0.092$.

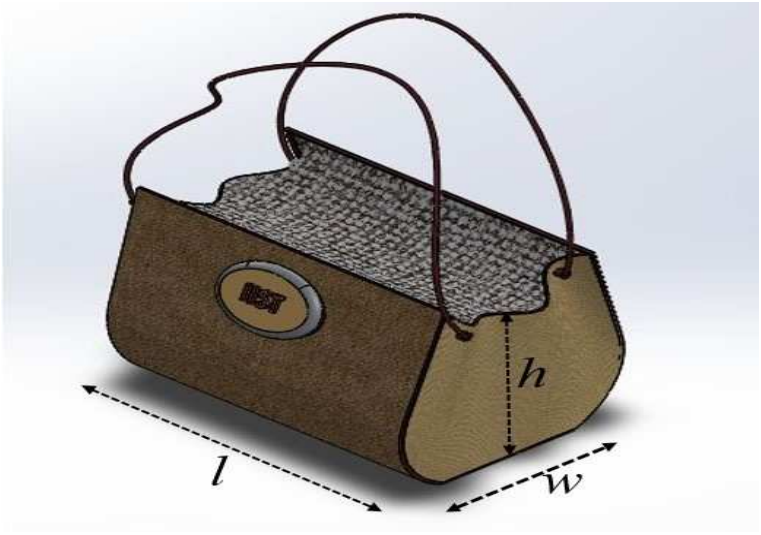

Fig. 4.12 Bag model simulated in SOLIDWORKS.

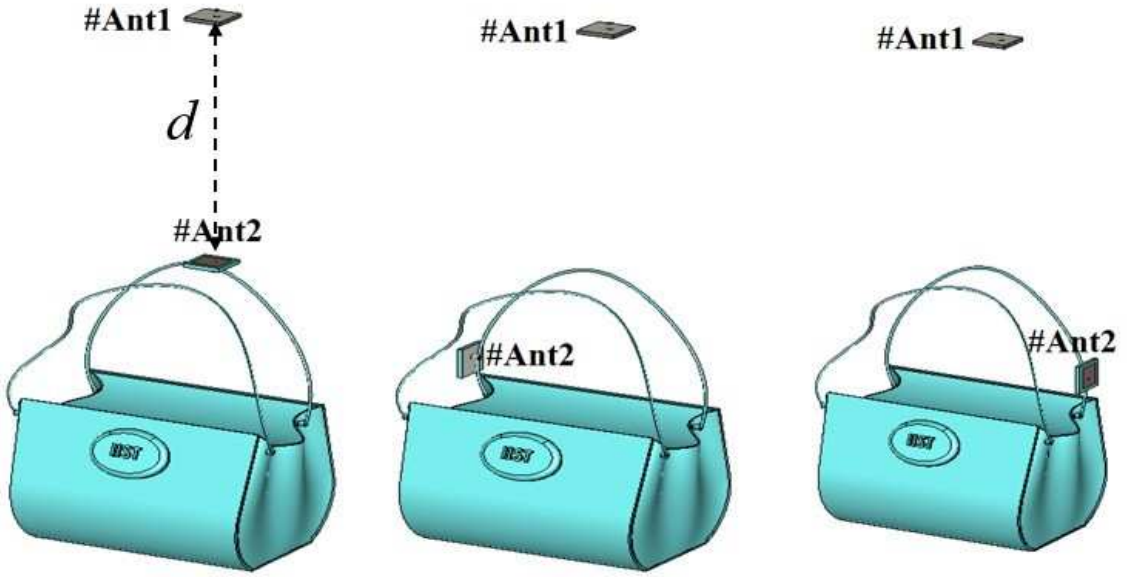

Fig. 4.13 Smart Bag system model: (a) #Ant1 and #Ant2 are in line of sight, (b) *Ant*2 is positioned on left side of #Ant1, and (c) #Ant2 is positioned on the right side of #Ant1.

Fig.4.13 depicts the system model of 'Smart Bag' (Bag integrated with antenna) simulated in CST for ON-Body to OFF-Body analysis. The antenna is placed on the bag strap providing the user flexibility to change the position of antenna on the bag thereby improving transmission with OFF-Body antenna. #Ant2 is the transmitting antenna positioned on cloth bag and #Ant1 is the receiving antenna in free space. #Ant1 is at a distance d = 21 cm from #Ant2 when they are in line of sight (LOS).

4.3.2 Antenna Design

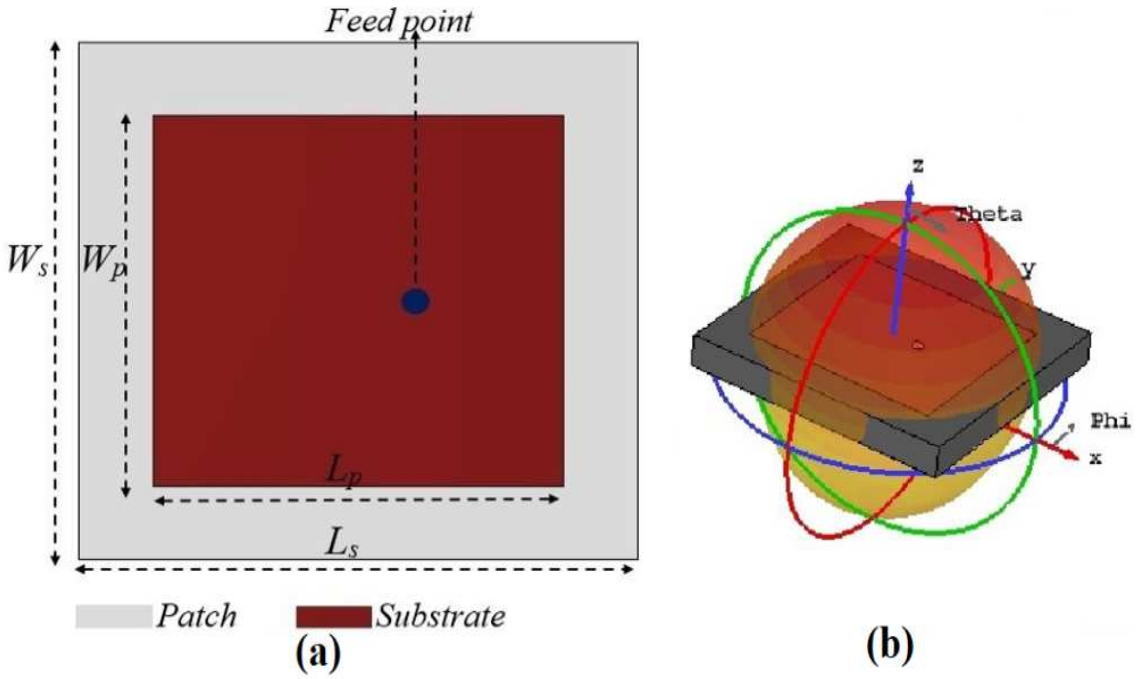

Fig. 4.14 (a) Schematic diagram of the antenna, (b) 3D radiation pattern of the antenna.

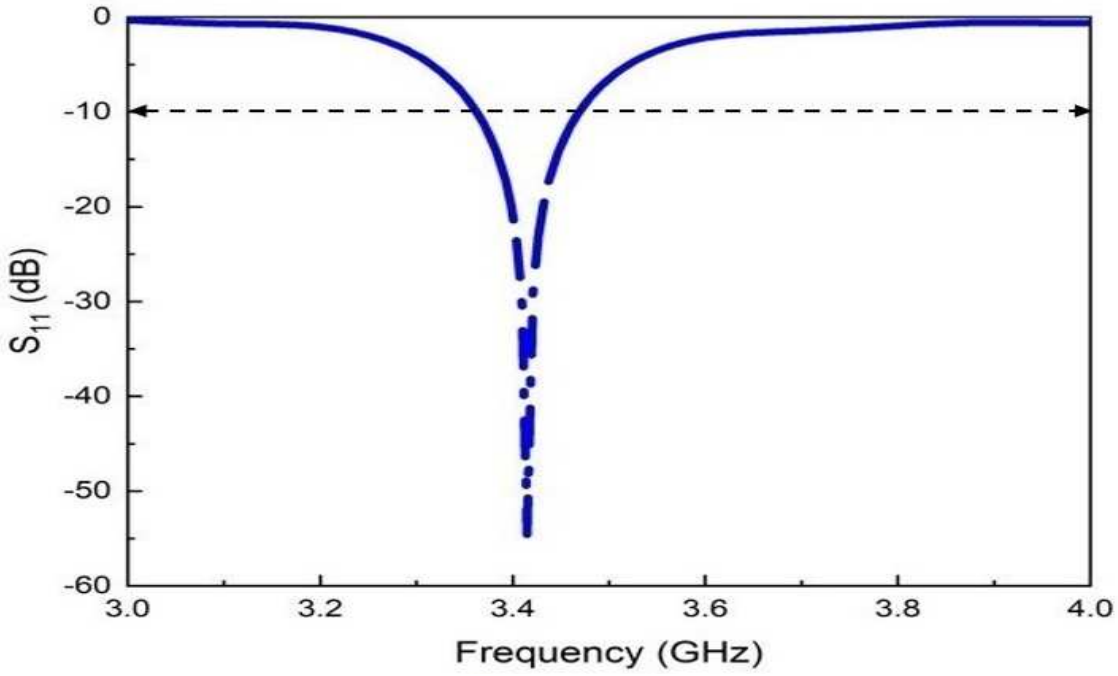

Fig. 4.15 S_{11} of the antenna.

#Ant1 and #Ant2 used in the 'Smart Bag' set-up is a rectangular microstrip patch antenna (MSA) printed on the FR4 substrate (ε_r = 4.4) with dimensions, L_s = 26 mm, W_s = 24 mm and h = 1.5 mm operating at 3.45 GHz. The schematic diagram of the MSA is as seen in Fig.4.14(a). Figure 4.14 (b) depicts the 3D radiation pattern of the MSA. The reflection coefficient of the MSA is as depicted in Fig.4.15. The dimensions used in bag and antenna design are given in Table-4.4.

Table 4.4 Dimensions of the Smart Bag Model

Parameter	Dimension (mm)	Parameter	Dimension (mm)
l	154.2	w	72.3
h	118 .	L_s	26
W_s	24	L_p	19
W_p	17.25	H_s	1.5

4.3.3 Results and Discussion

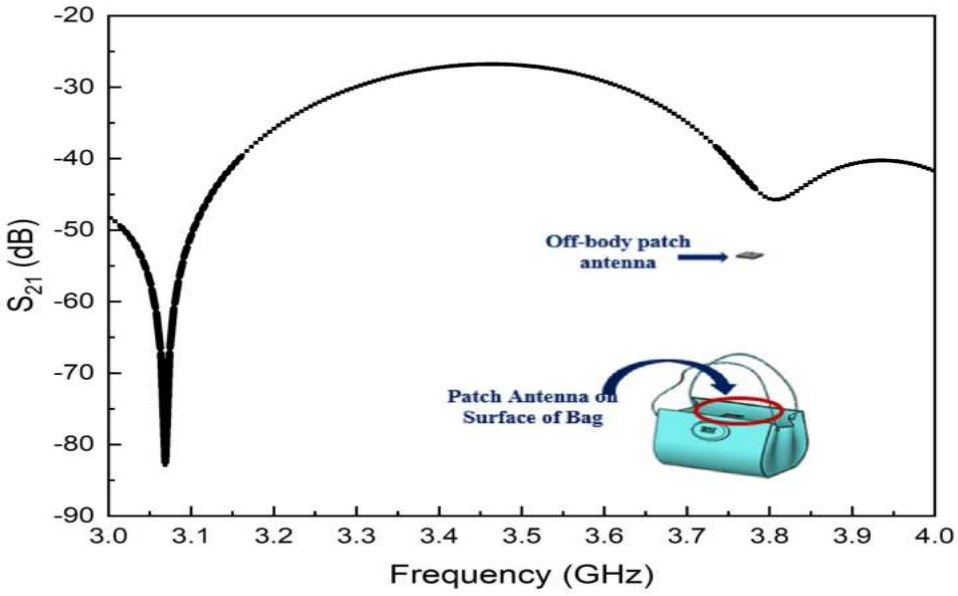

Fig. 4.16 Transmission Characteristics when #Ant2 is kept on the surface of bag model and #Ant1 in free space at d = 21 cm away from #Ant2.

The S_{21} when #Ant2 is positioned on the bag surface (ON-Body antenna) and #Ant1 functioning as OFF-Body/free space antenna is depicted in Fig.4.16.Figure 4.17 depicts the

S_{21} when #Ant2 is placed on the bag handle. Positioning the Ant2 on handle allows the user to move the antenna along the handle to the top, left and right unlike on any other part of the bag. Simulation of 'Smart Bag' is done for three scenarios: (i) #Ant2 on top (LOS with #Ant1) (ii) #Ant2 on left (NLOS with #Ant1) and (iii) #Ant2 on right (NLOS with #Ant1) of the bag model. In all these cases #Ant1 is fixed at distance d from the bag top.

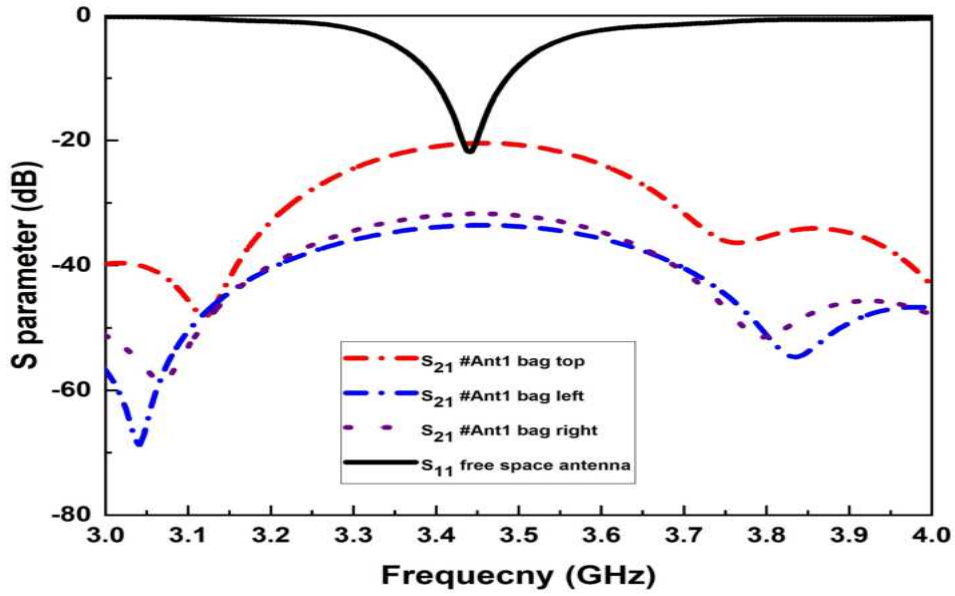

Fig. 4.17 Transmission characteristics of various positions of Ant2 with Ant1.

The reflection coefficient and transmission characteristics of the study for three scenarios are depicted in Fig.4.17. The maximum transmission occurs in case(i). The transmission value is lowered by 10 dB in case (ii) and (iii) which shows the requirement of flexibility for positioning the antenna.

4.4 Smart Bag on Human Body model

The 'Smart Bag' is then integrated with twelve cylinder body model to investigate the effect of human body on transmission characteristics. #Ant4 similar to the #Ant3 is located at a distance 760 mm from #Ant3.Figure 4.18 shows the twelve-cylinder body model integrated with 'Smart Bag'.

The S_{21} is analyzed with and without the human body model. Fig.4.19 depicts the S_{21} with and without using human body model.The value of S_{21} for MSA operating at a frequency

of 3.45 GHz is found to be -30 dB when antenna is not integrated on human body model. As observed from the Fig. 4.19, S_{21} is notably lowered when 'Smart bag' is integrated with twelve-cylinder body model. A lowering of 6 dB is found at 3.45 GHz which indicates that the lossy human body further weakens the transmission values. This indicates that a very efficient ON-Body antenna is required for ON-OFF Body communication considering human interference.

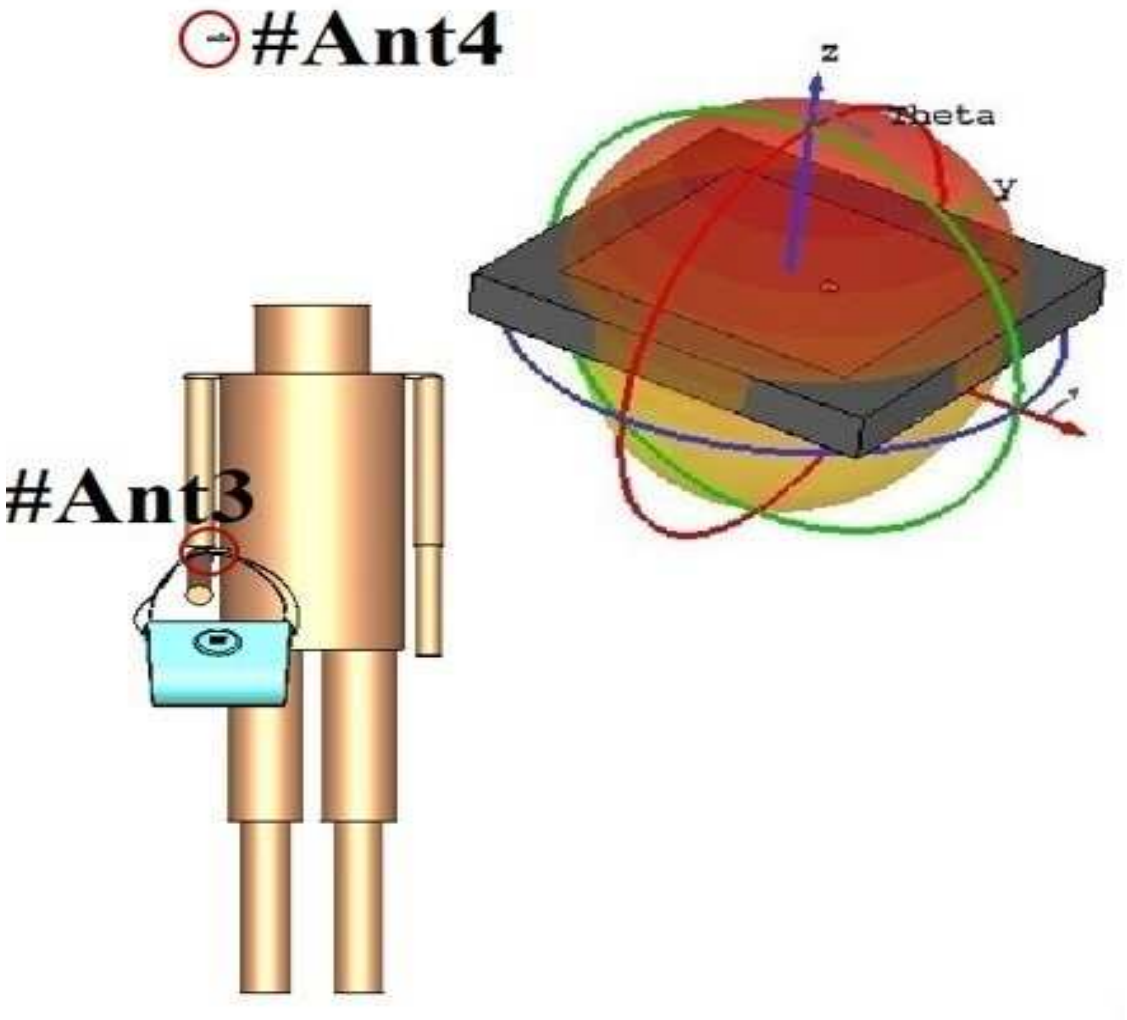

Fig. 4.18 Simulation set-up for twelve-cylinder phantom model integrated with a 'Smart Bag'.

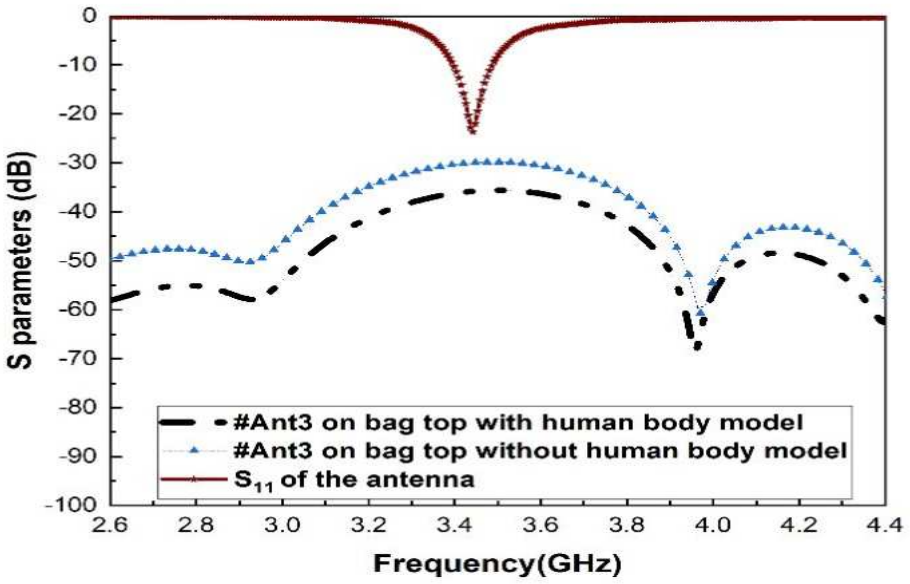

Fig. 4.19 Transmission characteristics of patch antenna on 'Smart Bag'.

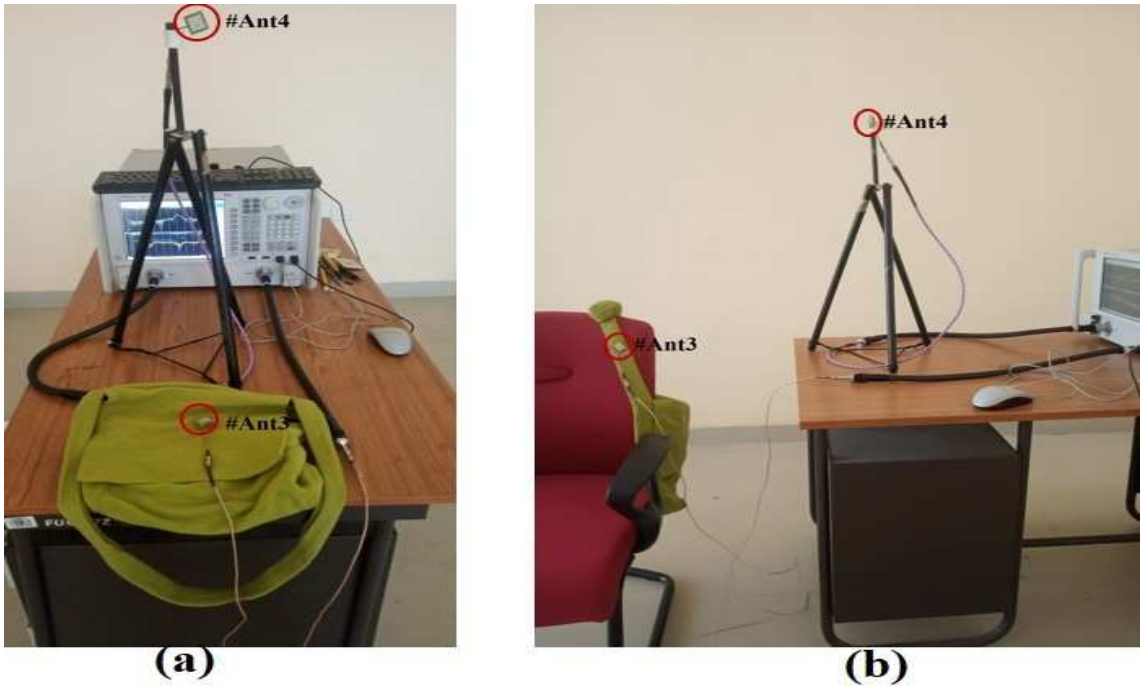

Fig. 4.20 Experimental set-up of 'Smart Bag' when #Ant3 and #Ant4 are (a) in line-of –sight, and (b) not in line-of sight.

4.4.1 Experimental analysis of ON-OFF Body Transmission

The ON-Body to OFF-Body analysis set-up is arranged with Ant3 as ON-Body antenna fixed on the cotton bag. This is performed for two cases: i) #Ant3 on a bag surface, in LOS with #Ant4, which is the OFF-Body antenna and ii) #Ant3 on a bag handle and #Ant4 as OFF-Body antenna. In the set-up ii) Ant3 and Ant4 are not in LOS as in case of set-up i). The OFF-Body antenna, #Ant4 is positioned on a tripod stand so as to make the vertical span between #Ant3 and #Ant4 64 cm. The picture of the experimental set-up is as seen in Fig.4.20.

The S_{21} is plotted for different cases and is as seen in Fig.4.21. At 3.45 GHz the observed transmission value is -42.5 dB for case i while it reduces to -55.5 dB in case ii. This is due to the fact that the #Ant3 and #Ant4 in NLOS are not positioned to attain maximum radiation in case ii.

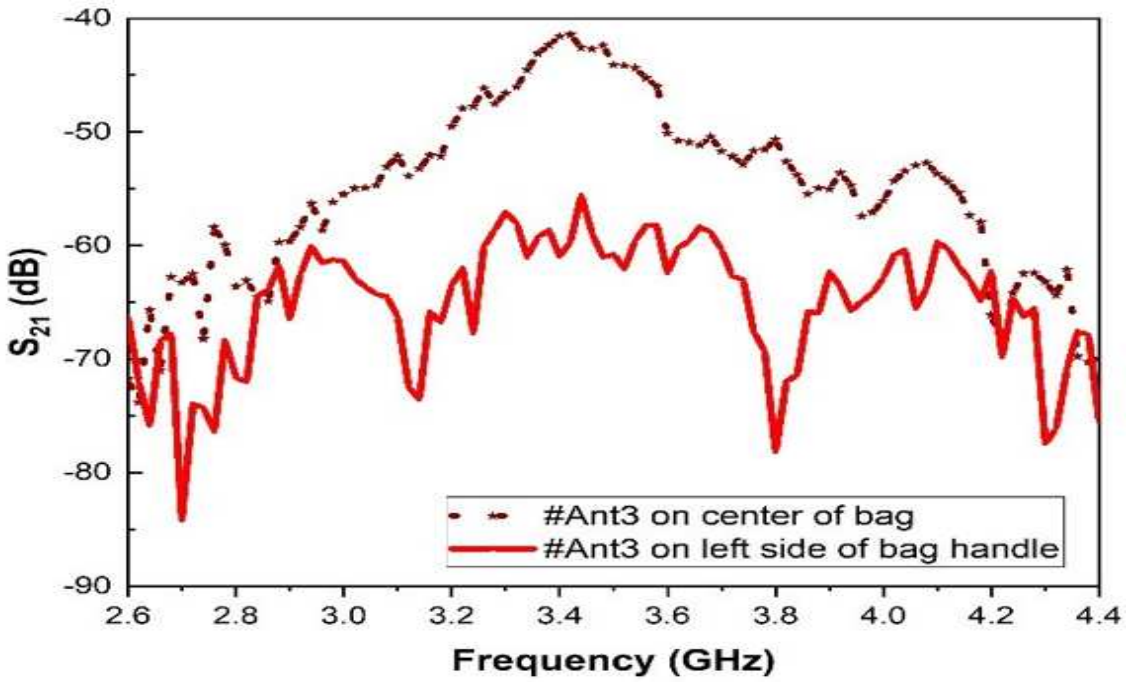

Fig. 4.21 Transmission characteristics of 'Smart Bag' when #Ant3 and #Ant4 are (a) in line-of –sight, and (b) not in line-of sight.

4.5 Conclusion

The twelve-cylinder phantom model presents an exciting horizon for EM wave analysis as it can model rest and dynamic postures of human body. Varying the dimensions of these models

in synthetic environments allows to supplement or may even substitute the requirement of experiment on human volunteers in complex scenarios. Elaborations of the analysis can be performed by using heterogeneous human body model rather than homogeneous body model. This model finds its application in ON-Body to ON-Body as well as ON-Body to OFF-Body transmission study and can be broadly used in EM wave analysis around/along body as it can be replicated easily.

Chapter 5

ON-Body to ON-Body analysis: Effect on UWB Transmission Characteristics

The present era finds the extensive research in the area of body area network systems as they find versatile applications in the field of sports, health care systems, media [35], indoor and outdoor data transmission system [86] and many more. A very low transmission power is an important requirement of wearable wireless devices. UWB (ultra-wideband) communications gives high data rates along with low power spectral densities in comparison with the MICS and 2.4 GHz ISM band [87]. UWB has large bandwidth and provides robustness to jamming and has low detection probability. The requirement of much lower transmit power provides increased battery life for wearable devices. [87]. Hence, UWB antennas finds applications for body-centric wireless networks [87]. Many features of the UWB BCWC in stochastic as well as experimental realms are found in literature [87]-[97]. The parameter explored by different research groups for UWB channel model includes, Channel Impulse Response (CIR), which is a significant Figure of merit for time domain characterization of an Ultrawideband system [91]-[97].

In this chapter, following simulation and experiment based approach for investigating ON-Body to OFF-Body Channel Modeling is considered: (i) a simulation methodology to analyze the ON-Body to OFF-Body channel using UWB monopole antenna (Ant1) considering the time domain characteristics of the transmit/receive antenna using [56],[98] , (ii) an indoor line of sight (LOS) ON-Body to OFF-Body measurement procedure using three antennas (ε_r = 2.33 and $tan\delta$ = 0.00012) operating in the FCC recommended bandwidth of 3-10 GHz. Various antennas such as, an UWB monopole antenna (L × W = 50mm × 60mm) with circular monopole diameter of 25mm (Ant 1) , a Vivaldi antenna (L × W = 35mm × 45 mm) (Ant 2), and an UWB monopole of dimensions L×W = 22mm × 40mm (Ant 3) are considered for experiment based investigation. The method of characterizing the transient Figures of

Merit presented in this chapter is a stepping stone to achieve a comprehensive approach towards channel modeling as well as analysis with short pulse electromagnetics. The novelty of this method lies in the fact that an ON-Body UWB channel can be analyzed in terms of pulse dispersion. The proposed method after testing with NLOS, reverberant, and multipath scenarios can be used as a simplified method for estimating UWB ON-Body to OFF-Body channel characteristics without considering stochastic or path loss model.

5.1 Antenna and Phantom Model

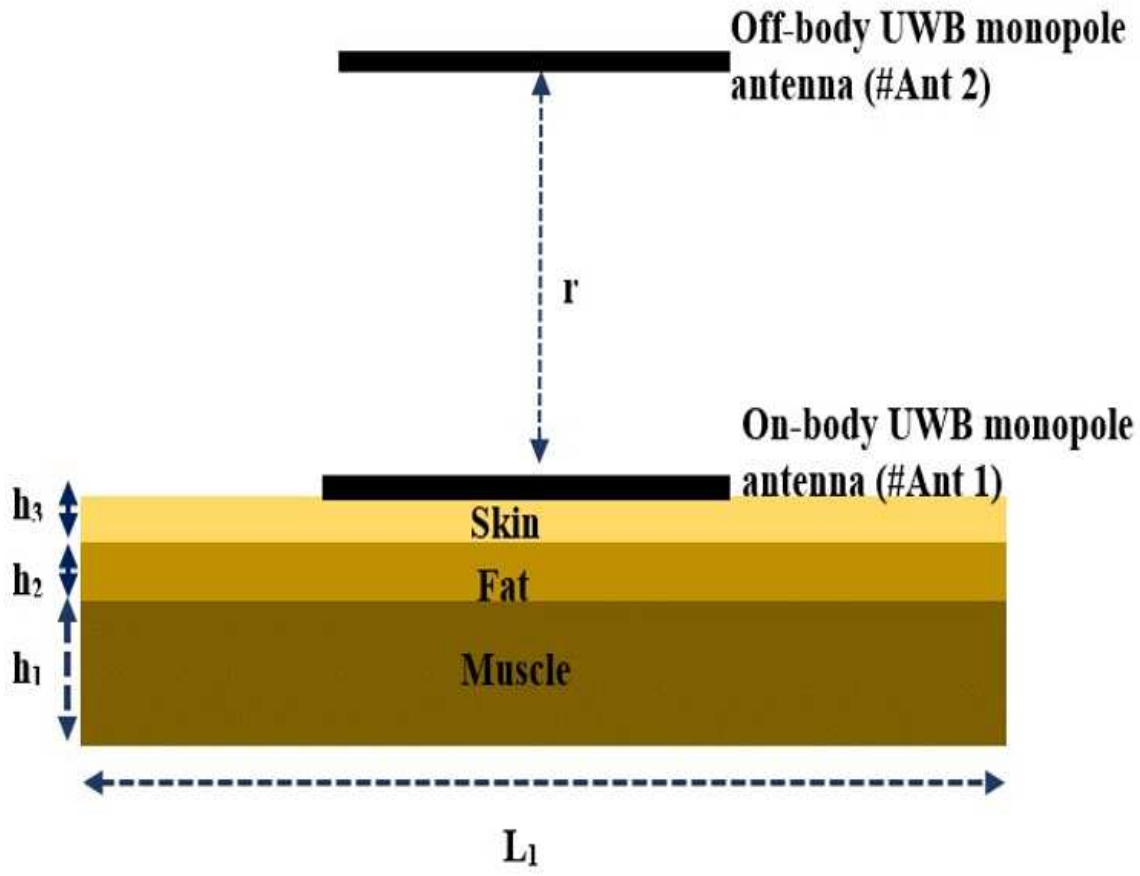

Fig. 5.1 Schematic diagram depicting position of the UWB monopole Tx on a three-layered human phantom arm model and UWB monopole Rx at far field distance r ($h_1 = 5$ mm, $h_2 = 10$ mm, $h_3 = 30$ mm, $L = 100$ mm).

Two similar UWB antennas (Ant1) acts as transmitting (Tx) and receiving (Rx) antennas for ON-Body to OFF-Body analysis. The OFF-Body antenna acts as the Rx antenna while Tx is located on the body. The placement of the Rx is in the far field of the Tx antenna. The

far field distance is measured by the thumb rule $\frac{2D^2}{\lambda}$, where D is the longest dimension of the Ant1 and λ is the wavelength which corresponds to the lowest frequency of operation. The three layered rectangular phantom model is designed considering effective permittivity and conductivity of each of the layers at 5.5 GHz: The top layer is the epidermal skin layer with a permittivity $\varepsilon_r = 35$ and $\sigma = 3.46$ S/m, the middle layer is the fat with permittivity $\varepsilon_r = 4.9$ and $\sigma = 0.27$ S/m, and the bottom layer is the muscle with a permittivity of $\varepsilon_r = 49.4$ and $\sigma = 4.8$ S/m [96],[99]. The Tx Ant1 is placed on the top epidermal layer as a wearable antenna and RX Ant1 in free space. The schematic diagram of the set-up described is as seen in Fig.5.1.

5.2 Results and Discussion

5.2.1 Simulation Results and Time Domain Analysis

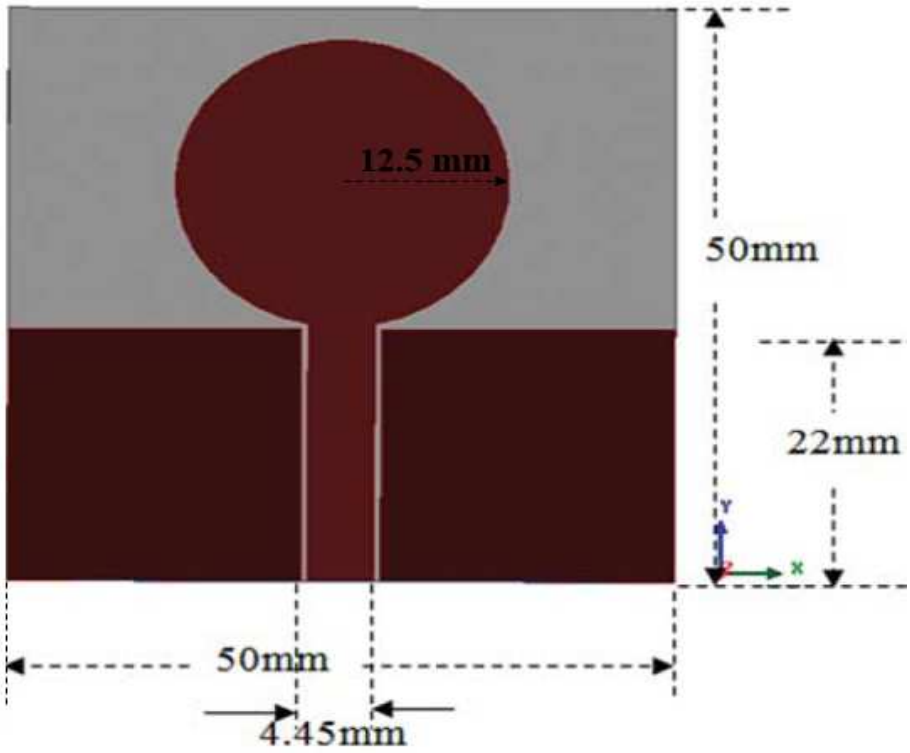

Fig. 5.2 Schematic of the standalone monopole antenna

An approach to characterize the channel in time domain is performed here. To begin with, the stand-alone UWB monopole, depicted in Fig 5.2, is analyzed in the time domain. The reflecion coefficient of the UWB monopole is as shown in Fig.5.3. The study provides

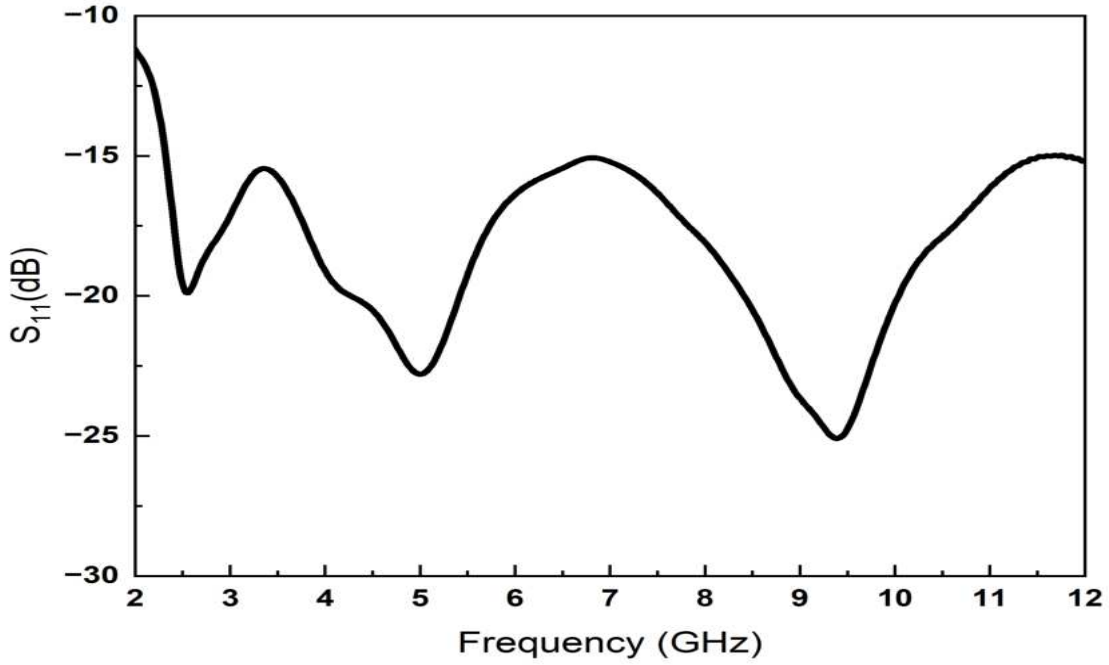

Fig. 5.3 S_{11} characteristics of the stand-alone monopole.

a relative interpretation on the effect of using same UWB monopole in a Tx-Rx system simulation in terms of pulse dispersion when UWB monopole (Ant1) is placed on the rectangular phantom model as a Tx antenna and as an OFF-Body Rx antenna set apart by a free space channel. For the analysis, the input signal for ON-Body Tx Ant1 is a narrow monocycle pulse which has a pulse width of 400 ps without any inherent ringing. It is to be noted that every monocycle pulse width cannot make the antenna radiate, a step-by-step procedure should be followed to determine the required pulse width [100]. The time domain parameters like radiated electric field sensed by a far field probe and its associated ringing time interval δ_r, and group delay characteristics are portrayed in Fig.5.4 and Fig. 5.5 respectively. The radiated field of in case of a stand-alone UWB monopole is the inverted second temporal derivative of the input monocycle as shown in Fig. 5.4 but its nature changes when it is positioned on the three layered rectangular phantom model as can be observed in Fig.5.6.

The group delay of the system changes as depicted in Fig. 5.7 as compared to stand-alone monopole. Figure 5.8 (a) depicts the block diagram for computing impulse response of a system and Fig.5.8(b) depicts the transfer function of Ant1 on three layered phantom model.

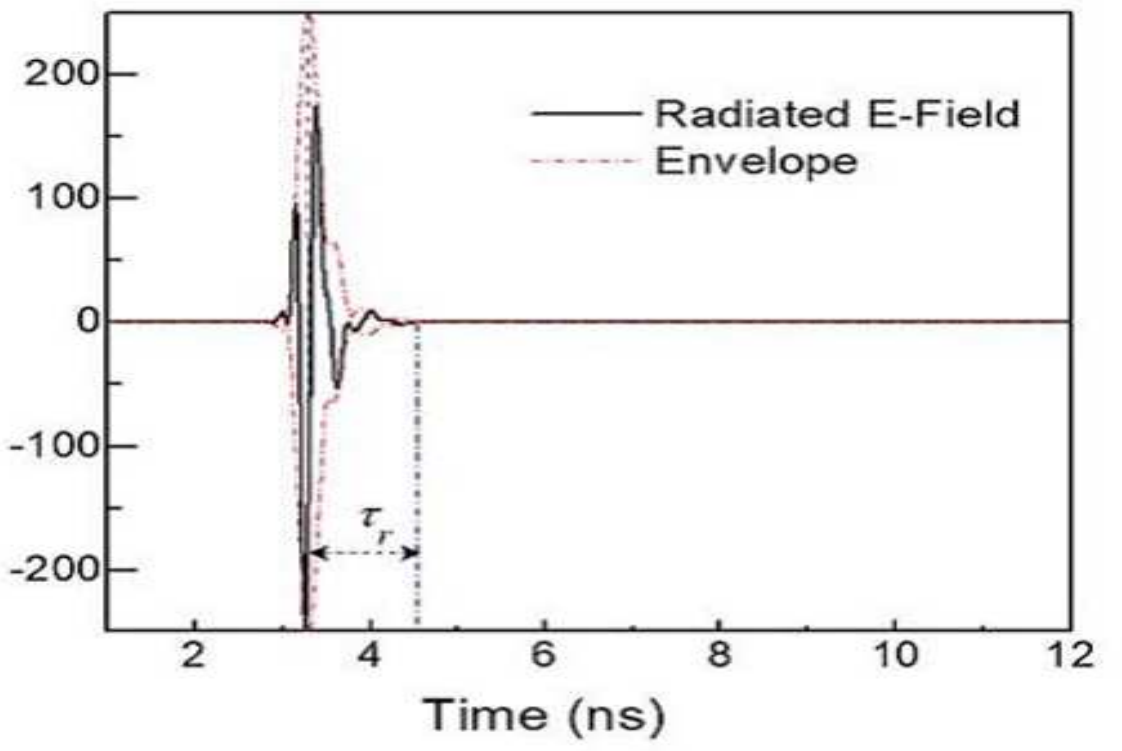

Fig. 5.4 Radiated Electric field; ringing interval $\delta_r = 1.58$ ns.

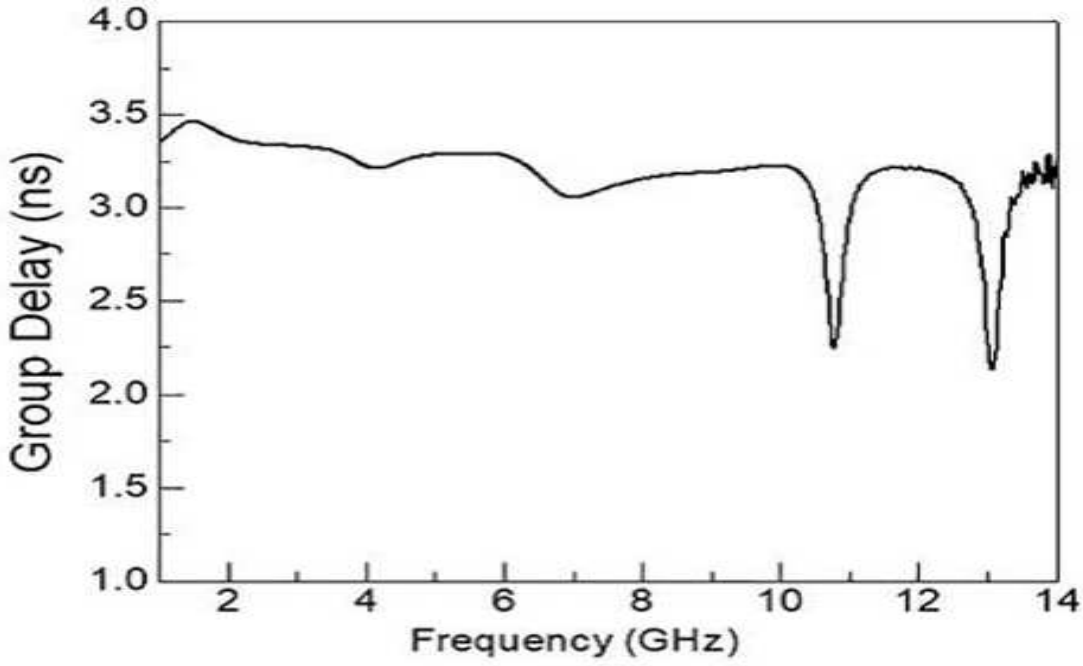

Fig. 5.5 Group delay computed using MATLAB.

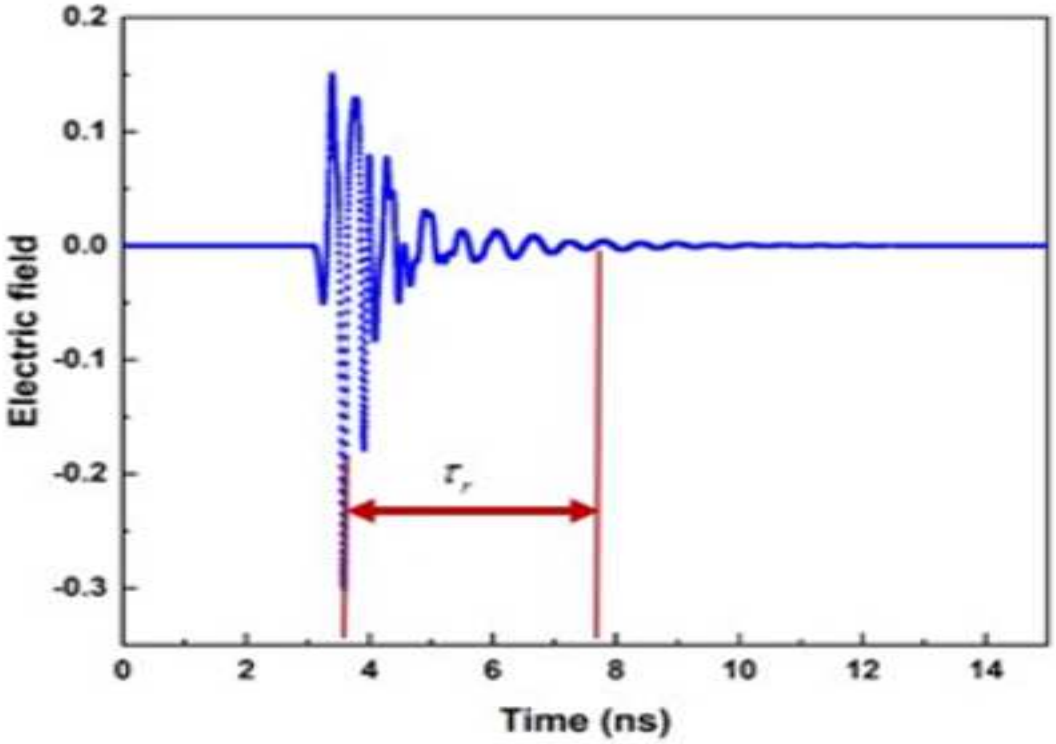

Fig. 5.6 Probe signal with ringing time interval of 4.33 ns

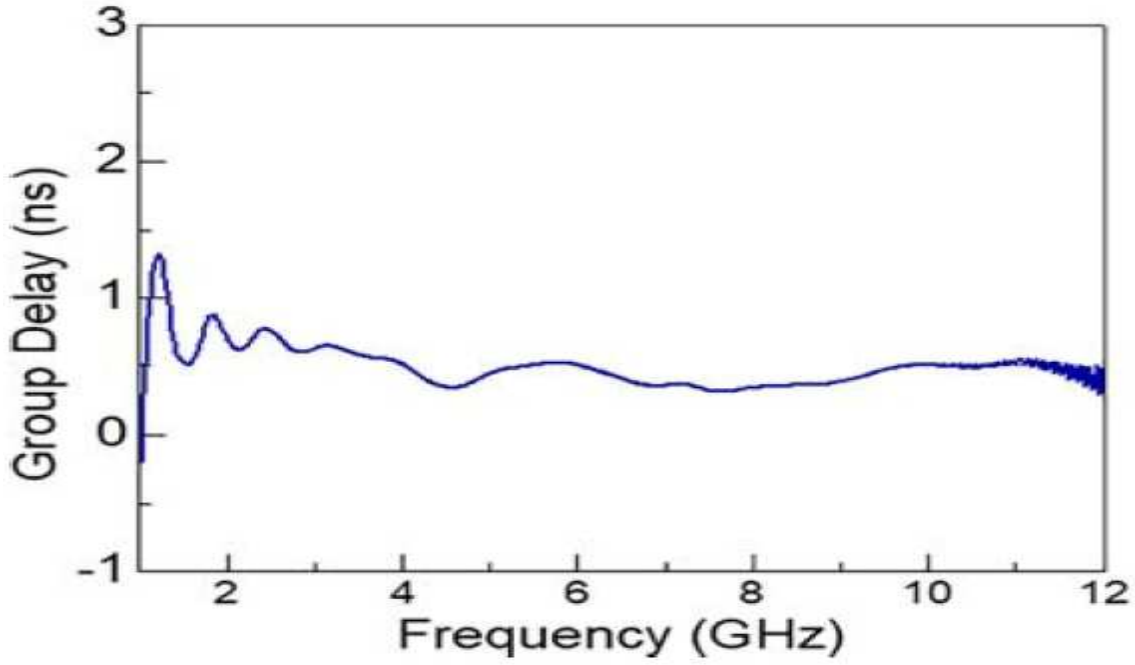

Fig. 5.7 Group delay computed using MATLAB.

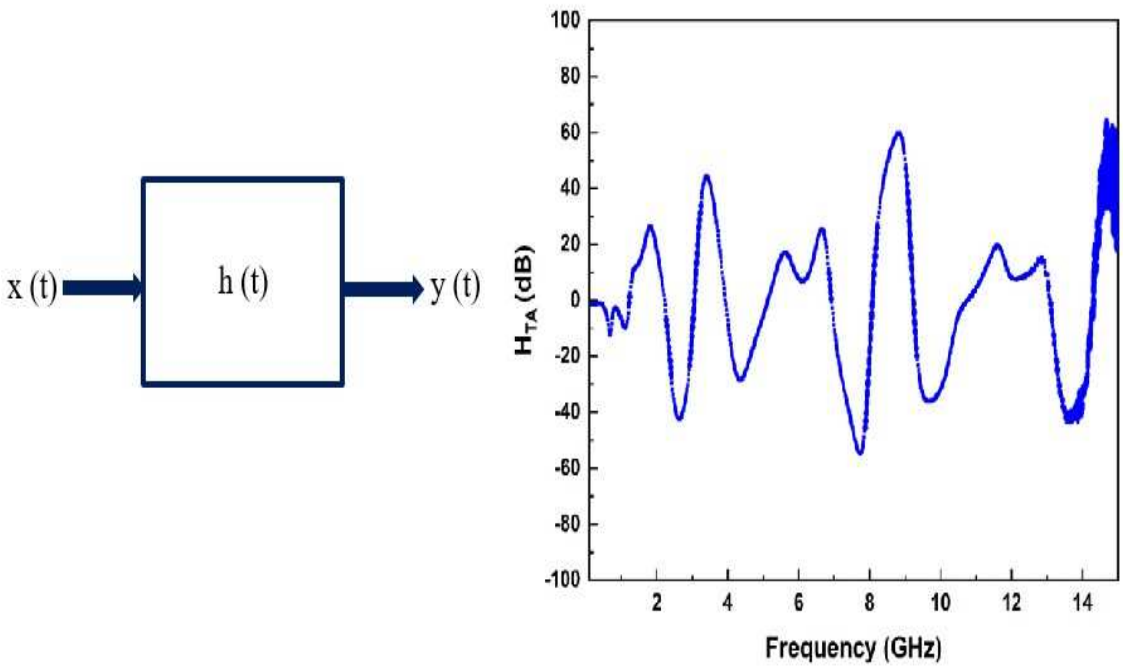

Fig. 5.8 (a) Block diagram for Impulse response of a system, and (b) Transfer function of antenna on the phantom

5.3 Experimental Findings

Experiment is performed for three cases:i) The Tx Ant1 is kept ON-Body and the Rx Ant1 as OFF-Body antenna. The Rx Ant1 is kept in the near field of Tx Ant1 in this case, ii) Tx Ant1 as ON-Body antenna and Rx Ant1 as OFF-Body. Here, the Rx Ant1 is located in the far field of Tx Ant1 iii) Tx Ant1 as ON-Body antenna and Rx Ant1 as OFF-Body antenna. The Rx Ant1 is in the far field and characteristics is studied by varying its elevation angle. The measurement set-up used is as seen in Figure.5.9 (a), where the Tx Ant1 antenna is fixed on the palm of a female volunteer with height 157 cm and weight 54 kg and Rx Ant1 is placed in free space. Experiment is conducted for near field and far field arrangement by varying the position of Rx Ant1 with respect to Tx antennas to obtain the transmission characteristics in both scenarios. Measured values of transmission vary with frequency for different elevation angles in the far field and near field region as depicted in Figure. 5.9(b). This data is then processed in MATLAB to estimate the group delay characteristics depicted in Figure.5.9(c).The negative slope of transmission phase angle with frequency results in group delay, given by,

$$\delta_d = -\frac{\delta\Phi}{\delta\omega} \tag{5.1}$$

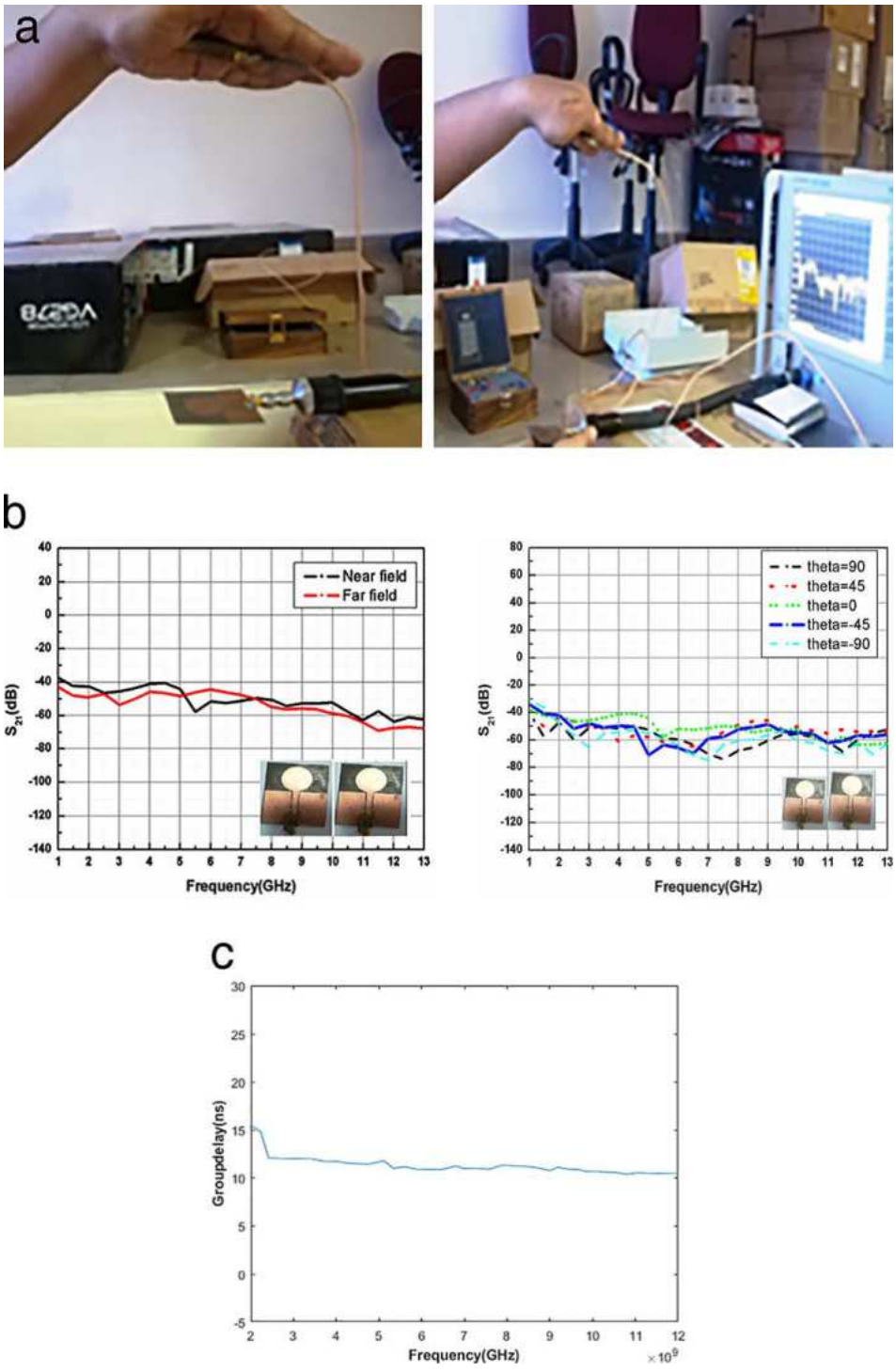

Fig. 5.9 (a) Experimental setup showing TX Ant1 on palm of the volunteer and RX Ant1 as OFF-Body antenna.(b) S_{21} characteristics for different cases: near-field, far-field, and varying elevation angles.(c) Computation of group delay from complex S_{21} data obtained from experiments.

where ϕ represents the phase angle and ω is the frequency [88]. Even though a good confirmation between the nature of transmission values and group delay characteristics are obtained from simulated and measured data, the magnitude scale is different from that in simulation for measured S_{21} and group delay characteristics. This might be due to the spurious reflections in the experimental setup that occurs when the OFF-Body Ant1 Rx is given external support to maintain stability.

5.4 Conclusion

The EM wave radiation analysis in case of UWB antenna systems for ON-Body to OFF-Body channel modeling are systematically analyzed in simulation as well as with experiments in this chapter. These primary studies gives some representative results for channel modelling. The simulation and experimental data helps to analyze the transfer function of the UWB systems.

Chapter 6

Conclusion and Future Scope

Current desertion, divided into five main chapters, have contributed on the investigation of propagation of electromagnetic waves around the human body, study of transmission characteristics in ON-Body to ON-Body scenario as well as ON-Body to OFF-Body scenario and design of antenna for associated applications. The requirement of performance enhancement of antennas is also evident from the study. This serves as the motivation and prime factor for the current research work. The main objective of this thesis is to investigate the propagation of EM waves around the human body and enhancement of the gain of OFF-Body antennas. Following are the main contributions of our research work which makes the major part of the thesis:

- Technique for gain enhancement in linearly and circularly polarized microstrip antenna using a hybrid substrate is proposed.
- Technique for gain enhancement in Dielectric resonator antennas using metasurface lens is proposed. The positioning of the MSL above the DRA is discussed theoretically. This is realized and experimentally validated.
- Analysis of creeping waves on a cylindrical phantom model is studied using simulation as well as experiments.
- A twelve-cylinder body model is proposed which can be used for modelling rest as well as different dynamic activity of humans. This model is used for the study of double arm swing activity as well as to analyze the transmission characteristics of a patch antenna integrated on a bag model in presence of human body model.
- A line of sight (LOS) scenario for ON-Body to OFF-Body transmission characterisyics is simulated using a three layered phantom model with two similar UWB monopole

antennas functioning in the bandwidth of 3-10 GHz to provide the time domain characterization of the channel. Experiments corresponding to the simulations are also carried out. Multiple experiments at different positions of the body gives an insight to the variation transmission characteristics of the antenna.

The work can be extended to get more insights on EM wave propagation on human body. These include:

- An up-gradation for twelve cylinder body model can be attained by using three layers namely skin, muscle and fat in each cylinder with their characteristics and varying sizes.
- The simulations can be replicated with different body sizes and positions for 'n' number of times and understanding gained from this can be used for design of efficient on-body antennas.
- Simulations and experiments with the efficient antennas will give a better understanding towards channel modelling.
- Collection of baseline data from healthy individuals as reference will provide a better understanding of motor disabling diseases including conditions caused by various diseases like Parkinson's, physical injury as well performance of athletes.

References

1. Y. Wang, J. Zhang, F. Peng, S. Wu, “A glasses frame antenna for the application in Internet of Things” *IEEE Internet Of Things Journal*, Vol. 6, NO.5, PP. 8911-8918, October 2019.

2. K.N. Paracha, S. Kamal Abdul Rahim, P. Jack Soh, M. Khalily “Wearbale Antennas: A review of Materials, Structures and Innovative Features for Autonomous Communication and Sensing” IEEE Access Vol.7 PP. 56694-56712, May 13, 2019.

3. D. Besnagan, Y. Li, “Investigation of Creeping wave propagation around the human head at ISM frequencies” IEEE Antennas and Wireless Propag. Letters, Vol. 16, PP. 2767-2770, August 2017.

4. V. Mishra , A. Kiourti ,“Wrap-Around Wearable Coils for Seamless Monitoring of Joint Flexion” IEEE Transactions on Biomedical Engineering, Vol. 66, No. 10, PP.2753-2760, October 2019.

5. G. Lee, B. Garner, Y. Li, "Simulation and Measurement of electromagnetic wave propagation on Dynamic Human Bodies” IET Microwave Antennas and Propag., Vol.11, No.10, PP. 1347-1355.

6. Y. Li, D. Xue, E. Forrister, G. Lee, B. Garner, Y. Kim, “Human Activiy Classification Based on Dynamic Time Wrapping of an On-body Creeping wave signal” IEEE Transactions on Antennas and Propag., VOL.64, NO.11, PP.4901-4905, November 2016.

7. P. S. Hall, “Antennas and Propagation for Body Centric Communication” IET Seminar on Antennas and Propagation for Body Centric Wireless Communication, London, 24 April 2007.

8. C. Liu, Yong-Xin Guo, R. Jegadeesan, and S. Xiao, “In Vivo Testing of Circularly Polarized Implantable Antennas in Rats” IEEE Antennas And Wireless Propagation Letters, VOL. 14, PP.783-786, December 2014.

9. T. Nakajima, M. Takahashi , K. Saito ,and K. Ito "Evaluation on characteristics of wristband type RFID antenna using a layer structural arm model" International Confere. on Applications of Electromagnetism and Student Innovation Competition Awards, Taipei, Taiwan, 11-13 August, 2010.

10. E. George, D. Ganguly, D. Sarkar, C. Saha, J. Siddiqui, and Y. Antar, "Time Domain Analysis of UWB Printed Monopole-Based Two-Port Systems for Characterization of On- to Off-Body Channels" URSI Radio Science Letters, Vol.2, September 2020.

11. M. Fazeli, Y. Hong, W. Lee, and J. Park, "Implantable Ferrite Antenna For Biomedical Applications" Microwave and Optical Technology Letters Vol. 58, No. 11, PP.2745-2749, August 2016.

12. S. N. Makarov , G. M. Noetscher, J.Yanamadala, M. W. Piazza, Sara Louie, A. Prokop, A. Nazarian, and A. Nummenmaa, "Virtual Human Models for Electromagnetic Studies and their Applications" IEEE Reviews In Biomedical Engineering, Vol. 10, PP.95-121, June 2017.

13. M. Abedian, S. K. A. Rahim, and M. Khalily, "Two-Segments Compact Dielectric Resonator Antenna for UWB Application" IEEE Antennas and Wireless Propag. Letters, Vol. 11, PP.1533-1536 , December 2012.

14. H.L. Zhu, S.W. Cheung, X.H. Liu, Y.F. Cao and T.I. Yuk, "Frequency Reconfigurable Slot Antenna Using Metasurface" 8th European Conference on Antennas and Propag, EuCAP 2014, The Hague, Netherlands, 6-11 April, 2014.

15. Y. H. Qian, Q. X Chu, "A Broadband Hybrid Monopole-Dielectric Resonator Water Antenna" IEEE Antennas and Wireless Propag. Letters, Vol. 16, PP. 360-363, June 2016.

16. S. Fakhte, H. Oraizi, L.Matekovits, "Gain Improvement of Rectangular Dielectric Resonator Antenna by Engraving Grooves on Its Side Walls" IEEE Antennas and Wireless Propag. Letters, Vol.16, PP.2167-2170, May 2017.

17. T.A. Denidni, Y. Coulibaly, H. Boutayeb, "Hybrid Dielectric Resonator Antenna with Circular Mushroom-Like Structure for Gain Improvement" IEEE Transactions on Antennas and Propag., Vol. 57, PP.1043-1049, April 2009.

18. Z.X. Xia, K.W Leung, "Gain Enhancement of Rectangular Dielectric Resonator Antenna Using EBG Surface", IEEE Asia-Pacific Conference on Antennas and Propag.,2018, Auckland, Newzland, 5-8 August, 2018.

19. B. Rana, A. Chatterjee, S. K. Parui, “Gain Enhancement of a Direct Microstrip Line fed Dielectric Resonator Antenna using FSS” IEEE Applied Electromagnetic Conference 2015, Guwahati, India, 18-21 December 2015.

20. Vigyanshu Mishra , Asimina Kiourti, “Wearable Magnetoinductive Waveguide for Low-Loss Wireless Body Area Networks” IEEE Transactions On Antennas And Propagation, Vol. 69, No. 5,PP.2864-2876, May 2021.

21. Nozomi Haga, Kazuyuki Saito, Masaharu Takahashi, Koichi Ito, “Characteristics of Cavity Slot Antenna for Body-Area Networks” IEEE Transactions On Antennas And Propagation, Vol. 57, No. 4,pp.837-843 April 2009.

22. Chia-Hsien Lin, Kazuyuki Saito, Masaharu Takahashi, Koichi Ito, “A Compact Planar Inverted-F Antenna for 2.45 GHz On-Body Communications” IEEE Transactions On Antennas And Propagation, Vol. 60, No. 9,PP.4422-4426 September 2012.

23. Bin Xu, Yang Li, and Youngwook Kim, “Classification of Finger Movements Based on Reflection Coefficient Variations of a Body-Worn Electrically Small Antenna” IEEE Antennas And Wireless Propagation Letters, Vol. 16, PP.1812-1815, March 2017.

24. Keren Zhu , Lisa Militello, and Asimina Kiourti, “Antenna-Impregnated Fabrics for Recumbent Height Measurement on the Go” IEEE Journal Of Electromagnetics, Rf, And Microwaves In Medicine And Biology, Vol. 2, No. 1, PP.33-39, March 2018.

25. Pongphan Leelatien , Koichi Ito , Kazuyuki Saito, Manmohan Sharma, and Akram Alomainy, “Channel Characteristics and Wireless Telemetry Performance of Transplanted Organ Monitoring System Using Ultrawideband Communication” IEEE Journal Of Electromagnetics, Rf, And Microwaves In Medicine And Biology, Vol. 2, No. 2,PP.94-101, June 2018.

26. Asimina Kiourti, Konstantina S. Nikita, “A Review of Implantable Patch Antennas for Biomedical Telemetry:Challenges and Solutions” IEEE Antennas and Propagation Magazine, Vol. 54, No. 3,PP.210-228 June 2012.

27. Sajid M. Asif, Adnan Iftikhar, Benjamin D. Braaten, Daniel L. Ewert, Keith Maile, “A Wide-Band Tissue Numerical Model for Deeply Implantable Antennas for RF-PoweredLeadless Pacemakers” IEEE Access, Vol.7, PP.31031-31042,March 2019.

28. Yunxiao Peng , Kazuyuki Saito, Koichi Ito, “Antenna Design for Impulse-Radio-Based Wireless Capsule Endoscope Communication Systems” IEEE Transactions On Antennas And Propagation, Vol. 66, No. 10, PP.5031-5042 October 2018.

29. Naeem Abba, Abdul Basir , Amjad Iqbal , Muhammad Yousaf , Adeel Akram ,Hyoungsuk Yoo, “Ultra-Miniaturized Antenna for Deeply Implanted Biomedical Devices” IEEE Access, Vol.10,PP.54563-54571, May 2022.

30. N.Chahat, Maxim Zhadobov, Ronan Sauleau, Koichi Ito, “A Compact UWB Antenna for On-Body Applications” IEEE Transactions On Antennas And Propagation, Vol. 59, No. 4, PP.1123-1131, April 2011.

31. Roy B. V. B. Simorangkir , Asimina Kiourti , Karu P. Esselle, “UWB Wearable Antenna With a Full Ground Plane Based on PDMS-Embedded Conductive Fabric” IEEE Antennas And Wireless Propagation Letters, Vol. 17, No. 3, PP.493-496, March 2018.

32. Erdem Cil, Sema Dumanli, "The Design of a Reconfigurable Slot Antenna Printed on Glass for Wearable Applications" IEEE Access, , Vol.8, PP.95417-95423, May 2020.

33. Luz. I. Balderas, Alberto Reyna, ,Marco A. Panduro, Carlos Del Rio, Arnulfo R. Gutierrez, "Low Profile Conformal UWB Antenna for UAV Applications" IEEE Access, Vol. 7,PP.127486-127494, September 2019.

34. S. Fakhte, H. Oraizi, and L. Matekovits, "High gain rectangular dielectric resonator antenna using uniaxial material at fundamental mode" IEEE Trans. Antennas Propag. Vol. 65, PP.342-347, January 2017.

35. R.D. Gupta, and M.S. Parihar, "Differentially fed wideband rectangular DRA with high gain using short horn" IEEE Antennas Wirel. Propag. Lett. Vol.16, PP.1804-1807, March 2017.

36. C.-H. Li and T.-Y. Chiu, "340-GHz low-cost and high-gain on-chip higher order mode dielectric resonator antenna for THz applications" IEEE Trans. Terahertz Sci. Technol. Vol.7, No.3, PP.284-294, March 2017.

37. S. Trinh-Van, Y. Yang, K.-Y. Lee, and K.C. Hwang, "Single-fed circularly polarized dielectric resonator antenna with an enhanced axial ratio bandwidth and enhanced gain" IEEE Access Vol.8, PP.41045-41052, February 2020.

38. B. Sahu, M. Aggarwal, P. Tripathi, R. Singh, "Stacked cylindrical dielectric resonator antenna with metamaterial as a superstrate for enhancing the bandwidth and gain" IEEE International Conference on Signal Processing, Computing and Control, 26-28 September, 2013.

39. B. Bahreini, H. Oraizi, N. Noori, and S. Fakhte, "Design of a circularly polarized parasitic array with slot-coupled DRA with improved gain for the 5G mobile system", IEEE Antennas Wirel. Propag. Lett. Vol.17, PP.1802-1806, August 2018.

40. Girish Kumar, K.P.Ray, Broadband Microstrip Antennas, Artech House Publishers,2003.

41. Constantine A. Balanis, Antenna Theory, Analysis and Design", John Wiley Sons, Inc. Second Edition 1997.

42. H.Wang, X.B. Huang, D.G. Fang, "A single layer wideband U-slot Microstrip Patch Antenna Array" IEEE Antennas and Wireless Propagation Letters, Vol.7, PP.9-12, February 2008.

43. Shing-Lung, Steven Yang, Kwai-Man Luk, "A wideband L-Probes Fed Circularly polarized reconfigurable microstrip patch antenna" IEEE Transacions on Antennas and Propagation, Vol.56, No.2, PP.581-584, February 2008.

44. Fan Yang, Xue-Xia Zhang, Xiaoning Ye, Yahya Rahmat-Samii "Wide-Band E-Shaped Patch Antennas for Wireless Communications", IEEE Trans. Antennas and Propagat., Vol.49,No.7, PP.1094-1100, July 2001.

45. Keisuke Noguchi, Harish Rajagopalan, Yahya Rahmat-Swami, "Design of Wideband/Dual-Band E-shaped Patch antennas with the transmission Line mode theory" IEEE Transactionson Antennas and Propagation, Vol.64, No.4, PP.1183-1192, April 2016.

46. Cheng Qi, Peter Hillyard, Amal Al-Husseiny, Neal Patwari, Gregory D.Durgin, "On-Wall, Wide bandwidth E-shaped Patch Antenna for Improved Whole-Home Radio tomography" IEEE Journal of Radio Frequency Identification, Vol.1, No.1, PP.22-31, March 2017.

47. Ka Ming Mak, Hau wah lai, Kwai Man Luk, Chi Hou chan "Circularly Polarized patch antenna for future 5G mobile Phones" IEEE Access, Vol.2, PP.1521-1529, December 2014.

48. Fa-Shian Chang, Kin-Lu Wong, and Tzung-Wern Chiou "Low cost broadband circularly polarized patch antenna" IEEE Transactions On Antennas And Propagation, Vol. 51, No. 10, PP.3006-3009, October 2003.

49. Anggit Dwi Novella, Heroe Wijanto, Agus Dwi Prasetyo "Dual feed Circularly Polarized Microstrip Antenna for S-band Transmitter of Synthetic Aperture Radar" International Conference on Quality in Research, 10-13 August, 2015.

50. Mang He, Xihong Ye, Pingyuan Zhou, Guoqiang Zhao, Chuanfang Zhang, Houjun Sun "A small size Dual feed Broadband Circularly Polarized U-Slot Patch Antenna" IEEE Antennas and Wireless Propagation Letters, Vol.14, PP.898-901 December 2014.

51. Jianxing Zhuang, Yan Zhang, Wei Hong, Zhangcheng Hao, "A broadband circularly polarized patch antenna with improved axial ratio" IEEE Antennas and Wireless Propagation Letters, Vol.14, PP.1180-1183, January 2015.

52. Jaejin Lee, Yang-Ki Hong, Woncheol Lee, Gavin S.Abo, Jihoon Park, "Role of small permiability in Gigahertz Ferrite Antenna Performance" IEEE Magnetics Letters Vol.4, February 2013.

53. D.M Pozar,V.Sanchez, "Magnetic tuning of a microstrip antenna on a ferrite substrate" Electronic Letters, Vol.24, No.12,PP.729-731, June 1988.

54. V.Losada, R.R Boix, Medina, "Evaluvation of the radar cross-section of circular microstrip patches on anisotropic and chiral substrate" IEEE Transactions on Antennas and Propagation,Vol.49, No.11, PP.1603-1605, Nov.2001.

55. A.Henderson, J.R James, "Magnetized Microstrip Antenna with Pattern Control" Electronic Letters, Vol.24, No.1, PP.45-47, January 1988.

56. CST STUDIO SUITE, Version 2016, Darmstadt, Germany.

57. Rogers Corporation, RT Duroid 6002 datasheet.

58. Alix Rivera-Albino, Constantine A. Balanis, "Gain Enhancement in Microstrip Patch Antennas using Hybrid Substrate" IEEE Antennas and Wireless Propagation Letters, Vol.12, PP.476-479, April 2013.

59. D. Sievenpiper, "High-impedance electromagnetic surfaces," Departmentof Electrical Engineering, UCLA, Los Angeles, CA, USA, 1999.

60. H. Boutayeb, T. Djerafi, and K. Wu, "Gain enhancement of a circularly polarized microstrip patch antenna surrounded by a circular mushroom-like substrate," in Proc. EuMC, Sep. 2010, PP. 257–260.

61. H. Boutayeb, T. A. Denidni, K. Mahdjoubi, A.-C. Tarot, A.-R. Sebak, and L. Talbi, "Analysis and design of a cylindrical EBG-based directive antenna" IEEE Trans. Antennas Propag., Vol. 54, No. 1, PP. 211–219, January 2006.

62. Meng Xue, Jinhai Liu, Zhipeng Zhao, Xi Yang, Yingzeng Ying, “Wideband Dual Polarized Hybrid Fed Patch Antenna” International Journal of RF and Microwave Computer Aided Engineering, 20 March 2019, Wiley Online Library.

63. Simon Mener, Raphael Gillard, Langis Roy "A dual band Circular Polarization Antenna for Ka band Satellite Communications" IEEE Antennas and Wireless Propag. Letters, Vol. 16, PP.274-277, May 2016.

64. Tayeb A. Denidni, Larbi Talbi, “High gain Microstrip antenna design for broadband Wireless applications” International Journal of RF and Microwave Computer Aided Engineering, 18 June 2003, Wiley Online Library.

65. Nemai Chandra Karmakar, “Miniaturization and bandwidth enhancement of a cavity backed circular microstrip patch antenna”International Journal of RF and Microwave Computer Aided Engineering, 2 April 2007, Wiley Online Library.

66. Dunwei Liao, Feng Wei, Xintong Zou, “A dual polarized low-profile microstrip patch antenna with U- or M- shaped feed network”International Journal of RF and Microwave Computer Aided Engineering, 28 March 2019, Wiley Online Library.

67. Preeti Kumari, Pankaj Tripathi, S. Sahu, S.P. Singh, Devandra Kumar, “Four-Element Composite Triangular Dielectric Resonator Antenna Using Li2O-1.94MgO-0.02Al2O3-P2O5 Ceramic for Wideband Applications” Journal of Electronic Materials, Vol.47, No.9, PP.5218-5228, 2018.

68. X Chen, H Feng Ma, X Ying Zou, W Xiang Jiang, T Jun Cui, “Three-dimensional broadband and high-directivity lens antenna made of metamaterials” Journal of Appl. Phys. Vol. 110 , PP.044904, August 2011.

69. Wenmo Chang and Zhenghe Feng “Investigation of a Novel Wideband Feeding Technique for Dielectric Ring Resonator Antennas” IEEE Antennas and Wireless Propag. Letters, Vol.8, PP.348-351, February 2009.

70. S. George, S. Raman, P. Mohanan, M. T. Sebastian, “Polymer ceramic composites for microwave substrate and antenna applications”, Indian Antenna Week: A Workshop on Advanced Antenna Technology, 31 May-04 June 2010.

71. Suma M N, Sreedevi K Menon , P V Bijumon , M T Sebastian, P. Mohanan, “Experimental Investigation on Rectangular Dielectric Resonator Antenna Excited By Conductor Backed Coplanar Waveguide” IEEE Antennas and Propag. Society International Symposium, 03-08 July 2005.

72. S.Mridula, Binu Paul, Sreedevi.K.Menon, C.K.Aanandan, K.Vasudevan, P.Mohanan, P.V.Bijumon, M.T.Sebastian, "Wideband Rectangular Dielectric Resonator Antenna for W-LAN Applications", IEEE Antennas and Propag. Society Symposium, 20-25 June 2004.

73. D. Swathi1, Dr.HabibullaKhan, V.Pallavi, S.V.S.Shalini, Pratyusha, "Design and Implementation of Dual Feed Circularly Polarized Dielectric Resonator Antenna for High Gain Applications" Fifth International Conference on Inventive Computation Technologies, 26-28 February 2020.

74. Hailiang Zhu, Sing Wai Cheung, Tung Ip Yuk "Enhancing Antenna Boresight Gain using a small metasurface lens" IEEE Antennas and Wireless Propag. Magazine, Vol.10, No.1, PP.35-44, February 2016.

75. S. Keyrouz, D. Caratelli, "Dielectric Resonator Antennas: Basic Concepts, Design Guidelines, and Recent Developments at Millimeter-Wave Frequencies" International Journal of Antennas and Propag., Volume 2016, Article ID: 6075680, October 2016.

76. Aldo Petosa, "Dielectric Resonator Antenna Handbook" (Artech House, 2007)

77. Zsolt Szabó, Gi-Ho Park, Ravi Hedge, and Er-Ping Li, "A Unique Extraction of Metamaterial Parameters Based on Kramers–Kronig Relationship" IEEE Transactions on Microwave Theory And Techniques, Vol.58, No.10, PP.2646-2653, October 2010.

78. Peter S Hall, Yang Hao, Yuriy I.Nechayev, Akram Alomainy, Costas C. Constantinou, Clive Parini, Muhammad R. Kamarudin, Tareq Z.Salim, David T.M.Hee, Rostyslav Dubrovka, Abdus S. Owadally, Wei Song, Andrea Serra, Paolo Nepa, Michele Gallo, Michele Bozzetti , "Antennas and Propagation for On-Body Communication Syatems" IEEE Antennas and Propagation Magazine Vol.49, No.3, PP.41-58, June 2007.

79. Thierry Alves, Benoit Poussot, Jean Marc Laheurte, "Analytical Propagation Modelling of BAN Channels based on the creeping wave theory" IEEE Trans. on Antennas and Propag., Vol.59, No.4, PP.1269-1274, December 2010.

80. Jhih-Ming Chen and Jeen-Sheen Row, "Wideband Circularly Polarized Slotted-Patch Antenna With a Reflector", IEEE Antennas And Wireless Propag. Lett., Vol. 14, PP.575-578, November 2014.

81. Wei Xia, Kazuyuki Saito, Masaharu Takahashi, Koichi Ito, "Performance of an Implanted Cavity Slot Antenna Embedded in the Human Arm", IEEE Trans. Of Antennas and Propag., Vol.57, No.4, PP. 894-899, April 2009.

82. E Je´quier1 and F Constant, “Water as an essential nutrient: the physiological basis of hydration” European Journal of Clinical Nutrition Vol.64, PP. 115–123, February 2010.

83. D. K. Das, “Study of dual-band wearable antennas using commonly worn fabric materials,” M.S. Thesis, Dept. of Elecrical and Computer Engg. Oklahoma State University, Stillwater, United States, 2017.

84. SOLIDWORKS, Dassaults Sysems, Providence, Rhode Island.

85. C. Briso, C. Calvo, Y. Xu,"UWB Propagation Measurements and Modelling in Large Indoor Environments”, IEEE Access,Vol.7, PP.41913-41920, March 2019.

86. S. Cotton, R.D’Ericco, C.Oestges, “A Review of Radio Channel Models for Body Centric Communications”, Radio Sci.,Vol.49, June 2014.

87. Z. Irahhauten, H. Nikookar, and G.J. M. Janssen, “An Overview of Ultra Wide Band Indoor Channel Measurements and Modeling”, IEEE Microwave And Wireless Components Letters, Vol. 14, No. 8, PP.386-388, August. 2004.

88. A. Alomainy, Y. Hao, X. Hu, C.G. Parini and P.S. Hal., “UWB on-body radio propagation and system modelling for wireless body-centric networks”, Ultra Wideband Systems, Technologies And Applications Special Section,IEEE Proc.-Commun., Vol. 153, No. 1, PP.107-114, February 2006.

89. Q. Wang, T.Tayamachi, I. Kimura, and J. Wang, “An On-Body Channel Model for UWB Body Area Communications for Various Postures” IEEE Transactions on Antennas And Propagation, Vol. 57, No. 4, PP:991-998, April 2009.

90. T.S. P. See and Z. Chen, “Experimental Characterization of UWB Antennas for On-Body Communications”, IEEE Transactions on Antennas and Propagation, Vol. 57, No. 4, PP:866-874, April 2009

91. A. Alomainy, A. Sani, A. Rahman, J. G. Santas, and Y. Hao, “Transient Characteristics of Wearable Antennas and Radio Propagation Channels for Ultrawideband Body-Centric Wireless Communications”, IEEE Transactions on Antennas And Propagation, Vol. 57, No. 4, ,PP: 875-884, April 2009.

92. A. Sani et al., "Experimental Characterization of UWB On-Body Radio Channel in Indoor Environment Considering Different Antennas," IEEE Transactions on Antennas and Propagation, Vol. 58, No. 1, PP.238-241, January 2010.

93. K. Ito, N. Haga, M.Takahashi and K. Saito, “Evaluations of Body-Centric Wireless Communication Channels in a Range from3MHz to 3 GHz” , Proceedings of the IEEE , Vol. 100, No. 7, PP.2356-2363, July 2012.

94. A. Maskooki, C.Boon, S.Erry Gunawan, and Kay Soon Low, “Ultra-Wideband Real-Time Dynamic Channel Characterization and System-Level Modeling for Radio Links in Body Area Networks” , IEEE Transactions On Microwave Theory And Techniques, Vol. 61, No. 8, PP2995-3004 , August 2013..

95. Q. Zhang, J. Sarrazin, M. Casaletti, P. De Doncker, and A. Benlarbi-Dela, “Assessment of On-Body Skin-Confined Propagation for Body Area Network”, IEEE Antennas And Wireless Propagation Letters, Vol. 16, PP.2610-2613 , August 2017.

96. R. Bharadwaj and S. K. Koul, "Experimental Analysis of Ultra-Wideband Body-to-Body Communication Channel Characterization in an Indoor Environment,” IEEE Transactions on Antennas and Propagation, Vol. 67, No. 3, PP.1779-1789, March 2019.

97. R. Dautov and G. R. Tsouri, "Dynamic Off-Body Rician Channel Modeling for Indoor Wireless Body Area Networks," IEEE Journal of Biomedical and Health Informatics, Vol. 24, No. 5, PP.1246-1254, May 2020.

98. MATLAB R.2010

99. D. Mandal and S.S Pattnaik, “Quad Band wearable slot antenna with low SAR values for 1.8 GHz DCS, 2.4 GHz WLAN and 3.6/5.5 GHz WiMax Applications”, Progress in Electromagnetic Research B. Vol.81, PP.163-182, 2018.

100. D. Ganguly, D. Guha, S. Das, A.Rojatkar., “Systematic approach to estimating mono-cycle pulse for time domain studies of UWB antennas using numerical computations and simulation tools,” IEEE Antennas Propag. Magazine, Vol. 56, No.4, PP.73–87 August, 2014.

List of Publications

International Journals

- **Elizabeth George** and Chinmoy Saha, 2022. Investigation of Creeping Wave Characteristics and Double Arm Swing Activity using Twelve Cylinder Phantom Model. *IEEE Antennas and Wireless Propagation Letters*, Vol.21, No.10, PP.2090-2094,July 2022.

- **Elizabeth George**, Chinmoy Saha, 2022. Metasurface Lens Integrated Rectangular Dielectric Resonator Antenna with Enhanced Gain *Journal of Electronics Materials* (Issue **6**), Springer Publications, (DOI: 10.1007/s11664-022-09544-4).

- **Elizabeth George**, D. Ganguly, D.Sarkar, Chinmoy Saha, J.Siddiqui, Y.Antar 2020. Time Domain Analysis of UWB Printed Monopole Based Two-Port Systems for Characterization of On to Off-Body Channels, *URSI Radio Science Letters, 2020.*

- **Elizabeth George** and Chinmoy Saha, 2019. Ferrite Ring loaded Hybrid Substrate design for gain enhancement of linearly and Circularly Polarized Microstrip antennas *International Journal of RF and Microwave Computer Aided Engineering,* , (Vol.**29**, Issue.12.), Wiley Publications, (DOI: 10.1002/mmce.21933).

To be Communicated

- Investigation of ON-to OFF-Body Transmission Characteristics using Smart Bag for IoT applications.

Conference Proceedings

- **Elizabeth George**, Chinmoy Saha, Investigation of on-Body Creeping Wave Mechanism and Double-Arm Swing Activity for WBAN Applications, *IMaRC, IEEE MTTS-*

International Microwave and RF Conference, December 17-19, 2021, IIT Kanpur, India.
(Third Prize-Female Student Paper award)

- **Elizabeth George**, Chinmoy Saha, Effect of Varying Antenna Position on Smart Bag for 5G Internet of Things (IoT) Applications, *Indian Conference on Antennas and Propagation (InCAP)*, December 13-16, 2021, Jaipur, India.

- **Elizabeth George**, D. Ganguly, D.Sarkar, Chinmoy Saha, Y.Antar Time-Domain Characterization of UWB Monopole Antenna Based On-Body to Off-Body Communication Channels, *Proceedings of URSI General Assembly (GASS), 2020.*

- D.Ganguly, D.Sarkar, Y.Antar **Elizabeth George**, Chinmoy Saha, Experimental UWB ON-Body Channel Modelling: Effect on Antenna Transmission Characteristics, *Proceedings of IEEE AP-S Symposium on Antennas and Propagation and CNC/USNC-URSI joint meeting, 2020 (Virtual Symposium).*, July, 5-10, Montreal, Canada.